PEOPLE'S DEMOCRATIC REPUBLIC OF ALGERIA

MINISTRY OF HIGHER EDUCATION AND SCIENTIFIC RESEARCH

UNIVERSITY SAAD DAHLEB BLIDA-1

FACULTY OF TECHNOLOGIE

Institute of Aeronautics and Space Studies

Department of Space Studies

Memorandum

Master's Thesis in Aeronautics

Specialty: Space Propulsion

Title:

Contribution to the Design of a One-Newton Thruster Based on a Green Propellant for Satellite Applications.

Presented by:	Advisor:	Member of the Jury	
Mr. BOUDGHENE STAMBOULI OMAR Nour Islem	Dr. KHALI El hadi	Dr.KEBAB Hakim	President
Mr. BOULAHIA Mohamed EmadEddine	Dr. DARFILAL Djamal	Dr.ADDA Mourad	Examiner
		Dr.SBAA Lazab	Examiner

2020/2021

ABSTRACT

The purpose of master thesis is a contribution into the realization of an inexpensive and lightweight thruster of one Newton (1N), that local manufacturing companies can produce, and this using a green fuel : Hydrogen Peroxide H_2O_2 of a concentration equal to 87.5 % for satellites application.

The methodology used was based under a set of analysis steps starting from Thermochemistry to Theoretical Rocket Performance, and Preliminary Thruster Design. The effective factors used to study our system are dependent upon one another, meanwhile these factors are directed the decisions made throughout this design project that are the thrust, pressure, fuel, loading factor, catalyzer type and study state (vacuum – atmospheric).

Nozzle is the most important part for any thruster design, a set of conditions were made within storage system and thruster to determine the right design for the converging diverging nozzle, meanwhile determining the correct catalyst model sustain the desired efficiency.

Matlab program was used for the dimensioning step. ANSYS Fluent 19.0 was used for CFD analysis & SolidWorks 2017 for CAD generation respectively.

The value of this project is to aid in the reconnaissance and analysis of green propellant propulsion system by adding a catalyzer for higher efficiency corresponding to control attitude conditions as well as provide a stable and controllable platform for testing equipment that can be ultimately applied to space applications.

RESUME

Le but de ce projet de fin d'étude est une contribution à la réalisation d'un propulseur d'un Newton (1 N) peu coûteux et de conception légère que les entreprises locales peuvent produire et cela en utilisant un carburant vert : le Peroxyde d'hydrogène H_2O_2 de concentration égale à 87,5% pour une application satellite.

La méthodologie utilisée était basée sur un ensemble d'étapes d'analyse allant de la thermochimie à la performance théorique de la fusée et à la conception préliminaire du propulseur. Les facteurs efficaces utilisés pour étudier notre système dépendent les uns des autres, tandis que ces facteurs orientent les décisions prises tout au long de ce projet de conception qui sont : la

poussée, la pression, le carburant, le facteur de charge, le type de catalyseur et l'état d'étude (vide – atmosphérique).

Le Nozzle est la partie la plus importante de toute conception de propulseur, un ensemble de conditions a été créé dans le système de stockage et le propulseur pour designer la bonne conception pour la partie divergente convergente, tout en déterminant le bon modèle de catalyseur afin de maintenir l'efficacité souhaitée.

Le programme Matlab a été utilisé pour l'étape de dimensionnement. ANSYS Fluent 19.0 pour l'analyse CFD et SolidWorks 2017 pour la génération DAO (design assisté par ordinateur) respectivement.

La valeur ajoutée de ce projet était d'aider à la reconnaissance et à l'analyse du système de propulsion à propergol vert en ajoutant un catalyseur pour une efficacité plus élevée correspondant aux conditions d'attitude de contrôle ainsi qu'à fournir une plate-forme stable et contrôlable pour tester des équipements qui peuvent finalement être appliqués aux applications spatiales.

ملخص

الهدف من هذا مشروع التخرج هو المساهمة في انجاز محرك بقوة دفع تعادل واحد نيوتن باعتباره تصميم غير مكلف وخفيف الوزن يمكن لشركات التصنيع المحلية إنتاجه. وذلك باستخدام وقود اخضر: بيروكسيد الهيدروجين H_2O_2 بتركيز يساوي 87.5 % لتطبيقات الأقمار الصناعية.

المنهجية المستخدمة مبنية على مجموعة من خطوات التحليل بدءًا من الكيمياء الحرارية وحتى أداء الصاروخ النظري والتصميم الأولي للمحرك. تعتمد العوامل الفعالة المستخدمة لدراسة نظامنا على بعضها البعض، في نفس الوقت يتم توجيه هذه العوامل للقرارات المتخذة طوال هذا المشروع التصميمي وهي: الدفع والضغط والوقود وعامل التحميل ونوع المحفز وحالة الدراسة (الفراغ- الغلاف الجوي).

باعتبار الفوهة هي الجزء الأكثر أهمية في أي تصميم دافع، تم وضع مجموعة من الشروط داخل نظام التخزين، والدافع يقوم بتحديد التصميم المناسب للجزء المتباعد المتقارب، وفي الوقت نفسه يحدد النموذج المحفز الصحيح للحفاظ على الكفاءة المطلوبة.

تم استخدام برنامج Matlab لدراسة الأبعاد. و استخدام ANSYS Fluent 19.0 لتحليل CFD و CAD SolidWorks2017 للتصميم بمساعدة الكمبيوتر، على التوالي.

تتمثل القيمة المضافة لهذا المشروع في المساعدة على الاستطلاع وتحليل نظام الدفع بالوقود الأخضر عن طريق إضافة محفز لتحقيق كفاءة أعلى تتوافق مع ظروف التحكم بالإضافة إلى توفير منصة ثابتة يمكن التحكم فيها لاختبار المعدات التي يمكن تطبيقها في النهاية على التطبيقات الفضائية.

ACKNOWLEDGEMENT

We really do have to express our collective gratitude towards **Dr. El hadi KHALI**. We say a "BIG THANKS' not only for his guidance and patience during this project but also for his mentoring throughout all of our brief encounters with the research world, It was a great privilege and honour to work and study under his guidance.

We would like to express our deep and sincere gratitude to the coordinator of the Algerian Satellite Development Center **Dr. Djamal DARFILAL**, for giving us the opportunity to do research and providing invaluable guidance throughout this research. His dynamism, vision, sincerity and motivation have deeply inspired us. He has taught us the methodology to carry out the research and to present the research works as clearly as possible. We are extremely grateful for what he has offered us. We would also like to thank him for his friendship, empathy, and great sense of humour.

Special appreciation goes to our loving parents especially our family who are always on our side by their love, prayers, caring and sacrifices for educating and riding along with us on our difficulties as well as giving us the encouragement to pursue our dreams.

Finally, Thanks to our Institute of Aeronautics and Space Studies – Blida for the chance we get to enhance our dream's goal and everyone who gave us the push to continue to finish and to reach the end where we are now.

Table of content

LIST OF FIGURES

LIST OF TABLES

NOMENCLATURE

a	acceleration	[m/s2]
A	Area	[m2]
c	effective exit velocity	[m/s]
$C*$	Characteristic velocity	[m/s]
CF	Coefficient of thrust	
Cl	length of catalyst	[mm]
C_v	Specific heat for volume constant	[kJ/ kg K]
C_p	Specific heat for pressure constant	[kJ/ kg K]
d	Diameter	[mm]
Dd	Disque diameter	[mm]
Dw	Wire diameter equal	[mm]
F	Thrust	[N]
F_{div}	Thrust loss dua divergent form	[N]
$g0$	Acceleration due to gravity	[m/s2]
h	enthalpy	[KJoule]
Hs	Hole size	[mm]
$\Delta_f H$	Standard Enthalpy of formation	[kj/mol]
$\Delta_R H$	Enthalpy of reaction	[kj/mol]
Isp	Specific Impulse	[s]
It	Total impulse	[s]
Ma	Mach number	
M	Average molecular mass of the gas	[g/mol]

m	Mass	[kg]
$\dot{m}$	Mass flow rate of propellants	[g/s]
No	Number of moles	[mole]
P	Pressure	[Pa]
Q	heat quantity	[KJoule]
r	rayon	[mm]
R	Universal gas constant	[J/mol*K]
T	Temperature	[K]
t	Time	[s]
$\bar{V}$	Volume	[m3]
V	Velocity	[m/s]
$\tilde{V}$	Specific volume	$[m^3/Kg]$
ε	Expansion ratio	
ρ	Density	[kg/m3]
γ	Ratio of specific heats of exhaust gas	

ABBREVIATIONS

CAD	Computer Aided Design	
CBL	Catalyst bed loading	[kg/s/m2]
CBLCSA	Cross sectional area catalyst bed loading	[kg/s/m2]
CBLWSA	Catalyst bed wetted area loading	[kg/s/m2]
CFD	Computational Fluid Dynamic	
CSA	Cross sectional area	
DAO	Design Assisté par Ordinateur	
F/O	Fuel to oxidizer ratio	
HTP	High test peroxide	
L/D	Length to diameter ratio	
MIB	Minimum impulse bit	
NASA	National Aeronautics and Space Administration	
O/F	Oxidizer to fuel ratio	
RCS	Reaction Control System	

CLUES

avb	available
avg	average
cat	catalyst
c	chamber
e	exit
f	final
i	ideal
int	initial
inj	injection
p	product
$\hat{r}$	feed system
$\check{t}$	throat

INTRODUCTION

Space propulsion refers to a set of different systems mostly used in spacecraft, and rockets. Chemical propulsion is meant to be the oldest and the most commonly used in our world. Besides to the variety in the technology used in this domain there is a diversity performance obtained while moving from micro-thruster to the huge thruster. Systems that deliver high thrust are generally used to carry a heavy loading as satellite to be putted into orbit. Low thrust engine are used for attitude and manoeuvring control for spacecraft, and these engines are mostly using chemical or electrical system.

Nowadays, for orbit correction, majority of satellites propulsion system uses hydrazine which decompose into Nitrogen and Hydrogen in an exothermal reaction and these hot gases are then ejected to ensure a propulsion force, the use of hydrazine as a monopropellant has dominated the market for decades for the reason that it is reliable and gives good performance, but because of the toxic nature, researchers become more interested in developing engines based on green propellants. High Test Peroxide or HTP, a storable, cheap, easy to fabricate propellant is a solution and good replacement.

The aim of this thesis is to do a study on a small thruster that uses HTP as a monopropellant. The work contains four chapters and starts by presenting space propulsion and talking about the existing types propulsion and the advantages/ disadvantages of each one, also seeing how the High-test peroxide is used in this domain. Chapter two was concerned in propulsion fundamentals principle, explaining and giving the mathematical form of rocket performance parameters. After that in the same chapter, we have mentioned the basic component of a propulsion system, and we spoke about the catalysts that decompose HTP by showing their categories, deactivation and how they chemically decompose the propellant. A final part of the second chapter is to make a thermochemical study on the decomposition of HTP and then obtain the dimensions, theoretical performances of our thruster. All this work is done using a MATLAB R2017a programme, the results are then presented and compared to work done by other developers which shows a good approximation.

Chapter number three focused on the CFD software ANSYS FLUENT 19.0, this part is concerned in the theory of models used in the software and after that we saw the mesh definition, its importance, types and quality. The final chapter is a fluid simulation of the nozzle obtained

previously in the second chapter. We used for this simulation a commercially available CFD software ANSYS FLUENT 19.0.A successful simulation would make it possible to investigate the fluid flow inside the nozzle. The study was divided into two cases, a first one considering an inviscid isentropic flow in order to compare the results with the programme in the same assumptions taken. The second one is a simulation for a viscous flow using SST k-omega turbulence model to see how viscosity effects the performance. Results discussed were the pressure, temperature, velocity, Mach number and Reynolds number. Values of y+ obtained in the solution were used to conclude that the k-ω turbulence was accurately modelled or the overall goal of the simulation. To check thrust obtained by our thruster, we cut the outlet area of the nozzle into 1000 section, and with the CFD software we obtained the pressure, velocity, axial velocity in every section, these results are exported to MICROSOFT EXCEL software which is used to calculate the thrust in each section and obtain the total thrust. A final step is to design our thruster in a 3D form using CAD software SOLIDWORKS 2017.

CHAPTER 1

SPACE PROPULSION

1.1   Introduction

Human beings have always developed their transportation by inventing and creating new vehicles and engines which helped to explore further places in a short time. Now a days space-crafts are in top list of transport technologies because most of our activities are reliant to satellites and space vehicles, communication, navigation and planet exploration are a good example.

Many propulsion systems have been developed to ensure a safe and successful space mission phase, from rocket launch, orbit insertion to the attitude control.[1]

1.2   Space-craft propulsion history

Feng Jishen (970 AD) invented the first rocket 'fire arrow', his experiments consist of filling a bamboo tube that contains a hole in one end with gunpowder which is then ignited, the ignition causes the tube to start to move randomly. After that, he adds a stick for stability. Rockets have been used as weapons during the Japanese invasion in 1275 by Kublai khan, and as bombardments by the Mongols and Arabs in the 1300s.In 1770s Indian sultan tipoo used them against British army.[1]

After these periods, humans start thinking of rocket as a vehicle capable of accessing space, Konstantin Tsiolkovsky (1857-1935), a Russian mathematician & a teacher, he was a scientist in aeronautics and astronautics and had many research in rockets and space [2]. In 1883 he wrote a paper about space travel and proposed the use of rocket equipped with engines that ejects gases at high velocities. He then published his book in 1903 that talks about space travelling and exploration, the book defined for the first-time rocket equation which shows in detail rocket movement theory [3], after that in 1929 he had a publication about multi stage rockets theory which is based on his knowledge of propulsion dynamics [4].

Figure 1-1: Konstantine Eduardvich Tsiolkovsky. [1]

Robert Goddard (1882-1945) was one of the famous persons who did a quantum leap in this rocketry, he was a professor of physics at Clark University Massachusetts in USA[5], in 16 March 1962 he successfully launched liquid fuel oxygen and gasoline rocket, it reached 12.5 meters and lasted 2 seconds at a speed of 96.5 kph[6], the same technology has been developed and improved by the German Wernher von Braun and used in the German V2 rocket 15 years later in world war 2 with an operational range of 320 Km[5,**7**].

Figure 1-2: Robert Goddard. [1]

Figure 1-3: Wernher von Braun. [1]

4 October 1957 U.S.S.R launched the first artificial satellite made of aluminium in space and put it in low earth orbit with 227 kilometres of perigee and 945 kilometres of apogee for a 21 days mission duration [8] Since that day, countries are developing more propulsion systems with different source of energy and for different missions.
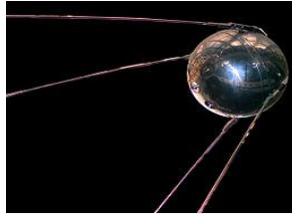
Figure 1-4: Sputnik 1 Satellite. [8]

1.3   Different types of propulsion

1.3.1   Introduction

Propulsion comes from the Latin word propulsus, it means to drive a way something. Propulsion generally is the action of changing the motion of a body, this change provides a force and this force will move bodies from position A to position B.[9]

In order to propel a space craft and launch it from earth or to put it in orbit and control its attitude we need to develop a propulsion system, so in this section we are going to talk about the various categories of these systems and see the advantages\disadvantages of each one.

Generally, in space propulsion the classification between different systems is made according to the source of energy used to produce and deliver thrust, we can then classify our systems into[10]:

- Energy from pressure we use it in cold gas thrusters
- Energy that comes from chemical reactions and we use it for chemical propulsive systems.
- Energy obtained from electricity or electric energy for electric propulsion systems.
- Energy from nuclear reactions.
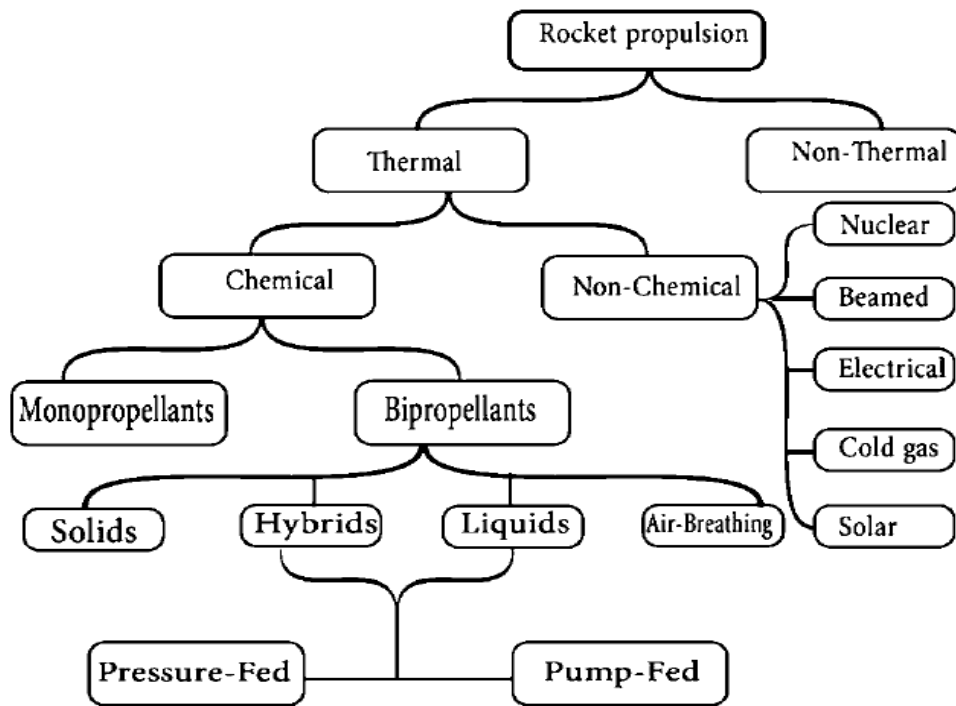
Figure 1-5: Propulsion System Classification. [11]

1.3.2 Cold Gas

This system generally uses nitrogen and helium as fuel because they are highly inert gases and have low molecular mass, an inert gas does not react with any other substance [12]. The idea of this type of propulsion is to store the propellant in a tank at high pressure, the gas is then expanded through a convergent divergent nozzle to space void, so the energy is obtained from that pressurized gas [13]. Cold gas system is simple to design because is contains a storage tank, there is no pressurization system in the tank so the pressure will decrease by time (blow down mode), feed pipe to deliver the gas to the nozzle and a valve to let the fuel enter to the convergent divergent part. these systems have proved that they are very suitable for low thrust propulsion and or LEO maneuvers [14].
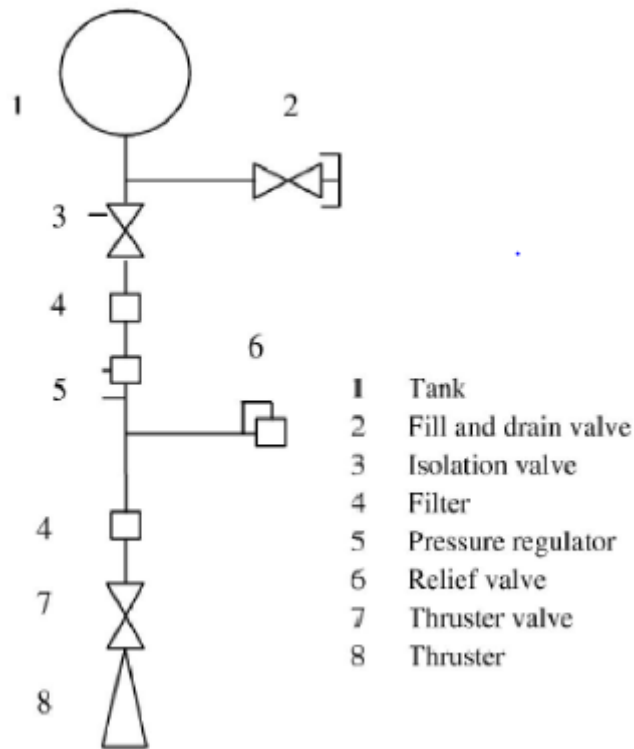
Figure 1-6: N2 Cold gas propulsion system schematic. [12]

ADVANTAGES [15]:

- Simple design
- Safe
- Inexpensive
- Reliable
- Lightweight

DISADVANTAGES [16]

- Thrust profile decreases due to pressure drop
- Low thrust and low Isp <100 s

1.3.3 Chemical propulsion

Chemical rockets use the energy released from combustion reaction, the reactant generally fuel and oxidizer meets in a chamber at certain conditions and react chemically, they produce very hot gases (2000-3500°C), a nozzle is used to expand these products and accelerate them at high velocities (2000-4500 m/sec) and provide necessary thrust. We can divide chemical propulsion into 3 major categories based on the nature of propellant [17].

- Solid
- Liquid
- Hybrid

1.3.3.1 Solid chemical propulsion

Solid propellant or the grain contains both fuel and oxidizer in one which is able to be burned while ignited. The combustion happens on the inner surface of the propellant charge. A hole in the combustion chamber is founded to let hot gases escape to nozzle and after that expand thermodynamically [18]. At microscopic level if fuel and oxidizer are chemically bounded, we say the propellant is homogenous, if not then it will be physically linked and we say it is heterogenous propellant that forms heterogenous physical structure [19].

A grain of propellant is made of different chemical substitutions, the chemical ingredients and their function are listed below [20]:

- Oxidizer, a necessary ingredient, it is important because it produces high energy on combustion
- Metal fuel like aluminium is added in form of spherical particles, it takes 14-20% of grain weight, the aim after adding it is to improve temperature of combustion and increase propellant density
- Binder special structure hold granular ingredients together, it is made of prepolymers and used to give a good chemical and mechanical properties. Binder gets oxidized in combustion like a normal fuel.
- Modifier, Catalyst or also called burning rate catalyst. Its role is to change the burning rate of the propellant, a burning rate determines the rate at which exhaust gases are generated from the burning propellant).
- Plasticizer improves the properties of propellant; it is an organic liquid with low-viscosity
- Curing agent is used to solidify the binder by forming longer chains

In propulsion, each mission requires certain profile of thrust vs time. To achieve this goal various of grain configurations are used, this will change the burning area from type to type and by consequence changes the amount of thrust delivered [21]. The most common shapes are tubular, star, dog bone [22].

The characteristics of performance of pounders depends on the percentage of different elements entering in its composition. Table 1.1 gives some examples with the approximate percentages

Table 1-1: Solid propellants. [10]

Oxidizer fuel	Ammonium perchlorate 75% Polybutadiene 10% Aluminium 15%	Ammonium perchlorate 75% Polybutadiene 20% Aluminium 15%	Ammonium nitrate Polybutadiene	Nitrocellulose 70% Nitrogrecyline 20% Stabilizer 10%
Theoretical Isp	260	260	190	220
Combustion temperature/K	3500	3400	1450	2100
Combustion velocity(cm/sec)	0.8	0.7	0.2	1.15
Density (Kg/m^3)	1770	1770	1470	1520
Molecular mass (g/mole	29	21	19	23

ADVANTAGES [23]:

- Simple design that helps for reducing maintenance costs

- Storable for a period that can reach 30 years

- High mass flow rates that lead to high thrust

DISADVANTAGES [23]:

- The variation of thrust during launch is limited and difficult

- Low specific impulse
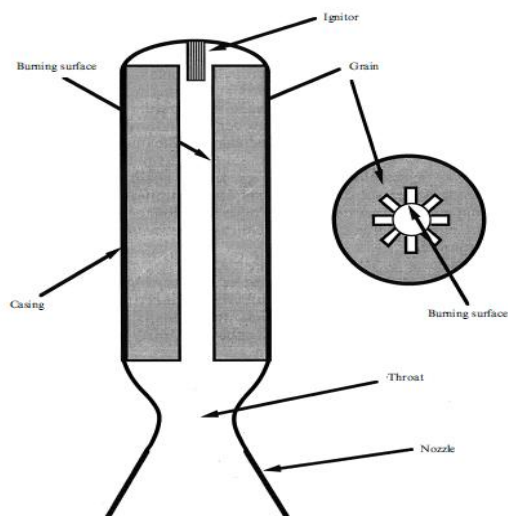
Figure 1-7: Schematics of a solid fuelled rocket motor. [18]

1.3.3.2 Liquid chemical propulsion

This system uses propellant which is in liquid state, we have two types of liquid, one is the fuel and the other one is oxidizer. If these liquids are separated and stored in different tanks we call it bipropellant, and if they are mixed together to become a single substance and stored in a single tank, we name it monopropellant. For the first type liquids are fed under pressure or with pumps and delivered to combustion chamber where they get mixed and ignited, hot gases produced from combustion are then expanded through a convergent-divergent nozzle. For the second type monopropellant is injected into catalysts chamber where it contacts a catalyst and decompose it, the products are expanded thermodynamically [24].

An important part in chemical rockets and liquid propulsion is the nozzle, it is made of three parts, convergent where the subsonic gases enter in it and get accelerated until reaching throat where the speed is equal to sound velocity, then a divergent to accelerate the supersonic flow [25].

In liquid propulsion, we can classify bipropellant into two categories [26]:

- Hypergolic bipropellant which ignites automatically when the fuel and oxidizer contact each other
- Nonhypergolic bipropellant, in this type need energy to start combustion, so an external ignition device is used.

In the other hand liquid propellant in general can be divided also into two categories [27]:

- Cryogenic propellant a gas which is liquefied and has extremely low melting point, -253°C for liquid hydrogen.
- Storable propellant has high melting point, this type can be stored for long time.

ADVANTAGES [27,28]:

- Thrust vs time profile is controllable due to the possibility to start/shutoff engines at any time.
- Specific impulse is large comparing to other chemical rockets, modern solid rocket can have 250 sec of Isp, while a liquid rocket can reach 450 sec of Isp
- High combustion temperature is achieved
- Cryogenic propellants give the highest specific impulse
- Thrust delivered is by a factor of 10^8
- They are suitable for controlling quick attitude changes

DISADVANTAGES [27]:

- The major problem in liquid rockets is that they need pumps for delivery and separate tanks, that means extra weight.
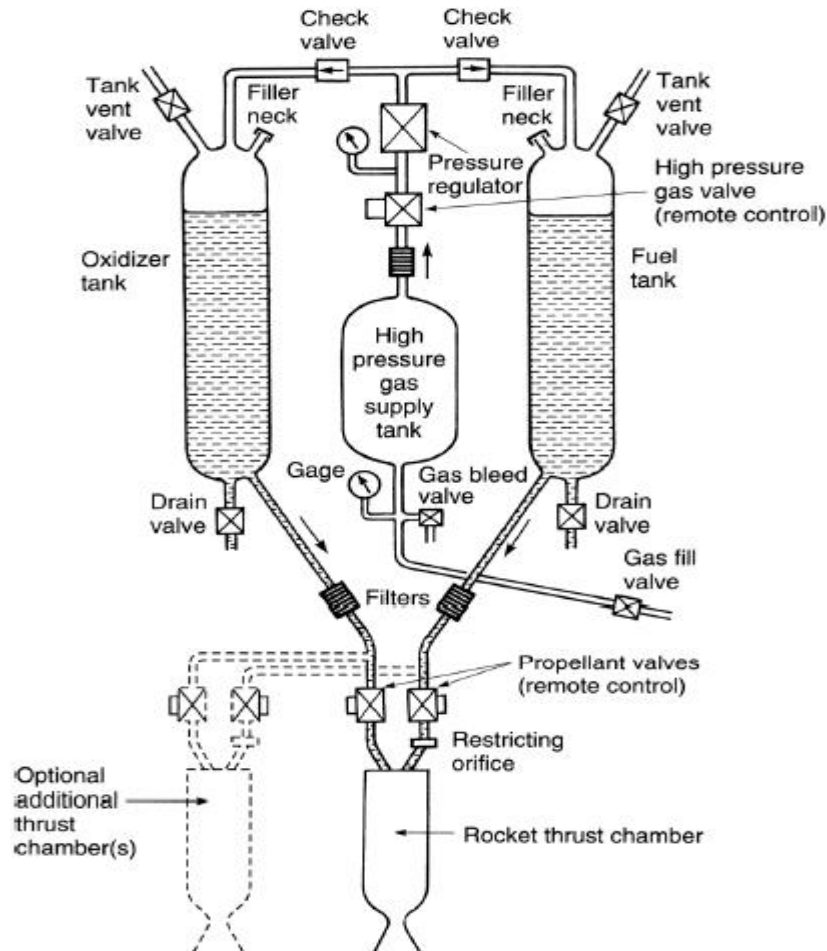
Figure 1-8: Schematics flow diagram of a liquid propellant rocket with a gas pressure feed system. [29]

1.3.4 Hybrid propulsion

A third type of chemical rockets, this one is a combination of the two previous ones. In hybrid propulsion propellants are stored in different phases. Generally, we use liquid oxidizer and solid fuel, if the configuration is the opposite, we call it reversed hybrid [30]. Fuel is stored in cylinder with different section shapes to deliver desired thrust profiles, the inner surface of fuel melts due to heat transfer, an oxidizer is injected and combustion occurs, an after burner is added because the

time for the previous combustion is short and causes incomplete combustion [30]
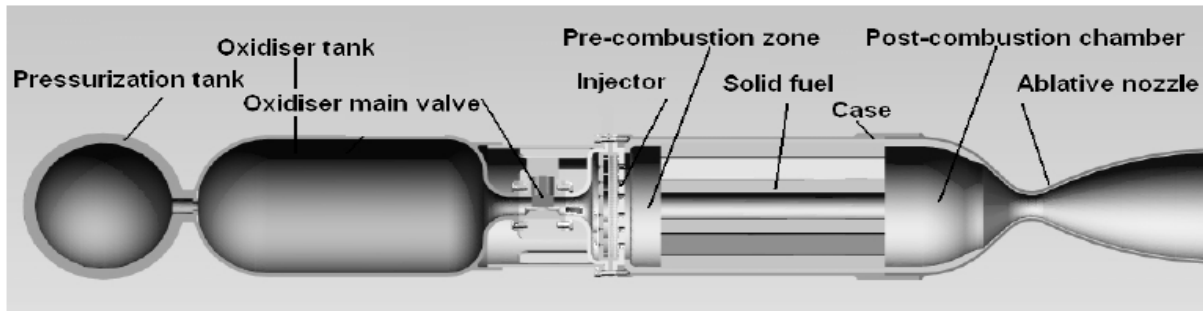
Figure 1-9: Simplified schematic diagram of a typical hybrid rocket engine. [30]

1.3.5 Electric propulsion

Electric rockets from its name we understand that they use electric energy, this energy will heat and/or directly accelerate and eject propellant gases. Like other types, this system is composed from several subsystems [31]:

- First there is energy source, it can be solar energy or nuclear plus some components like panels, radiators.
- Secondly, we find devices that convert the first raw energy into electricity at a specific voltage.
- A third subsystem that is responsible for the storage and the delivery of propellant
- A last one is the thruster that convert electric energy into kinetic energy.

In propulsion science, electric rockets are regrouped in three main branches, these branches are as follow [32]:

- Thermal thrusters: Where the gases are heated electrically the acceleration happens thermodynamically like chemical rockets through a nozzle
- Electrostatic thrusters: Propellant gas is positively ionized, and then accelerated through the interaction between ions and electrostatic field
- Electromagnetic thrusters: highly ionized gas called plasma that characterized by its total electric neutrality, this plasma interact with electromagnetic fields, this interaction causes the acceleration and ejection of hot gases
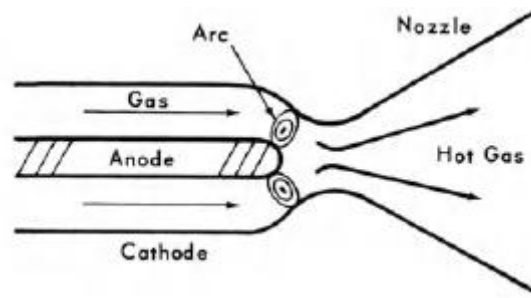
Figure 1-10: Simplified schematic of arc jet engine (an electrothermal thruster). [32]
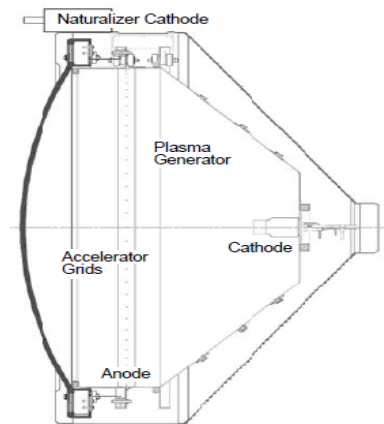
Figure 1-11: Ion thruster schematics (electrostatic thruster). [33]
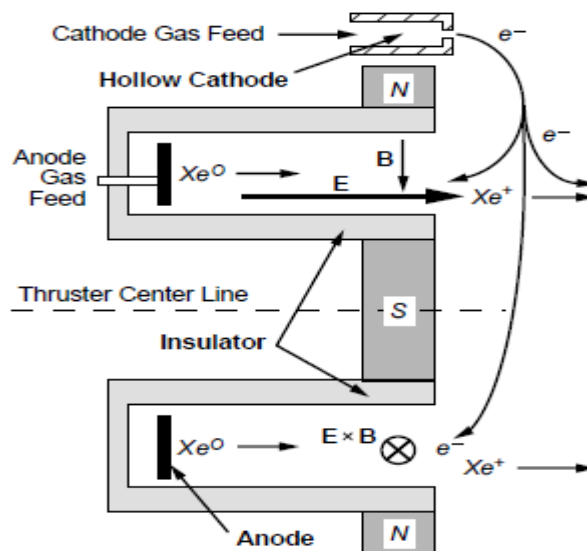
Figure 1-12: Hall thruster (electromagnetic thruster). [33]

ADVANTAGES [34]:

- Electric rockets are safer
- They are more efficient than chemical rockets, because they require less propellant and deliver same effect

- Hot gases are ejected in speeds twenty time faster than other thrusters
- Very high specific impulse
- Force can be applied for long period, months or years.

DISADVANTAGES [34]:

- Can't eject massive amount of propellant
- They can't achieve high velocities in short time, which means in cases of mission that require high acceleration we can't use them.

1.3.6   Nuclear propulsion

This system is similar to liquid propellant systems, the difference is mechanism that gives thrust. Only one propellant is used (generally hydrogen) because of its low molecular weight stoked in a tank, with a feeding system, propellant enters inside reactor, a fission nuclear reaction produces heat, heated propellant passes through a heat exchanger. Hot gases are then ejected through a convergent-divergent nozzle [35,36]. System advantage is that its performance is very high but it is very complex and politically not accepted [36,37].

Table 1-2: Propulsive systems applications. [10]

Function → Type ↓	Launch	Orbit insertion	Orbit manoeuvre	Attitude control
Cold gas			*	*
Monopropellant			*	*
bipropellant	*	*	*	*
Solid	*	*		
Hybrid	*	*	*	
Nuclear		*	*	*
Electric		*	*	

Table 1-3: Satellite propulsive systems performances and energy source. [35,29,31]

Type	Propellant	Energy	I_{sp} / sec
$Cold-Gas$	N_2, NH_3, He	High pressure	$50-75$
$Monoproppellant$	H_2O_2, N_2H_4	exothermic decomposition	$150-225$
$Bipropellant$	$O_2 + kerosene$ $O_2 + H_2$ $N_2O_4 + MMH$ $F_2 + N_2H_4$	chimical	350 450 $300-340$ 425
$Solid$		chemical	$220-300$
$Electric$	N_2, NH_3, N_2H_4, Xe	electric	$200-5000$

1.4   Green propulsion

1.4.1   Green propellant in space propulsion

During years of space propulsion, Hydrazine was the dominant monopropellant in the field, because of its high performance and design simplicity[38].New research done by the European chemical agency in R.E.A.C.H (Registration, Evaluation, Authorization, Restriction of chemicals) classified Hydrazine as chemical substance that we should worry about it, this decision will cause the ban of this propellant in European countries[39].For that reason, people start thinking to use and develop a green propellant which is safe to use, to store, to transport and low toxic. [40]

Many countries start different programs and missions in this field to replace the toxicity and handling difficulty founded in hydrazine, such as, Green Propellant Infusion Mission by NASA, the European projects Pulsed Chemical Rocket with Green High-Performance Propellants and Replacement of hydrazine for orbital and launcher propulsion systems. Since the beginning of green propellant projects, the results were very satisfying in both performance, environment safety, cost and physiochemical properties [41].

Green propellants are classified into three major categories [42]:

- Hydrogen peroxide in aqueuse solution
- Liquid nitrogen oxide monopropellant (an oxidizer salts dissolved in aqueous solutions, called ionic liquids mixed with ionic fuel forming a premixed propellant).
- Energetic ionic liquids

1.4.2   Hydrogen peroxide in space propulsion

Louis Jacques Thenard discovered hydrogen peroxide in July 1818, it was first known as "oxygenated water". Many other scientists did the production of H2O2 but the advantage that made thenard the founder of this substance is that he was the first who defined a procedure of manufacturing [43]. The beginning of hydrogen peroxide commercial production with different available process took place more than 60 years exactly in 1885 [44].

The use of hydrogen peroxide as source of energy for propulsion systems passes through many developments and inventions, in Germany they could produce high concentrations of HTP 80-82% in a period from 1933 to 1936, a man named Walter used these high concentrations and manufactured a submarine turbine and an engine for the plane Heinkel He176, the motor used 80% HTP with liquid permanganate salt as catalysts, after Walter's experiments and inventions a big project was done by Germans in WWII, it was the V-2 rocket that used the same concentrations as Walter's engine and liquid potassium permanganate solutions catalysts[43].

In United Kingdom they were using German's engines, but after 1952, UK started to developed its own HTP/Kerosene aircraft rocket engines [45].UK after that had two significant project with hydrogen peroxide. The first one was the Black knight rocket designed for re-entry studies, it was built in 1955 and used four Gamma engines developed by Armstrong Siddeley Motors, this engine had our thrust chambers using kerosene as fuel and 85% HTP as oxidizer [46,47]. The black knight was not a good satellite launcher, so a second programme was developed which is black arrow rocket with 3 stages, the first stage was eight rocket chambers with two turbopumps to feed engines, mixture ratio between HTP and kerosene was 8.2:1 and the engine delivered 50000 lb of thrust, the second stage was almost the same except it delivered less thrust 15300 lb and had special nozzle for high altitude, the third one was solid engine [48].

In USA they start reaction control system (RCS) programme with the X-vehicles,RCS of space shuttle provide the attitude control and translation through the 3-axis.For example X-15 vehicle, it uses 90% HTP as monopropellant that decomposes with 15silver screen catalyst bed and 1 corrosion resistant screen, the products of the decomposition heated steam and oxygen are exhausted through a nozzle[49,50]

During the 1980s to 1990s the world saw a huge use of hydrazine comparing to H2O2 because at that time work focus on which substance give better performance without taking in consideration toxicity and pollution and also many issues found in HTP like developing a good catalysts were solved with hydrogen[44,43],but after that period till our present day the production and use of hydrogen peroxide for propulsion has seen the light again because of the the good properties and environment safety of this substance which can be resumed in [51]:

- High density
- High oxidizer to fuel ratios
- Storable propellant
- Non-toxic
- Non-reactive with the atmosphere.

1.5   <u>State of art</u>

Satellite technology is currently advancing at a breakneck pace. The progress of satellite technology needs a variety of desired properties in rocket propulsion. Lowering the average transport cost per kilogram of payload is one of the most important goals [52]. to make space more available, it is important to reduce the cost of propulsion systems used for space transportation. This reduction must not affect the safety of the environment, for that reason green propellants satisfy these criteria and also deliver good performance [53].

One of the good solutions is the use of the green propellant High-Test Peroxide, it can be used as monopropellant or as oxidizer for bipropellant systems [54,55].in this section we are going to set different project and research that have used HTP catalytic decomposition for designing and developing propulsive systems.

1. Experimental Validation of a 1-Newton Hydrogen Peroxide Thruster

This work consists on experimental tests done to 1N thruster prototypes that use 87.5% HTP as propellant in order to have a final design with good performances. For all prototypes the inlet pressure varies from 5.5 to 25 bar. The first prototype MK0 used ceria cylindrical pellets catalyst and was tested under atmospheric conditions, results showed bad performance at low pressure inlet due to non-optimized catalysts bed. The second prototype MK1 had some geometry modifications, for this case two catalysts were chosen, MnO_x-coated ceria pellets and platinum coated gamma alumina particles, both catalysts gave almost the same performance except one difference that the platinum didn't have a degradation when scanned with CT scans, for that reason it was chosen for future developments. The MK3 prototype has seen big modifications and it was tested in both vacuum and atmospheric conditions, after tests it was seen that the catalysts beds performed well for both cases without any physical damage of the catalysts. To sum up, for a small or medium size satellite, a 1N HTP would perform much better if we choose the exact catalyst bed model, geometry and study state [56].

Table 1-4: Thruster design parameters. [56]

Variable	MK0	MK1	MK2
Injector pressure drop, bar	2	2	3
Catalysts bed length to diameter ratio	2.5	2	1.34
Nozzle Expansion ratio	167	3	300
Target vacuum specific impulse, s	165	166	172
Design propellant mass flow rate, g/s	0.62	0.61	0.59
Nozzle throat diameter, mm	0.63	0.64	0.63
Injector hole diameter, mm	0.24	0.22	0.2
Catalysts bed diameter, mm	12	12	13
Catalyst bed length	30	24	17.5

2. Development of Hydrogen Peroxide Rockets at Alta S.p.A.: The Past, the Present and the Future.

The work passed through many steps. In the beginning they had to develop an advanced catalytic bed for hydrogen peroxide, activity test performed on different sample catalysts demonstrated that platinum is the most active metal to effectively and rapidly decompose hydrogen peroxide. Four candidate platinum catalysts with various characteristics are selected to be tested on a thruster prototype that operates with 5g/s 90%HTP and to choose the best of them. Tests showed that all catalysts had C^* efficiency higher than 90%. However, the study ends up to release that the LR-III-106 catalyst's bed perform very efficiently and promising in terms of resistance, pressure drop, and catalytic bed lifetime [57].

Table 1-5: Main characteristics of the selected candidate catalysts. [57]

	LR-III-97	LR-III-106	LR-IV-11	CZ-11-600
Catalyst	Pt	Pt	Pt	Pt
Support	$\alpha - Al_2O_3$	$\alpha - Al_2O_3$	$\theta - \alpha - Al_2O_3$	$Ce_{0,6}Zr_{0,4} / Al_2O_3$
Diameter(mm)	0,6	0,6	0,6	0,6
Surface area(m^2/g)	4	4	75	75
Nom. metal load(wt%)	2	1	1	10
SEM metal load(wt%)	35	3	2,5	10

3. Catalytic Ignition of Hydrogen Peroxide for Storable Bipropellant Thrusters.

This work is in the aim of testing a bipropellant combustion thruster auto ignition between 87.5% HTP as an oxidizer and n-decan as fuel. The idea was is to see if the products of hydrogen peroxide decomposition will be able to auto ignite the fuel while both injected in combustion chamber, to check this they first did an experience on real 87;5%HTP decomposition using MnO_x active phase catalyst in pellets form, the test took place in catalyst decomposition chamber of the thruster, the results shows that the maximum temperature achieved at the exit o chamber is 710°C,the obtained results proved that the decomposition was efficient, after this part they had to check and experience if the auto ignition will happen, the results led to the success of tests and the interaction of the two fluids(oxidizer and fuel)with the auto ignition and the stabilisation of the flame. The conclusion from this work is that the products of HTP catalytic decomposition were very efficient in playing role of an oxidizer to be used in bipropellant system and auto ignite the n-decan fuel [58].
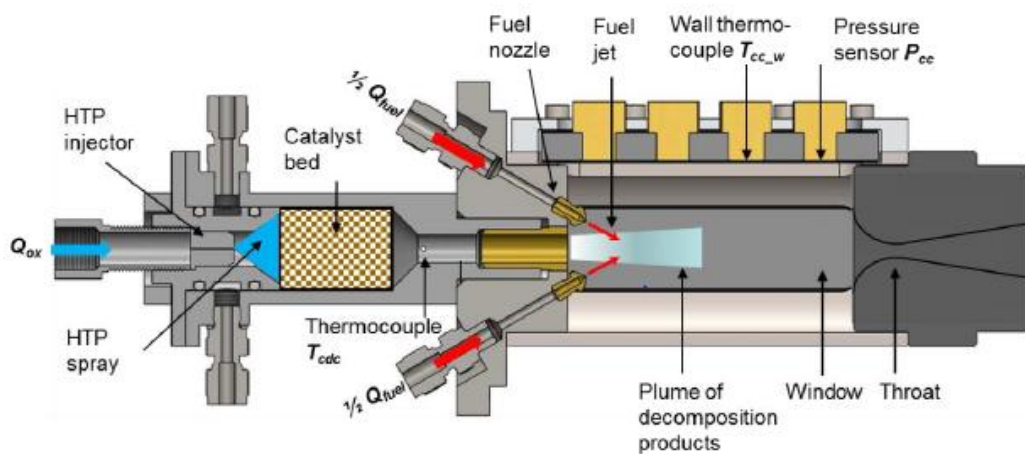
Figure 1-13: Assembly of the catalytic decomposition chamber on ACSEL optical combustor. [58]

CHAPTER 2

Mathematical Modelisation

2.1 Rocket Fundamentals:

Rocket propulsion's basic principles are essentially based on mechanics, thermodynamics, and chemistry. Propulsion is achieved by applying a force to a vehicle or that accelerating the vehicle or, alternatively, maintaining a given velocity against a resisting force. This propulsive force is obtained by ejecting propellant at high velocity.

2.2 Study Hypothesis

Hypothesis should be taken into consideration for our study, the first case study is inviscid -isentropic-ideal gas, and second case study for viscous flow. Hypothesis depend on the case study where assumptions are taken into consideration differently. The result would be achievable through three major stages MATLAB® program in Thermochemistry, Theoretical Rocket Performance, and Preliminary Thruster Design

Assumptions to the rocket performance stage of our study are summarized below:

1. The work is only considered by pressure forces inlet of the combustion chamber
2. Perfect gas law
3. Frozen flow - Quasi 1-D flow model
4. Inviscid flow
5. No appreciable friction of boundary effect
6. No shock waves
7. Direct reaction, we assume that the decomposition mechanism is described by a single step where HTP is directly converted into its products.
8. Purities within the reaction,

Assumptions to the thermochemical portion of the study are summarized as:

1. Heat Transfer adiabatic system with Adiabatic chamber system Q = 0, the system can be adiabatic using a multi-layer insulation, this will stop the heat exchange between system and external environment
2. Isentropic nozzle expansion
3. Chemical Reactants – the chemical reaction did not account for reactants beyond hydrogen peroxide and water.
4. No contaminate are present within the propellant, feedsystem, or chamber.

5. Reaction Products – the products of dissociation were gaseous oxygen and water. In a more rigorous sense, negligible traces of additional compounds or elements would be present.

6. At high concentrations (> 87.5%) of hydrogen peroxide aqueous solutions, the dissociation would also result in a negligible amount of OH, and other gaseous products.

7. During the reaction through the catalyst, the entirety of hydrogen peroxide dissociates

Assumptions to the preliminary thruster design stage of the study for the catalyst pack. The catalyst is paramount to hydrogen peroxide thruster design. For that, we should seek the following seven items:

1. High product yield per unit time
2. Minimal pressure drop
3. Low temperature engine starts, pulsed or steady state
4. Structurally capable for all loads
5. Maintains phase without melting of fusing
6. High total throughput capability
7. Maintains consistent performance over life

2.3 **Rocket equations**

To introduce principle of propulsion, we have to redress to the Newtonian principle of action and reaction, which states that for every action (force) in nature there is an equal, and opposite reaction. At the same time, it states that in an isolated system, the sum of the forces exerted on a mobile at zero speed or at constant speed is equal to zero. [59,87]

Indeed, for an isolated system such as a rocket in space to model this system, space will be considered as a pseudo-isolated system, and we will neglect the external forces such as the gravitational forces of the surrounding stars, the sum of the (internal) forces exerted on the different parts of the system is zero.

$$\sum \vec{F}_{ext} = 0 \tag{2-1}$$

Then consider the structure of the rocket on the one hand, the ejected gases on the other hand. We can therefore apply the fundamental principle of dynamics as well to the structure as to the ejected gases:

$$\sum \vec{F}_{ext} = m\vec{a} \tag{2-2}$$

23

Or

Where $\vec{p}$ is the quantity of movement $\qquad \sum \vec{F}_{ext} = \dfrac{\overrightarrow{dp}}{dt}$ (2-3)

2.3.1 Tsiolkovsky's Rocket Equation

From Eq. 2-3, we can say for n parties that:

$$\sum \frac{\overrightarrow{dp_n}}{dt} = 0 \qquad (2\text{-}4)$$

Which means

$$\sum \vec{P}(t)n = constante \qquad (2\text{-}5)$$

The principle of propulsion is expressed through the conservation of momentum. [60]

If we consider rocket with initial mass **m** and velocity **V,** and a small part of mass **dm** has injected with a relative velocity of rocket V_2 or V_e :
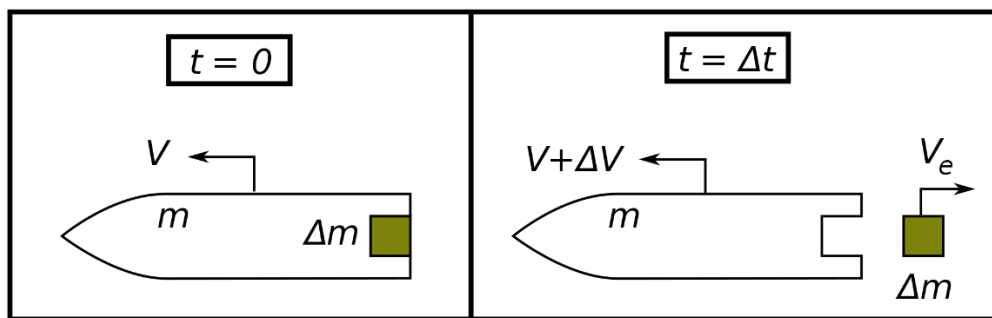
Figure 2-1: Principle of conservation of momentum for a spacecraft during the ejection of propellant gas. [61]

for instant t:

$$p = mV \qquad (2\text{-}6)$$

At the instant $t + dt$, at the speed $V + dV$, therefore:

$$mV = (m - dm)(V + dV) + dm(V + dV + V_e) \qquad (2\text{-}7)$$

we get:

$$mdV = -V_e dm \qquad (2\text{-}8)$$

dividing by **dt**:

$$-\frac{dm}{dt} V_e = m \frac{dV}{dt} \qquad (2\text{-}9)$$

On the left side we got the decrease rate of rocket mass, multiply it by the exit velocity V_e, on the other side we have the mass multiplied by the acceleration, where we can conclude the Second low of Newton, and we get:

$$\vec{dV} = -\vec{V_e}\frac{dm}{m} \tag{2-10}$$

After integration and taking $V_e = constant$

$$\int_{V_i}^{V_f}\vec{dV} = -\vec{V_e}\int_{m_{int}}^{m_f}\frac{dm}{m} \tag{2-11}$$

m_i initial mass

m_f final mass

$$V_f - V_i = V_e \ln\left(\frac{m_{int}}{m_f}\right) = g.I_{sp}\ln\left(\frac{m_{int}}{m_f}\right) \tag{2-12}$$

If we consider the gravity, we get:

$$\Delta V = V_e \ln\left(\frac{m_{int}}{m_f}\right) + g\cos(\theta)t \tag{2-13}$$

t: period of acceleration

To calculate mass propellent we derive it from the previous equation and we get:

$$m_p = m_{int}\left(1 - e^{-\frac{\Delta V}{g.I_{sp}}}\right) \tag{2-14}$$
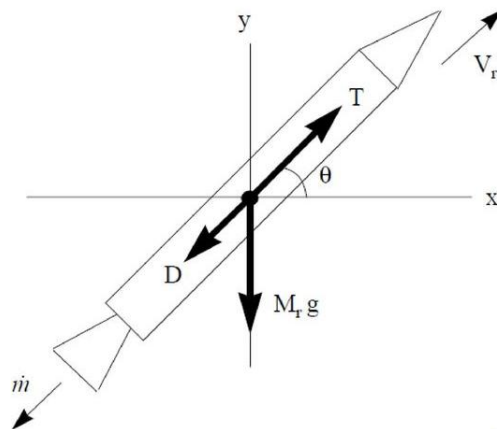
Figure 2-2: Propulsion principle. [62]

2.3.2 Thrust

The thrust of a rocket is the reaction experienced by its structure due to the ejection of high-velocity matter. Momentum is a vector quantity and is defined as the product of mass times velocity. All ship propellers and oars generate their forward push at the expense of the momentum of the water or air masses, which are accelerated towards the rear. Rocket propulsion differs from these devices primarily in the relative magnitude of the accelerated masses and velocities. In rocket propulsion relatively small masses are involved which are carried within the vehicle and ejected at high velocities [63].

Deriving from the equation of Newton, we find:

$$F = \frac{dm}{dt}V_e = \dot{m}V_e = \frac{\dot{w}}{g_0}V_e \tag{2-15}$$

This force represents the total propulsion force when the nozzle exit pressure equals the ambient pressure. Because of a fixed nozzle geometry and changes in ambient pressure due to variations in altitude, there can be an imbalance of the external environment or atmospheric pressure p_a and the local pressure p_e of the hot gas jet at the exit plane of the nozzle. Thus, for a steadily operating rocket propulsion system moving through a homogeneous atmosphere, the total thrust is equal to

$$F = \dot{m}V_e + (p_e - p_a)A_e \tag{2-16}$$

The first term is the *momentum thrust* represented by the product of the propellant mass flow rate and its exhaust velocity relative to the vehicle. The second term represents the *pressure thrust* consisting of the product of the cross-sectional area at the nozzle exit A_e
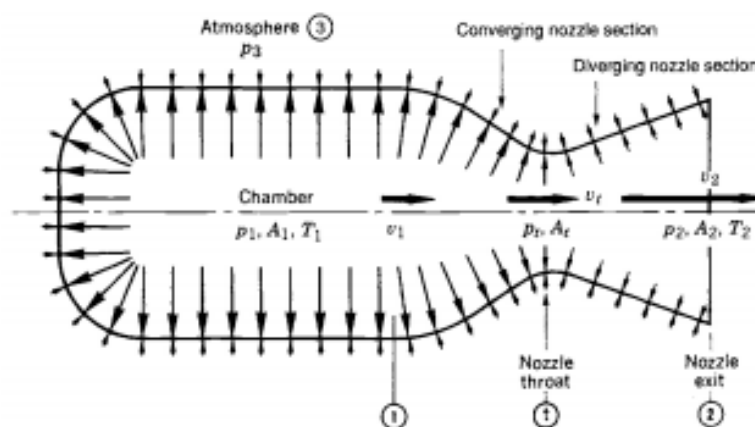
Figure 2-3: Pressure distribution inside the thruster.

When the ambient atmosphere pressure is equal to the exhaust pressure, the pressure term is zero and the thrust is the same as in Eq.2-16. In the vacuum of space $p_a = 0$ and the thrust becomes

$$F = \dot{m}V_e + p_e A_e \tag{2-17}$$

Eq.2-17 shows that the thrust of a rocket unit is independent of the flight velocity. Because changes in ambient pressure affect the pressure thrust, there is a variation of the rocket thrust with altitude.

2.3.3 Specific Impulse

The specific impulse I_s is the total impulse per unit weight of propellant. It is an important figure of merit of the performance of a rocket propulsion system. A higher number means better performance. If the total mass flow rate of propellant is $\dot{m}$ and the standard acceleration of gravity at sea level g_0 is 9.8066 m/s² then

$$I_s = \frac{\int_0^t F \, dt}{g_0 \int \dot{m} \, dt} \tag{2-18}$$

This equation gives a time-averaged specific impulse value for any rocket propulsion system, particularly where the thrust varies with time. During transient conditions (during start or the thrust buildup period, the shutdown period, or during a change of flow or thrust levels) values of I_s can be obtained by integration or by determining average values for F and $\dot{m}$ for short time intervals. [64]

The *total impulse* I_t is the thrust force F (which can vary with time) integrated over the burning time t.

$$I_t = \int_0^t F \, dt \tag{2-19}$$

For constant thrust and negligible start and stop transients this reduces to

$$I_t = Ft \tag{2-20}$$

For constant thrust and propellant flow this Eq.2-18 can be simplified; m_p is the total effective propellant mass.

$$I_s = \frac{I_t}{m_p g_0} = \frac{I_t}{w} = \frac{F}{\dot{m} g_0} = \frac{F}{\dot{w}} \tag{2-21}$$

The product $m_p g_0$ is the total effective propellant weight w and the weight flow rate is $\dot{w}$

2.3.4 Effective Exhaust Velocity

In a rocket nozzle, the actual exhaust velocity is not uniform over the entire exit cross-section and does not represent the entire thrust magnitude. The velocity profile is difficult to measure accurately. For convenience, a uniform axial velocity c is assumed which allows a one-dimensional description of the problem. This *effective exhaust velocity c* is the average equivalent velocity at which propellant is ejected from the vehicle. Exhaust velocity applies to all rockets or spacecraft that thermodynamically expand hot gas in a nozzle and, indeed, to all mass expulsion systems.[64]

$$c = \frac{I_s}{g_0} = \frac{F}{\dot{m}}$$
(2-22)

From Eq. 2-16 and for constant propellant mass flow this can be modified to

$$c = V_e + (p_e - p_a)A_e/\dot{m}$$
(2-23)

As can be seen that c can be determined from thrust and propellant flow measurements

2.3.5 Exit velocity

We use the first principle of thermodynamic for the gas injected from nozzle

$$\Delta E_c + \Delta E_p + \Delta U = Q + W$$
(2-24)

We take P pressure, T temperature, and Vc gas velocity in the combustion chamber

In addition, Te, Pe, Ve the same variables but at the exit area, to simplify the calculation we consider the hypothesis considered at the beginning of the chapter.

Then:

$$\Delta E_c + \Delta U = W_{pressure\ forces}$$
(2-25)

Which give:

$$\Delta E_c + \Delta U + \Delta PV = 0$$
(2-26)

$$\Delta E_c + \Delta H = 0 \quad \text{(Consider P = const)}$$
(2-27)

Deriving this equation by using the previous assumption:

$$V_e = \sqrt{\frac{2\gamma}{\gamma-1}RT_c\left[1 - \left(\frac{P_e}{P_c}\right)^{\frac{\gamma-1}{\gamma}}\right]}$$
(2-28)

2.3.6 Hugoniot law

For isentropic flow inside convergent divergent nozzle, Hugoniot had determined the relation that shows how the velocity change when changing the section area for subsonic and supersonic flows using continuity, Bernoulli and speed of sound equations. [65]

(continuity)
$$\frac{d\varphi}{\varphi} + \frac{ds}{s} + \frac{dv}{v} = 0 \qquad\qquad (2\text{-}29)$$

(Bernoulli)
$$vdv + \frac{dp}{\varphi} = 0 \qquad\qquad (2\text{-}30)$$

(speed of sound)
$$a^2 = \frac{dp}{d\varphi} \qquad\qquad (2\text{-}31)$$

From (2-30) and (2-31) we can write

$$\frac{d\varphi}{\varphi} = \frac{d\varphi}{dp}.\frac{dp}{\varphi} = \frac{1}{a^2}(-vdv) \qquad\qquad (2\text{-}32)$$

We can then insert (2-32) in (2-29), continuity equation will become

$$\frac{ds}{s} = -\frac{dv}{v}\left(1 - \frac{v^2}{a^2}\right) \qquad\qquad (2\text{-}33)$$

We finally can find Hugoniot theorem written as:

$$\frac{ds}{s} = -\frac{dv}{v}(1\text{-}M^2) \qquad\qquad (2\text{-}34)$$

- For M < 1, subsonic flow, velocity is inversely proportional to section area.
- For M > 1, supersonic flow, velocity is proportional to section area

2.4 <u>Components of Spacecraft's propulsion systems</u>

2.4.1 General description of rocket engine

In general, a space propulsion engine is made up of several large subassemblies:

1. Combustion chamber
2. Propulsive chamber
3. Injection system
4. storage tanks
5. Nozzle
6. Gas distributors
7. Throttles (hydraulic, high-temperature, two-mode of cam type)

8. valves (shut-off, safety, diaphragm, stop, check, electric, electrohydraulic, pyro and electric pyro valves)

9. Switches

10. regulators (of pressure, pressure drop, fuel flow rate);

11. Pressure drops stabilizers

These subassemblies have to be considered while designing a rocket engine, some types of engines use all of them however some others doesn't need to consider all of them

2.5 <u>Hydrogen Peroxide and its Catalysis</u>

There is a wide range of catalysts that can be used to decompose hydrogen peroxide but only a few that provide the performance required by the space industry. Catalysts can be divided into two main categories, namely homogenous (in the same phase as HTP, liquid) and heterogeneous (in a different phase to HTP, normally solid). [66]

Although thermal decomposition can dominate at high temperatures in monopropellant thrusters' catalysts are required to initiate the reaction. , the catalyst reduces the potential energy barrier over which the reactants must pass to form products. This lowering in energy barrier is shown in Figure 2.4, reducing the activation energy required to initiate the decomposition, it is known that the rate of decomposition is highly dependent on temperature, surface area and the concentration of reactant(s), by decreasing the activating Gibbs free energy. It is important to note that the catalyst does not modify the total Gibbs free energy released the reaction that is a function of state of the system and therefore has no effect on the equilibrium constant. [67]
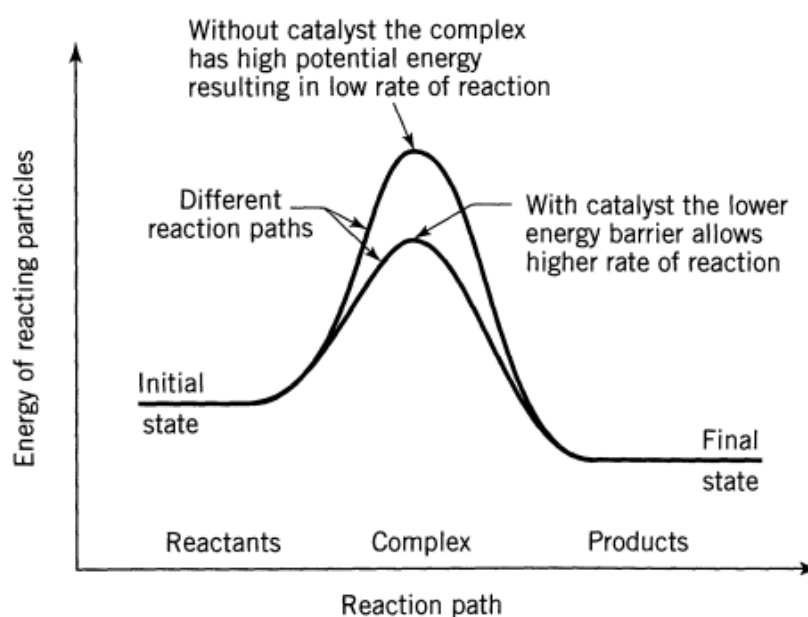
Figure 2-4: The use of catalyst. [67]

In addition to the performance parameters described, two design parameters are also often quoted. These are the catalyst bed loading and the wetted area loading. These are used along with the length-to-diameter ratio, L/D, to dimensionalise the catalyst bed. The catalyst bed loading or cross-sectional area catalyst bed loading (CBLCSA) is defined as the mass flow rate of propellant per unit cross sectional area (CSA):

$$CBL_{CSA} = \frac{\dot{m}_{prop}}{Catalyst\ bed\ CSA}$$ (2-35)

Meanwhile the catalyst bed wetted area loading (CBLWSA) is defined as the mass flow rate of propellant per unit wetted surface area (WSA) of catalyst:

$$CBL_{wSA} = \frac{\dot{m}_{prop}}{Catalyst\ bed\ WSA}$$ (2-36)

It will be seen later in this thesis that a low value of either of these two terms increases the catalyst bed life by reducing the quantity of peroxide each unit area of catalyst has to decompose. However, this leads to a large thruster increasing mass and reducing performance, the choice of catalyst can rely on some criteria that combine between the selectivity and life span:

1. High surface area to facilitate the decomposition of hydrogen peroxide in the shortest length. This is important for minimizing catalyst bed length.
2. High thermal shock resistance to reduce the possibility of the substrate failing due to the thermal loads that take place within the support. This is facilitated by high thermal conductivity and a thermal coefficient of expansion similar to that of the active phase deposited on it.
3. A chemically inert support that does not react with the peroxide in such a way as to compromise the carrier itself or have a detrimental effect on the catalytic properties of the active phase.
4. A high mechanical strength that is able to resist damage caused by the highly energetic and turbulent flow. This can be assessed using the physical properties of the support such as ultimate tensile strength or tested experimentally within a representative bed. In the case of ceramic pellets high strength is also needed since the pellets can vibrate and impact each other. [68]

A catalytic decomposition process can be subdivided into 7 steps [69] as depicted in Figure 2.5:

1. External diffusion - diffusion of the reactant from the bulk liquid or gas phase through the boundary layer to the outside of the catalyst material.

2. Internal diffusion - diffusion of the reactant from the outside material into the catalyst material

3. Adsorption

4. Actual decomposition

5. Desorption

6. Internal diffusion - diffusion of the products from the catalyst material to the outside

7. External diffusion - diffusion of the product through the boundary layer to the bulk liquid or gas phase liquid or gas phase
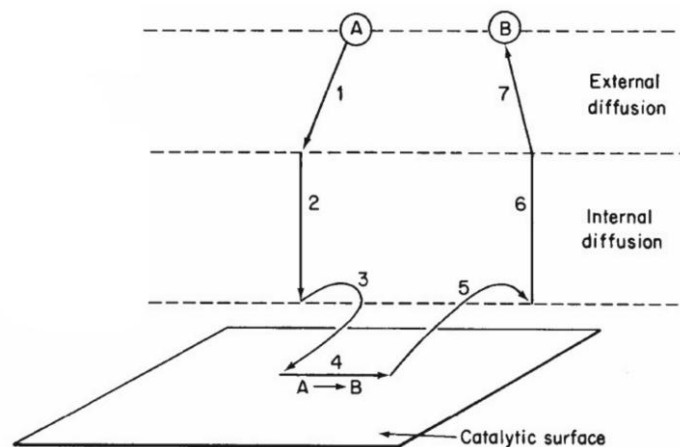
Figure 2-5: Steps in a heterogeneous catalytic reaction. [70]

However, an important factor that will influence the catalytic decomposition rate of HTP is how well the surface can be wetted by the liquid HTP. When a liquid is dropped on a surface with poor wettability properties the droplet will sustain its form on the surface, with a given angle, dependent upon the surface characteristics as seen in Figure 2.6. When the fluid flow has transition into a region where the liquid is only present in the form of bubbles, the wettability would then determine the contact area between the liquid and the surface.

Figure 2-6: Figure of different wetting properties of different fluids with increasing wetting from left to right. [71]

2.5.1 Different types of catalyst

Ceramic supported catalyst

They have shown good promise in decomposing high concentration hydrogen peroxide (>90%) due to their high melting temperature. They can also have an exceptionally high surface area, exceeding 200m2/g, with good thermal shock resistance. They can be found primarily in two different forms; monoliths and pellets. There are various advantages and disadvantages to each design. [66]

- Monoliths are usually extruded, single ceramic catalyst supports containing internal channels through which the HTP flows and is decomposed. The advantages stated by Kappenstein [72] include; low pressure drop, better thermal shock and attrition resistance, uniform flow distribution and high surface-to-volume ratio.

- Ceramic pellets can move relative to each other within the bed leading to mechanical abrasion and possible structural failure. Structural failure leads to the formation of voids which act to further exacerbate the problem

Figure 2-7: Ceramic pellets based. [73]
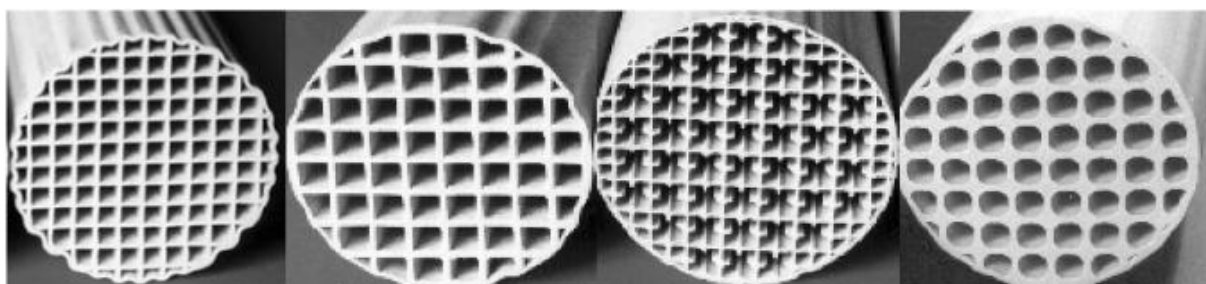
Figure 2-8: Monolith catalyst ceramic based. [74]

Metallic Gauzes

Metal gauze catalysts have a significant heritage for decomposing hydrogen peroxide. Gauzes are normally defined by two parameters; wire size, hydraulic diameter, and mesh number. The mesh number relates to the size of the gaps between the wires. The effective surface area is much less than that of ceramic supports.

Reporting that the gauze catalysts were made in a deposit a smooth layer of silver onto a nickel support where the gauze was activated with samarium nitrate, Significant work was also being conducted by NASA with the main focus being on decomposing 90-98% HTP. Wanhainen [75] investigated the effect of temperature on thrust build-up for two different types of metal gauze catalyst. ACS thrusters, which require extended operation. Two main causes were identified that limited catalyst bed life of gauz catalyst. The first was

- Catalyst poisoning; this was due to chlorides, normally chromium chloride found within the HTP.
- The second was due to the sodium stannate used to stabilize the HTP. This would strip away a significant quantity of silver from the gauze. [66]
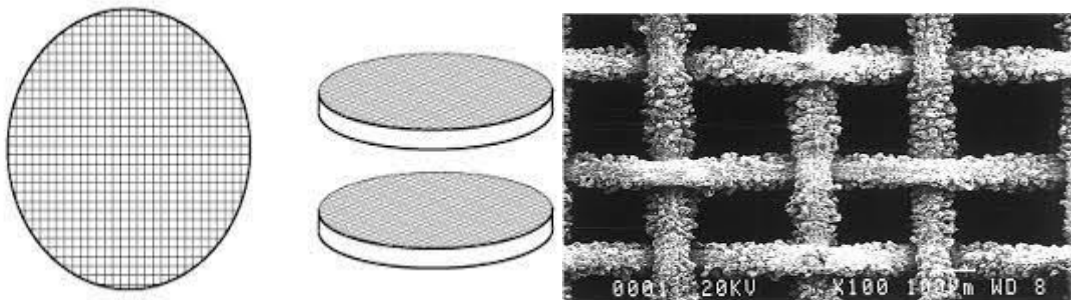
Figure 2-9: Gauze support catalyst. [76]

Metallic Foam

Metallic foams have not been used that much for the decomposition of hydrogen peroxide; however, impregnated or coated ceramic foams are much more common. Metallic foams have several advantages ;

The surface area is much greater than gauzes, miss of vibration and impact phenomena between each other like pellets and if catalytically active metals are used, there is no need to attach a separate active phase. Moreover, ceramic foams have a greater surface area than metal foams when used in combination with a wash coat. [66]

One of the drawbacks of foams relates to the significant pressure drop those results from the unordered structure. Although the structure facilitates intimate contact between HTP and

catalyst, the path the hydrogen peroxide takes is tortuous; therefore, the pressure required to force the flow through the bed tends to be greater than for pellets and gauzes. [66]
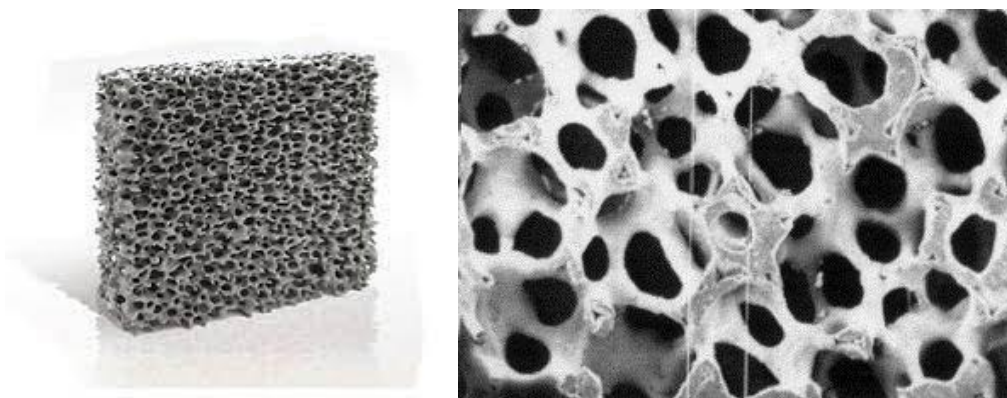
Figure 2-10: Foam support catalyst [77]

2.5.2 Catalyst Deactivation

An important factor that can reduce the decomposition rate in a catalyst is the extent of degradation over time. Several different processes are involved, and the traditional classifications of degradations are sintering or aging, fouling and poisoning [69].

- **Sintering**

Sintering is a thermal degradation of the catalyst due to prolonged exposure to gases with high temperature [68]. When the temperature inside the catalyst exceeds or is operating in a region close to the melting point of the solid, small sections of the catalyst will melt together. The new formed geometry will thereby have a smaller surface area than its original form as separated mesh structures. This will in turn decrease the available surface for reaction. When designing a catalyst, it is important to select a catalytic material that has the proper reaction characteristics in addition to a large enough melting point to prohibit sintering degradation.

- **Fouling**

Fouling is a mechanical degradation of the catalyst and occurs when unwanted material is physically deposited on the surface, which prevents further catalytic reaction. In its advanced stages it may result in disintegration of catalyst particles and plugging of the catalyst voids. This type of degradation is most often seen in catalyst involved with hydrocarbon reactions, where coke is formed on the surface. In the process described in this thesis these types of molecules are not involved, and this effect is assumed to be negligible. [78]

- **Poisoning**

Poisoning is a chemcial degradation due to strong chemisorption of species on catalytic sites. The poisoning molecules become irreversibly chemisorbed to active sites, thereby reducing the number of sites available for the main reaction. In addition to physically blocking of adsorption

sites, adsorbed poisons may induce changes in the electronic or geometric structure of the surface. The poisoning molecule, P, may be a reactant and/or a product in the main reaction or an impurity that has entered into the feed stream. Whether a species acts as a poison depends upon its adsorption strength relative to the other species competing for catalytic sites. [78]

2.5.3   The use of a monopropellant thruster

The use of a monopropellant thruster respects a set of regulations to maintain the best of it:

- **Handling**

simple monopropellant liquid thruster concept is shown in Figure 2.11. It is composed basically by three main components: the pressurization tank, the propellant tank and the thrust chamber. The tanks are connected via pipeline and a pressure regulator, while a firing valve separates the propellant from the thrust chamber. This last one component is made by:

1. An injector to get an efficient propellant distribution.
2. A combustion chamber filled with the catalytic material to decompose the propellant.
3. The convergent-divergent nozzle to accelerate the high temperature products of the reaction and generate thrust
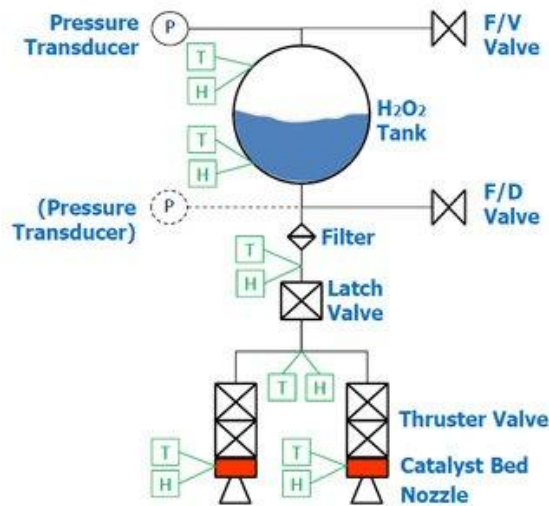
Figure 2-11: H_2O_2 Monopropellant system architecture. [79]

- **Performance**

Currently, hydrogen peroxide thrusters are designed for very low intensity thrusts (up to a few hundred N). [80] This type of propulsion systems can currently satisfy many applications in the space field such as:

1. Orbital changes;
2. Orbital maintenance;
3. End of life disposal;
4. Desaturation of Reaction Wheels;

In order to satisfy the modern (new) space economy, the features that a monopropellant thruster should have are:

1. Low cost;
2. Performance;
3. Environmental friendliness;
4. Reliability;
5. Controllability;
6. Customization capability.

When the mission is defined and the requirements in terms of accuracy and authority are established, the thruster specifications that lead the design procedure are:

1. The total operating life;
2. The number of cycles that the catalytic bed has to withstand;
3. The minimum impulse bit, which is related to the accuracy of the control and is influenced by the engine transient response;
4. The system specific impulse which is related to the total propellant mass

Hydrogen peroxide may be used effectively as a rocket propellant above 70% concentration [81]. A more common rocket propellant grade, high-test hydrogen peroxide (HTP), extends above 85% concentration [82]. The higher concentration the higher performance and chamber temperature is giving. However, as the concentration increases, the dangers of storage and handling increase as well as the difficulty of manufacturing [81].

- **Analysis Modelling Method**

The first step to the development of the computer program was the generation of a flow chart. The steps on Figure 2.12 support the purpose of the master's project, through three major stages from Thermochemistry, Theoretical Rocket Performance, to Preliminary Thruster Design.
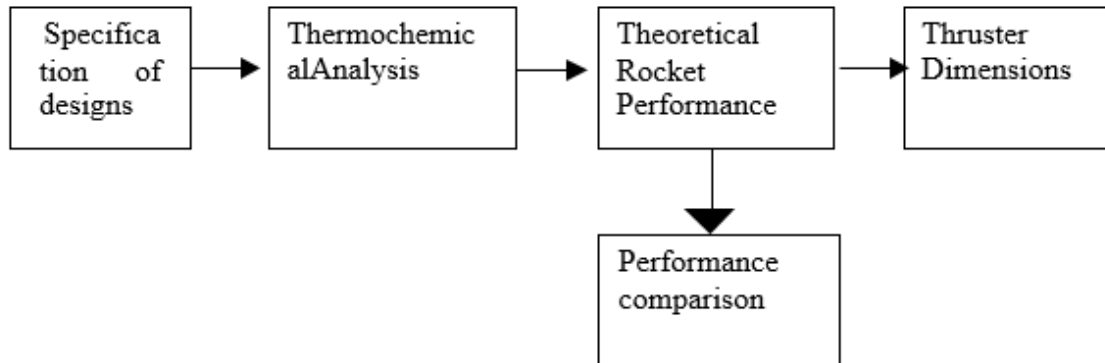
Figure 2-12: Chemical Rocket Preliminary Design Flow Chart

2.6 Specification of design

A mathematical model initially supplies the main characteristics for the design of a monopropellant thruster, which yield to the use of one-dimensional flow equations. Simplifications included the assumption that the flow is isentropic and the effect, and the mixture of oxygen vapor and water produced only by the decomposition of hydrogen peroxide and behaves like an ideal gas. [83]

The flow field is fully described when the following variables are known in all points:

To describe the flow field four equations (three Navier-Stockes equations plus the equation of state) expressed as a function of the last four variables considered. These equations are derived from the following principles

The principle of conservation of mass which gives the continuity equation:

$$\dot{m} = \rho . \text{V} . \text{A} = \frac{V.A}{\tilde{V}} = constante \qquad (2\text{-}37)$$

$\dot{m}$ mass flow ($kg.s^{-1}$) through a section A

The principle of conservation of momentum which gives the Euler equation:

$$\text{V} . \text{dV} + \frac{\text{dp}}{\rho} = 0 \qquad (2\text{-}38)$$

Or

$$\text{V} . \text{dV} + \tilde{V} . dP = 0 \qquad (2\text{-}39)$$

The principle of conservation of energy which gives the Barré de Saint-Venant equation:

$$\frac{V^2}{2} + C_p dt = Cst \qquad (2\text{-}40)$$

Perfect gas law:

$$\frac{P}{\rho} = rT = P.\tilde{V} \qquad (2\text{-}41)$$

r : Specific constant of ideal gases , where $r = \check{R}/M$ [j/kg.k]

$\check{R}$: perfect gas constant = 8.314 [j/k.mol]

M: the effective molecular weight of the decomposition products [kg/mol]

2.6.1   Thermochemistry Analysis

Hydrogen peroxide decomposes in one of two ways; either thermally or catalytically. For our case study the decomposition is considered catalytically, it was assumed that the reaction for the dissociation of hydrogen peroxide was stoichiometric. According to [84], the products of dissociation are water vapor and oxygen.

$$H_2O_2 \Rightarrow H_2O + \tfrac{1}{2}O_2 \qquad (1)$$

The stoichiometric assumption was enhanced to better describe the concentration of hydrogen peroxide (by weight).

$$a\ H_2O_2\ (liquid) + b\ H_2O\ (liquid) \Rightarrow c\ H_2O\ (vapor) + d\ O_2\ (gas) \qquad (2)$$
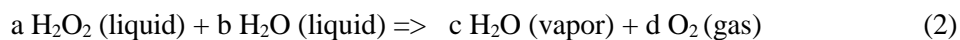
The mole values of the products (c, d) and reactants (a, b) were calculated based upon molecular weight and the given concentration by weight.

We have:

$$\text{Mass } H_2O(l) = b * M_b \qquad (2\text{-}42a)$$

For the numerical study of the propulsion system, it is assumed that b = 1 mol; We have:

$$\text{Mass } H_2O_2(l) = \left[\frac{concentration}{1-concentration}\right] * \text{Mass } H_2O(l) \qquad (2\text{-}42b)$$

With

$$a = \left[\frac{\text{Mass}(H_2O_2)}{M(H_2O_2)}\right] \qquad (2\text{-}42c)$$

$$c = a + b \qquad (2\text{-}42d)$$

$$d = \left[\frac{a*2+b-c}{2}\right] \qquad (2\text{-}42e)$$

When all the standard enthalpy values of formation of the species in a chemical reaction are known under standard conditions, the following equation is used to calculate $\Delta_R H$. [85]

$$\Delta_R H = [\{c * \Delta_f H(H_2O(v)) + d * \Delta_f H(O_2(g))\} - \{a * \Delta_f H(H_2O_2(l)) + b * \Delta_f H(H_2O(l))\}]/a \qquad (2\text{-}43)$$

In general form:

$$\Delta_R H = \sum v \Delta_f H(products) - \sum v \Delta_f H(reactif) \qquad (2\text{-}44)$$

The value of $\Delta_R H$ corresponds to the energy available to do a work, if in our reaction for a value of $\Delta_R H = -27.60$ kj, we can make a maximum of 27.60 kj of heat H. [68]

$$-\Delta_R H = Q_{disp} \qquad (2\text{-}45)$$

To calculate the chamber temperature from this solution we have the Triangle law

$$T_C = \left(\frac{Q_{disp}-Q_X}{Q_{X+1}-Q_X}\right) * (T_{X+1} - T_X) + T_X \qquad (2\text{-}46)$$

To find the enthalpy of the product for Eqt.2-43 we used Chemical Equilibrium Applications (**CEA**) The **CEA program by NASA** or **JANAF table** which are used to calculates chemical equilibrium product concentrations from any set of reactants and determines thermodynamic and transport properties for the product mixture

```
THERMODYNAMIC FUNCTIONS CALCULATED FROM COEFFICIENTS FOR H2O2
```

T deg-K	Cp cal/mol-K	H-H298 kcal/mol	S cal/mol-K	-(G-H298)/T cal/mol-K	H kcal/mol	delta Hf kcal/mol	log K
0	0.	-2.667	0.	INFINITE	-35.143	-31.045	INFINITE
300	10.148	0.019	56.116	56.053	-32.457	-32.483	18.3668
400	11.103	1.081	59.166	56.463	-31.395	-32.826	12.4217
500	11.998	2.237	61.742	57.267	-30.239	-33.099	8.8203
600	12.767	3.477	63.999	58.205	-29.000	-33.315	6.4014
700	13.417	4.787	66.017	59.179	-27.690	-33.485	4.6635
800	13.977	6.157	67.846	60.150	-26.319	-33.618	3.3542
900	14.475	7.580	69.522	61.100	-24.896	-33.720	2.3322
1000	14.921	9.050	71.071	62.020	-23.426	-33.795	1.5124
1100	15.322	10.563	72.512	62.909	-21.913	-33.848	0.8404
1200	15.690	12.114	73.861	63.766	-20.363	-33.882	0.2797
1300	16.026	13.700	75.130	64.592	-18.776	-33.899	-0.1951
1400	16.330	15.318	76.329	65.388	-17.158	-33.901	-0.6021
1500	16.606	16.965	77.465	66.156	-15.511	-33.891	-0.9549
1600	16.856	18.638	78.545	66.897	-13.838	-33.872	-1.2634
1700	17.083	20.335	79.574	67.612	-12.141	-33.845	-1.5355
1800	17.290	22.054	80.556	68.304	-10.422	-33.811	-1.7771
1900	17.480	23.793	81.496	68.974	-8.684	-33.773	-1.9930
2000	17.653	25.549	82.398	69.623	-6.927	-33.732	-2.1871

Figure 2-13: CEA Thermodynamic properties for H2O2.

```
THERMODYNAMIC FUNCTIONS CALCULATED FROM COEFFICIENTS FOR O2
```

T deg-K	Cp cal/mol-K	H-H298 kcal/mol	S cal/mol-K	-(G-H298)/T cal/mol-K	H kcal/mol	delta Hf kcal/mol	log K
0	0.	-2.075	0.	INFINITE	-2.075	0	INFINITE
300	7.024	0.013	49.075	49.032	0.013	0	0
400	7.198	0.723	51.117	49.309	0.723	0	0
500	7.431	1.454	52.748	49.839	1.454	0	0
600	7.670	2.210	54.124	50.442	2.210	0	0
700	7.885	2.988	55.323	51.055	2.988	0	0
800	8.065	3.785	56.388	51.656	3.785	0	0
900	8.213	4.600	57.347	52.236	4.600	0	0
1000	8.337	5.427	58.219	52.792	5.427	0	0
1100	8.445	6.266	59.019	53.322	6.266	0	0
1200	8.531	7.115	59.757	53.828	7.115	0	0
1300	8.606	7.972	60.443	54.311	7.972	0	0
1400	8.673	8.836	61.083	54.772	8.836	0	0
1500	8.736	9.707	61.684	55.213	9.707	0	0
1600	8.797	10.584	62.250	55.635	10.584	0	0
1700	8.857	11.466	62.785	56.040	11.466	0	0
1800	8.915	12.355	63.293	56.429	12.355	0	0
1900	8.973	13.249	63.776	56.803	13.249	0	0
2000	9.031	14.150	64.238	57.163	14.150	0	0

Figure 2-14: CEA Thermodynamic properties for O2.

2.6.2 Chemical proprieties for the product

- Average Molecular weight of products:

$$M_{avg} = \frac{\sum n_p M_p}{\sum n_p} \tag{2-47}$$

With

$$\sum n_p M_p = c * M_c + d * M_d \tag{2-48}$$

$$\sum n_p = c + d \tag{2-49}$$

M_p: molaire mass kg/mol

n_p : number of moles of product

- Average Specific Heat

$$Cp_{avg} = \frac{\sum n_p Cp_p}{\sum n_p} \tag{2-50}$$

With

$$\sum n_p C_{pp} = c * C_c + d * C_d \tag{2-51}$$

C_{pp} specific heat for the product

- Specific Heat Ratio

From the ideal gas state equation, r is the ideal gas constant is also expressed as a function of the specific heats at constant pressure Cp and at constant volume Cv where r = Cp - Cv (Mayer's relation). We denote by γ the ratio of specific heats, also called isentropic exponent defined as being:

$$\gamma = \frac{C_p}{C_V} \tag{2-52}$$

From Mayer relation we get $\qquad \gamma = \frac{Cp_{avg}}{Cp_{avg} - R} \tag{2-53}$

2.6.3 Theoretical Rocket Performance

With respect to the combustion chamber, it was assumed that the system was adiabatic, and all available energy released from the dissociation was transferred entirely into the products [86]. Flow through the throat and nozzle was assumed quasi-one-dimensional frozen flow.

To account for actual (non-ideal) thruster performance, established correction factors were utilized which is equivalent to the λ factor.

- **Exit velocity Ve**

The energy equation (the Barré de Saint-Venant equation) is a portrait of the principle of conservation of energy Eq.2-42. For an adiabatic flow between two points, x1 and x2, it is given by:

$$h_1 - h_2 = \frac{1}{2}(V_2^2 - V_1^2) = C_p(T_1 - T_2) \tag{2-54}$$

We consider the stagnation state (in the decomposition chamber) as the reference state. The properties of stagnation can be thought of as the properties that would result if the fluid were decelerated to a speed of zero. [87,59]

- **Chamber pressure Pc**

To effectively decompose the fuel system from the propellant engine, typically a 6% loss of tank pressure at the catalytic chamber. A pressure drop of 4 bar is expected for the propellant injector; for a mass flow rate equal to 0.8 g/s [88]. the pressure is meant to be at the 22 bar at the beginning of the mission, it decrease until 5 bar at the end of life of a satellite, which give us a variation of thrust between 2 N to 0.5 N approximately. Therefore, to insure a good dimension of thruster, expansion ratio (Ae/Ac), variation of thrust and specific impulse it is favorable to fix the pressure to be 12 bar.

$$P_c = P_{\hat{r}} - \Delta P_{inj} - \Delta P_{cat} \tag{2-55}$$

ΔP_{cat}: Pressure loss in the catalytic chamber

From Eq. 2-54 the exit velocity as a function of the stagnation temperature T0, (T0 $\equiv Tc$) is found by the energy equation (assuming the velocity in the chamber is zero) is:

$$V_e = \sqrt{2 * C_p(T_c - T_e)} \tag{2-56}$$

For isentropic flow, the following relationship between the exit properties and the stagnation properties for temperature, pressure and mass volume of the fluid are very important:

$$\frac{T_e}{T_c} = \left(\frac{P_e}{P_c}\right)^{\frac{\gamma-1}{\gamma}} = \left(\frac{\widetilde{V_e}}{\widetilde{V_c}}\right)^{1-\gamma} \tag{2-57}$$

And:

$$C_p = \frac{\gamma r}{\gamma - 1} \tag{2-58}$$

And then we get to the Eq. 2-28

$$V_e = \sqrt{\frac{2\gamma}{\gamma-1} RT_c \left[1 - \left(\frac{P_e}{P_c}\right)^{\frac{\gamma-1}{\gamma}}\right]}$$

This equation is one of the most useful, since it allows to calculate the speed of the exit at the level of the nozzle; and gave a better understanding of the behavior of the system that can be obtained

- **Thrust coefficients C_F**

Pe / Pc being the rate of expansion at the nozzle exit (function of the ejection section) The thrust factor (or coefficient) C_F represents the thrust input provided by the diverging part, compared to that of a nozzle simply convergent. This quantity, which measures the effectiveness of the trigger, is expressed as [89]:

$$C_F = \frac{F_T}{P_c * A_T} \tag{2-59}$$

$$C_F = \sqrt{\frac{2\gamma^2}{\gamma-1}\left(\frac{2}{\gamma+1}\right)^{\frac{\gamma+1}{\gamma-1}} \left[1 - \left(\frac{P_e}{P_c}\right)^{\frac{\gamma-1}{\gamma}}\right]} \tag{2-60}$$

Ideal F_T thrust is obtained if the expansion flow is purely axial at the outlet section. In practice, for obvious reasons of thrust / weight optimization, the diverging part of a real nozzle is truncated to a substantially conical shape, which for a flow at constant γ, induces a loss of thrust proportional to the angle of divergence [90]:

$$F_{div} = F_T * \lambda \tag{2-61}$$

F_{div} : thrust loss dua divergent form

And $\lambda \leq 1$ correction factor for nozzle

$$\lambda = \frac{1}{2}(1 + cos\alpha) \tag{2-62}$$

An ideal thrust ($\lambda = 1$); and a rocket nozzle with a cone divergence angle of 28 ° (half angle $\alpha = 14$ °), the output pulse will be reduced, and therefore the ejection speed will be equal to 98% of the speed calculated by Eq. 2-25 [89]

- **Characteristic velocity**

The characteristic velocity has been used frequently in the rocket propulsion literature. Its symbol c*, pronounced "cee-star," is defined as:

$$c^* = (p_c A_t)/\dot{m} \tag{2-63}$$

The characteristic velocity c*] measure the effectiveness of the combustion of a rocket engine at high temperature and pressure, separate from nozzle performance. It is used to compare different propellant and propulsion systems [91] it is easily determined from measured data of $\dot{m}$, p_1, and A_t.

Using the equation of continuity Eq.2-30, we get:

$$c^* = \frac{\sqrt{\gamma r T_c}}{\gamma \sqrt{\left(\frac{2}{\gamma+1}\right)^{\frac{\gamma+1}{\gamma-1}}}} \tag{2-64}$$

- **Ideal specific impulse for the engine $I_{s\,i}$:**

From equation (2-21) we get :

$$I_{s\,i} = \frac{V_e}{g_0} = \frac{c^* . C_F}{g_0} \tag{2-65}$$

g_0 is the gravitational acceleration $= 9.81$ m/s²

2.6.4 Chamber parameters:

The characteristics of the expansion flow are calculated from the laws of conservation of mass and energy in addition to the equations of state of the mixture and isentropy. By using the generating conditions with those at the outlet of the chamber (Tc and Pc) [92]:

- **Mass flow $\dot{m}$**

Using the thrust force equation allows us to express the ideal mass flow as:

$$\dot{m} = F/V_e \tag{2-66}$$

- **Throat velocity**

The local sonic speed c (m / s), and the Mach number Ma, defined as the ratio of the flow speed and the local sonic speed, is given by:

$$M = V/c \tag{2-67}$$

$$c = \sqrt{\gamma r T} \tag{2-68}$$

From this equation and using Eq.2-46 to Eq.2-54 and Eq.2-67 to Eq.2-68 the relation between temperature and the velocity in an adiabatic flow between two point x1 and x2, given as :

$$\frac{T_2}{T_1} = \frac{1+\frac{\gamma-1}{2}M_1^2}{1+\frac{\gamma-1}{2}M_2^2} \tag{2-69}$$

We consider the critical conditions at the nozzle throat where the Mach number is unitary, Ma = 1 (the flow speed is equal to the sonic speed):

$$\frac{T_{\tilde{t}}}{T_c} = \left(\frac{P_{\tilde{t}}}{P_c}\right)^{\frac{\gamma-1}{\gamma}} = \left(\frac{\widetilde{V}_t}{\widetilde{V}_c}\right)^{1-\gamma} = \frac{2}{\gamma+1} \tag{2-70}$$

With Tt, Pt, and vt, are respectively the temperature, the pressure and the mass volume at the throat of the nozzle.

And then we can get the velocity at the throat:

$$V_{\tilde{t}} = \sqrt{\left(\frac{2}{\gamma+1}\right)\gamma r T_c} \tag{2-71}$$

A volume method was used to optimize the dimensions of the thruster in order to obtain the best configuration, reduction of thruster volume and mass, and also to give maximum thrust

- **The specific volume at the nozzle inlet $\widetilde{V}_c$**

From the equation of state of ideal gases the specific volume at the nozzle inlet can be expressed as follows:

$$\widetilde{V}_c = \frac{RT_c}{P_c} \tag{2-72}$$

- **Specific volume at throat $\widetilde{V}_{\tilde{t}}$**

from Eq.2-69 while considering the flow as isentropic and critical conditions in throat we get:

$$\widetilde{V}_{\tilde{t}} = \widetilde{V}_c \left(\frac{\gamma+1}{2}\right)^{\frac{1}{\gamma-1}} \tag{2-73}$$

- **specific volume of nozzle exit $\widetilde{V}_e$**

-

and from Eq.2-54 we get :

$$\widetilde{V}_e = \widetilde{V}_c \left(\frac{P_c}{P_e}\right)^{\frac{1}{\gamma}} \tag{2-74}$$

2.6.5 Preliminary Thruster Design

This section is to shape the catalyzer dimensions the length and the diameter of the catalyst in such way to gain a perfect decomposition of the hydrogen peroxide, and we consider:

- The stability of the pressure inside the catalyser while the reaction and the absence of oscillations,
- Constant thrust from the starting to end life.
- The endurance: a long operating life of the catalyst with little degradation in performance,
- Speed: the decomposition time must be of the order of a few milliseconds; Figure 2.15 shows a flow through a catalyst of cross section (A) [88].
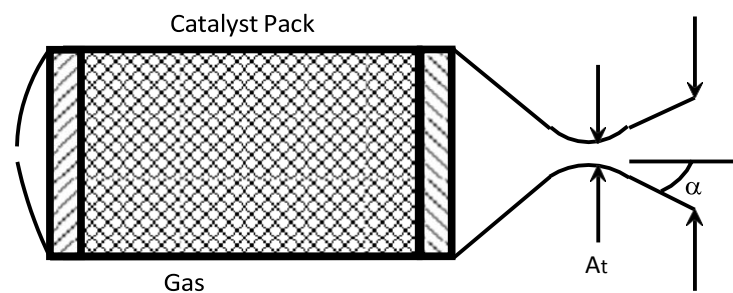

Figure 2-15: Nozzle Dimensions, Low Thrust Application. [88]

Based upon nozzle theory [64, 86, 93], the throat area (A_t) and exit area (A_e) are derived from the properties of the gaseous products (temperature, pressure, molecular weight, and specific heat), the laws of thermodynamics, and conservation criteria.

$$A_{\check{t}} = \frac{\dot{m}\tilde{V}_t}{V_t} \tag{2-75}$$

$$A_e = \frac{\dot{m}\tilde{V}_e}{V_2} \tag{2-76}$$

Where we get nozzle expansion ratio:

$$\varepsilon = A_e / A_{\check{t}} \tag{2-77}$$

For low thrust applications and manufacturing simplicity, the computer program models a conical nozzle (Sutton, [81, 82, 86]). Loss to exhaust momentum, based upon the nozzle half

angle (α), is calculated through l (nozzle correction factor). The final computer simulation derived the remainder of internal thruster dimensions thatwere dependent upon empirical data. Figure 2.14 identifies the dimensions from final computer simulation
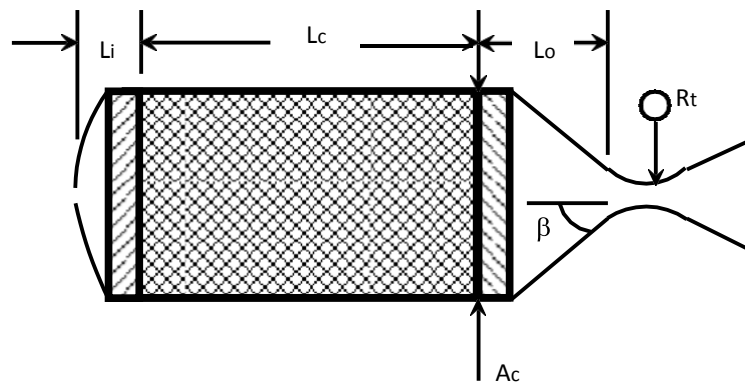

Figure 2-16: Catalyst Geometry. [87]

Identified that the throat contour, or radius of curvature (R_t), is not critical for performance, and "any radius is usually acceptable." The designer is suggested to define a radius that meets manufacturability requirements and the angles of α (nozzle half-angle) and β (contraction angle). Also provided that the contraction angle may approach 90 degrees without significant performance loss. Thus, the designer should focus upon the requirements of L_o (chamber length, post-catalyst).

Relative to the chamber, special considerations for hydrogen peroxide monopropellant thrusters were incorporated into the program. Three stages to the chamber exist. The first stage (L_i) is where liquid hydrogen peroxide is introduced. The second stage is the catalyst, which is assumed to completely dissociate the hydrogen peroxide. The third stage (L_o) is where the gaseous products are accelerated into the throat. The dissociation of hydrogen peroxide is completed within the catalyst, and there is no combustion occurring within L_o. Hence, the length of the chamber after the catalyst (L_o) should be minimized to limit heattransfer and starting transients [66].

The cross-sectional area of the catalyst (A_c), which coincides with the chamber, and the length of the catalyst (L_c), are entirely dependent upon the catalyst design. The equation for A_c is available in Eq.2-70. The length (L_i) of the chamber between the flow orifice and the catalyst is entirely dependent upon the catalyst design. L_i must be of sufficient length to allow for uniform hydrogen peroxide flow through the catalyst. However, to limit start-up transients, the pre-catalyst length (L_i) should be minimized.

$$A_C = \frac{\dot{m}}{LF} \qquad (2\text{-}78)$$

$$L_C = \bar{V}_C / A_C \qquad (2\text{-}79)$$

2.7   <u>Numerical Modelling - Equation Derivation and Implementation</u>

Taken from the steps of the analysis model, a detailed flow diagram of the computerprogram is provided within Figure 2.15. by using MATLAB® 2017
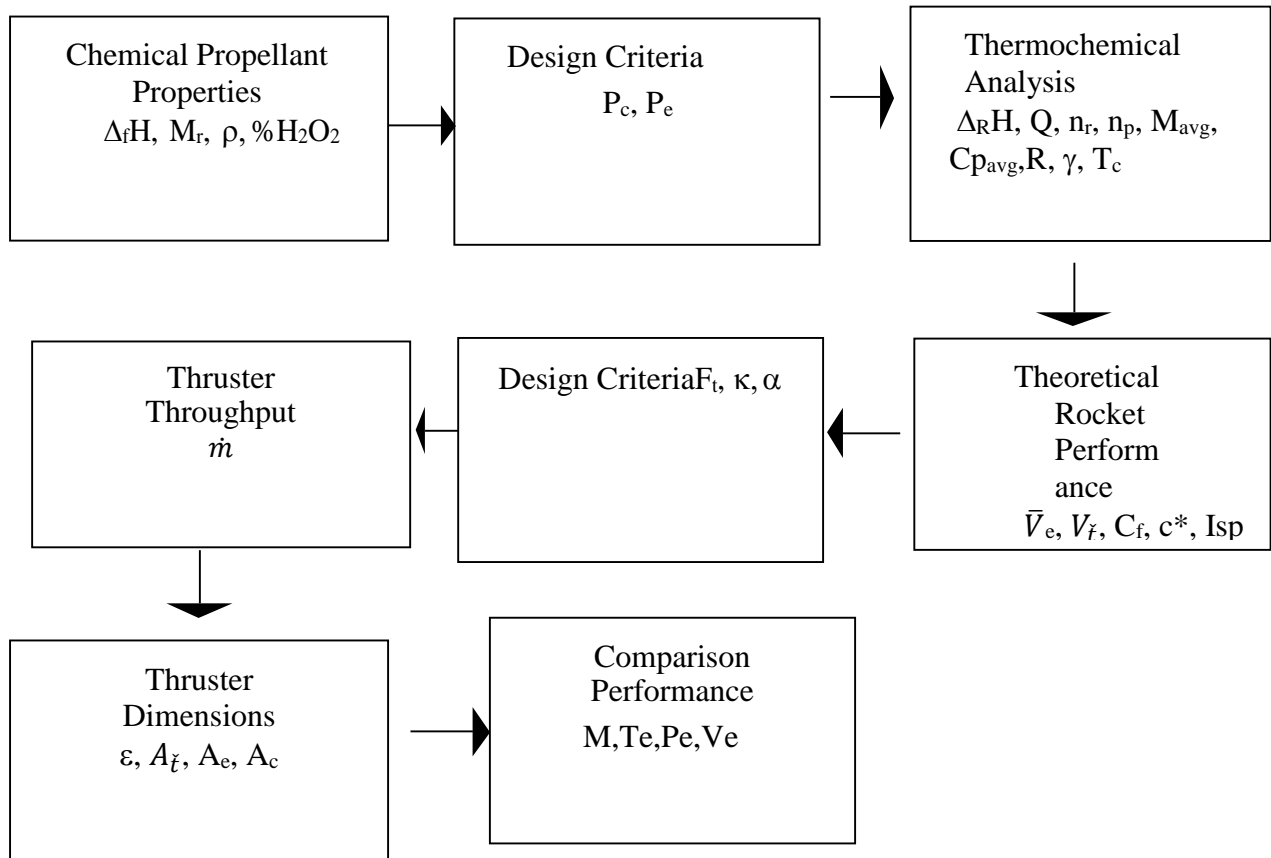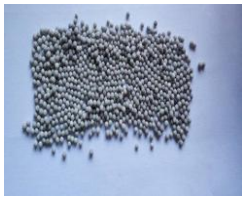

Figure 2-17: Computer Program Flow Diagram.

Given the assumptions previously identified part 2.1 within the analysis model, the equation for the program were derived or taken directly from textbooks (with confirmation of correct assumptions). The equations were sequenced to provide the desired output. The individual equations and the stages of the computer analysis are provided. The computer analysis was performed through MATLAB® 2017

2.7.1 Review of state of the art

Owing to the ongoing rapid research activities in the green-propulsion field, it was necessary to extensively study and collect various data of green monopropellants properties and performance that would further assist analysts and designers in the research and development of liquid propulsion systems. This review collected and presents these necessary data for a wide range of state-of-the-art for green monopropellants from relevant literature sources with highest reliability, to have the credibility to our analysis.

Table 2-1: State of art of some based references

Reference / Parameters	[94]	[94]	[95]	[96]
H_2O_2 concentration %	**87.5%**	**87.5%**	87.7%	89%
Loading factor (kg/s/m^2)	73.21	72.00	19.26	78.94
Catalyst	Pt/ Al2O3 2nd type (LR-59)	Silver Grids	Pt/ Al2O3-COM	Ag silver disque
Models				
Reason	+ very active and relatively insensitive to poisoning - sensitive to pellet rupture	+ decomposition efficiency (characteristic velocity efficiency and the temperature efficiency) - channeling phenomena	+ yielding nearly spherical granules for more uniform bed packing and reduced pressure drop, long duration - thermal shock resistance excellent chemical activity	+ easy to build without degradation + give a temperture higher than 873 K
Chamber pressure Pc (bar)	10.5-5.5	10.5-7	21.5-19.6	21.8-11
Chamber Temperature (K)	952.85-703.15	952.85-773.15	958-870	901-1006.76
Mass flow rate (g/s)	3.68	3.62	4.90	0.598

Specific impulse (s)	113-57	113-80	130-110	172.743 vacuum
Characteristic velocity (m/s)	904-470	904-724	900.5-840	925
Nozzle expansion Ratio Ae/ At	3.48	3.48	3.3	100
Exhaust diameter	3.73	3.73		8
Throat diameter Dt (mm)	2	2	1.7	0.8
Conical nozzle half angle (deg)	15	15	15	
Nozzle lengh (mm)	3.23	3.23		
Injector hole diameter (mm)	1.5	1.5		
Distribution plate diameter (mm)	8	8		
Catalyst bed diameter (mm)			18	10
Catalyst bed length (mm)			60	10
Thrust (N)	4.1 – 2.05	4 - 3	5.2-6.2	1.0125
Thrust coefficient	1.23 - 1.20	1.23-1.22	1.40-1.30	

2.7.2 System Modeling

The highest point of the three major stages of the program (thermochemistry, theoretical rocket performance, and preliminary thruster design) provided the tools necessary to develop a thruster. The calculation was based on silver mesh with a wire diameter equal to Dw = 0.357 mm and hole size equal to Hs = 0.84 mm and disc diameter Dd = 10 mm and a length of catalyst equal to 10 mm [68].

The input based upon the requirements on Table 2-2 where we consider two conditions, The Vacuum and the atmospheric pressure and the output are provided within tables 2-2 through Table 2-6

Table 2-2: Thruster Requirements.

Parameter	Description	Value
P_c	Chamber Pressure	12 bar
P_e	Exit Pressure	1 bar & 0.001 bar
%H_2O_2	Concentration of H_2O_2	87.5 %
Loading Factort	Lf	70 kg/s/m^2
Catalyst	Silver Mesh	
T	Design thrust	1 N

2.7.3 Theoretical Rocket Performance

Within the limits of hydrogen peroxide concentrations of 87.5%, the tables following is the steps used to have our final result, meanwhile comparing with the state of art found previously

Table 2-3: Results of Theoretical Rocket Performance.

Parameter	Case study atmospheric conditions	Case study Vacuum
H2O2 Concentration	87.5%	87.5%
Chamber Temp (K)	968	968
Specific Impulse, Isp (s)	119.56	170

2.7.4 Preliminary Thruster Design result

After scaling the thrust to match the observed results, the throat diameter exhibited direct correlation with the computer simulation.

Table 2-4: Results of Preliminary Thruster Design.

	Parameter	Case study atmospheric conditions	Case study Vacuum	Dr.Amri Redha [10]
$\dot{m}$	Mass Flow Rate (g/sec)	0.852	0.599	0.599
Dt	Throat Diameter (mm)	0.9053	0.7589	0.8
De	Exit Diameter (mm)	1.3703	12.56	8

Table 2-5: Theoretical Rocket Performance.

Isp	Theoretical Specific Impulse (s)	119.56	170	172.7
Tc	Chamber Temperature (K)	968	968	1006.76
c*	Characteristic Velocity (m/s)	906	906	925
C_F	Coefficient of Thrust	1.2947	1.2947	
Ve	Exit velocity (m/s)	1172.9	1669.1	
$\dot{m}$	Mass flow rate (g/s)	0.852	0.599	0.599
Mach	Mach number	2.26	7.23	

Table 2-6: Nozzle Dimensions Based Upon Theoretical Performance.

Parameter	Description	Condition 1	Condition 2	Dr.Amri Redha [10]
A_e	Exit Area of Nozzle (mm^2)	1.4748	146.12	50.26
A_t	Throat Area (mm^2)	0.6436	0.453	5.026
A_e / A_t	Expansion Ratio	2.2914	325	100
α	Nozzle Half-angle (°)	14	14	
A_C	Catalyst Pack Area (mm^2)	1.4551	0.74883	78.5
R_C	Catalyst pack Rayon (mm)	0.68057	0.48822	5

It is remarkable that the dimensions parameters and performance depends on the study conditions taken. However, the manufacturability is considered as a critical state where it is obvious that a catalyst of radius equal to 0.488 mm is impossible to be manufactured. For this case, we will use a catalyst of rayon 5 mm, which is the smallest silver catalyst that has been produced without degradation.[4]

CHAPTER 3

ANSYS System Study

3.1 ANSYS FLUENT MODELS

Many models to be implemented in Fluent had to be carefully considered in order to suit the needs of simulating the fluid flow in the thruster. The sections that follow detail the various models that are utilized and how they are implemented in Fluent.

3.1.1 Continuity and Momentum Equations

ANSYS Fluent solves mass and momentum conservation equations for all flows. An additional equation for energy conservation is calculated for flows involving heat transfer or compressibility. An extra energy conservation equation is solved. A species conservation equation is solved for flows involving species mixing or reactions, or conservation equations for the mixture fraction and its variance are solved if the non-premixed combustion model is utilized. When the flow is turbulent, additional transport equations must be solved.

The mass conservation equation, often known as the continuity equation, is written as follows[97]:

$$\frac{\partial \rho}{\partial t} + \nabla.(\rho \vec{v}) = S_m \tag{3-1}$$

S_m : is the mass added to the continuous phase from the dispersed second phase

The general form of the mass conservation equation, Equation 1.1, is valid for both incompressible and compressible flows.

The continuity equation for 2D axisymmetric geometries is

$$\frac{\partial \rho}{\partial t} + \frac{\partial}{\partial x}(\rho v_x) + \frac{\partial}{\partial}(\rho v_r) + \frac{\rho v_r}{r} = S_m \tag{3-2}$$

x is the axial coordinate, r is the radial coordinate, v_x is the axial velocity, v_r is the radial velocity.

Conservation of momentum is described by[97]:

$$\frac{\partial \rho}{\partial t}(\rho \vec{v}) + \nabla.(\rho \vec{v} \vec{v}) = -\nabla P + \nabla.(\overline{\overline{\tau}}) + \rho \vec{g} + \vec{F} \tag{3-3}$$

P is the static pressure, $\overline{\overline{\tau}}$ the stress tensor, $\rho \vec{g}$ is the gravitational body force and $\vec{F}$ is external body forces.

The stress tensor is expressed as:

$$\overline{\overline{\tau}} = \mu \left[(\nabla \vec{v} + \vec{\nabla}^T) - \frac{2}{3} \nabla.\vec{v} I \right] \tag{3-4}$$

μ is the viscosity

I is the unit tensor

The second term on the right-hand side is the effect of volume dilation.

For 2D axisymmetric geometries, the axial and radial momentum conservation equations are given by:

$$\frac{\partial}{\partial t}(\rho v_x) + \frac{1}{r}\frac{\partial}{\partial x}(r\rho v_x v_x) + \frac{1}{r}\frac{\partial}{\partial r}(r\rho v_r v_x) = -\frac{\partial p}{\partial x} + \frac{1}{r}\frac{\partial}{\partial x}\left[r\mu \left(2\frac{\partial v_x}{\partial x} - \frac{2}{3}(\nabla.\vec{v}) \right) \right]$$

$$\tag{3-5}$$

$$+\frac{1}{r}\frac{\partial}{\partial r}\left[r\mu \left(\frac{\partial v_x}{\partial r} + \frac{\partial v_r}{\partial x} \right) \right] + F_x$$

And

$$\frac{\partial}{\partial t}(\rho v_r) + \frac{1}{r}\frac{\partial}{\partial x}(r\rho v_x v_r) + \frac{1}{r}\frac{\partial}{\partial r}(r\rho v_r v_r) = -\frac{\partial p}{\partial r} + \frac{1}{r}\frac{\partial}{\partial x}\left[r\mu \left(\frac{\partial v_r}{\partial x} + \frac{\partial v_x}{\partial r} \right) \right]$$

$$+\frac{1}{r}\frac{\partial}{\partial r}\left[r\mu \left(2\frac{\partial v_r}{\partial r} - \frac{2}{3}(\nabla.\vec{v}) \right) \right] \tag{3-6}$$

$$-2\mu \frac{v_r}{r^2} + \frac{2\mu}{3r}(\nabla.\vec{v}) + \rho \frac{v_z^2}{r} + F_r$$

Where

$$\nabla . \vec{v} = \frac{\partial v_x}{\partial x} + \frac{\partial v_r}{\partial r} + \frac{v_r}{r}$$

(3-7)

3.1.2 Inviscid flow

Inviscid flow analyses ignore the effect of viscosity on flow and are best used in high Reynolds number applications where inertial forces dominate viscous forces. An aerodynamic analysis of a high-speed projectile is one example where an inviscid flow calculation is appropriate. In a case like this, the pressure forces on the body will dominate the viscous forces. An inviscid analysis will provide you with a rapid approximation of the body's basic forces. After you've adjusted the body shape to optimize lift and minimize drag, you may run a viscous analysis to account for the impacts of fluid viscosity and turbulent viscosity on lift and drag forces. ANSYS Fluent solves the Euler equations for inviscid flows. The mass conservation equation is the same as for a laminar flow, but because to the lack of molecular diffusion, the momentum and energy conservation equations are lowered [98].

Conservation of momentum is described by:

$$\frac{\partial \rho}{\partial t}(\rho \vec{v}) + \nabla . (\rho \vec{v} \vec{v}) = -\nabla P + \rho \vec{g} + \vec{F}$$

(3-8)

For 2D axisymmetric geometries, the axial and radial momentum conservation equations are given by:

$$\frac{\partial}{\partial t}(\rho v_x) + \frac{1}{r}\frac{\partial}{\partial x}(r\rho v_x v_x) + \frac{1}{r}\frac{\partial}{\partial r}(r\rho v_r v_x) = -\frac{\partial p}{\partial x} + F_x$$

(3-9)

And

$$\frac{\partial}{\partial t}(\rho v_r) + \frac{1}{r}\frac{\partial}{\partial x}(r\rho v_x v_r) + \frac{1}{r}\frac{\partial}{\partial r}(r\rho v_r v_r) = -\frac{\partial p}{\partial r} + F_r$$

(3-10)

3.1.3 Compressible flow

Compressibility effects occur in high-velocity gas flows and/or in those with considerable pressure changes. When the flow velocity approaches or exceeds the speed of sound of the gas or when the pressure change in the system $(\Delta p / p)$ is large, the variation of the gas density with pressure has a significant impact on the flow velocity, pressure, and temperature. ANSYS

Fluent provides a wide range of compressible flow modelling capabilities for subsonic, transonic, and supersonic flows [99].

3.1.4 Species transport

ANSYS Fluent can model the mixing and transport of chemical species by solving conservation equations describing convection, diffusion, and reaction sources for each component species. The species model must be incorporated in the simulation to resolve the aspect of multicomponent fluid flow where a given phase consists of a combination of distinct fluids. The species equation is calculated in Fluent for each phase k, and forecasts the mass fraction of each species by solving a convection-diffusion equation for the ith species [100,101].

3.2 <u>Turbulence models</u>

The random and chaotic diversity in velocity and other flow parameters characterizes turbulent flows. They also contain rotational flow structures which are termed turbulent eddies. Inertial factors dominate the properties of bigger eddies in turbulent flow [102]. The dimensionless Reynolds number is used to identify whether the flow regime is laminar or turbulent by describing the relationship between inertial and viscous forces [103].

$$R_e = \frac{\rho u L}{\mu} \qquad (3\text{-}11)$$

3.2.1 Choosing a turbulence model

Unfortunately, no single turbulence model is universally acknowledged as being preferable for all types of issues. The physics included in the flow, the accepted practice for a certain type of problem, the level of precision necessary, the available computer resources, and the length of time available will all influence the turbulence model used.[104]

3.2.2 Reynolds Averaging Navier-Stokes Equation

The Navier-Stokes's equation can be utilized with direct numerical simulation to calculate the flow field of a turbulent flow (DNS). This method is computationally intensive and costly, and it is often employed for research purposes on smaller size challenges. The Reynolds Averaged Navier-Stokes (RANS) equation is used alternatively in the example studied in this thesis. The numerical solution of the two-dimensional compressible Reynolds averaged

Navier–Stokes (RANS) equations in conjunction with six turbulence models is obtained using the FLUENT finite volume solver. [105].

3.2.3 SST K-Omega

According to Balabel[cd-dv modelling] who did a comparison between different turbulence models for a simulation of gas flow in a convergent divergent nozzle. The simulation displayed that the empirical turbulence model shear-stress transport (SST) k-ω exhibited the best over-all agreement with experimental data. For This reason, this model was therefore selected as the turbulence model for the simulation in this thesis[106].

The SST k-ω turbulence model [Menter 1993] is a two-equation eddy-viscosity model which has become very popular. The shear stress transport (SST) formulation combines the best of two worlds. The empirical turbulence model shear-stress transport (SST) k- ω had the best overall agreement with experimental data on a simulation of a nozzle flow.

SST k- ω is a hybrid of k- ω and k-ε, with the standard k- ω model operating near the wall and a modified k- ε model operating in the far field. This model allows for turbulent shear stress transport and is particularly well adapted to flow separations. The k- ω equations are described in Fluent as follow [107]:

k-equation:

$$\frac{\partial}{\partial t}(\varphi k) + \frac{\partial}{\partial x_i}(\varphi k u_i) = \frac{\partial}{\partial x_i}\left(\Gamma_k \frac{\partial k}{\partial x_j}\right) + G_K - Y_K + S_K \qquad (3\text{-}12)$$

ω -equation:

$$\frac{\partial}{\partial t}(\varphi \omega) + \frac{\partial}{\partial x_i}(\varphi \omega u_i) = \frac{\partial}{\partial x_i}\left(\Gamma_\omega \frac{\partial k}{\partial x_j}\right) + G_\omega - Y_\omega + S_\omega \qquad (3\text{-}13)$$

G_k :represents the generation of turbulent kinetic energy due to mean velocity gradients.

G_ω: is the generation of ω.

Γ_k and Γ_ω : are the effective diffusivity of k and ω .

Y_k and Y_ω : represent the dissipation of k andωdue to turbulence.

D_ω represents the cross-diffusion term.

S_K and S_ω : are user defined source terms.

3.3 Meshing

3.3.1 Mesh definition

Meshing is the process of breaking down an object's continuous geometric space into thousands or more shapes in order to adequately define the object's physical shape. The more detailed a mesh is, the more accurate the model will be, allowing for more realistic simulations. Mesh generation, also known as meshing, is the act of separating complex geometries into elements that can be used to discretize a domain into a two-dimensional and three-dimensional grid. Advanced automated meshing techniques can deliver faster and more accurate solutions because meshing takes up a substantial amount of time while obtaining simulation results[108].

3.3.2 Mesh importance

Creating the most appropriate mesh is the foundation of engineering simulations. The mesh influences the accuracy, convergence, and speed of the simulation. Computers cannot solve simulations on the CAD model's actual geometry shape as the governing equations cannot be applied to an arbitrary shape. Mesh elements allow governing equations to be solved on volumes that are mathematically defined and have a predictable shape. The equations that are solved on these meshes are usually partial differential equations. Because solving these equations by hand is impractical due to the iterative nature of the calculations, computational methods such as Computational Fluid Dynamics (CFD) are used.[108,109]
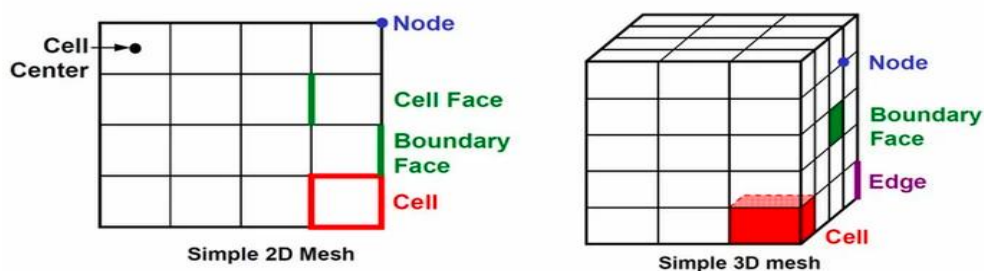

Figure 3-1: Simple 2D-3D mesh. [110]

3.3.3 Mesh types

Control volume forms are determined by the solver's capability. In 2D and 3D flows, structured-grid codes use quadrilaterals and hexahedrons, respectively. In unstructured-grid solvers, triangles (2D) or tetrahedrons (3D) are commonly used, but newer algorithms can employ any polyhedron.[110]

- **Structured mesh**

Grids can be either Cartesian or curvilinear in nature (usually body-fitting). Grid lines in the former are always parallel to the coordinate axes. Coordinate surfaces are curved to fit boundaries in the latter. This mesh can give a good convergence and high resolution.[110,111]
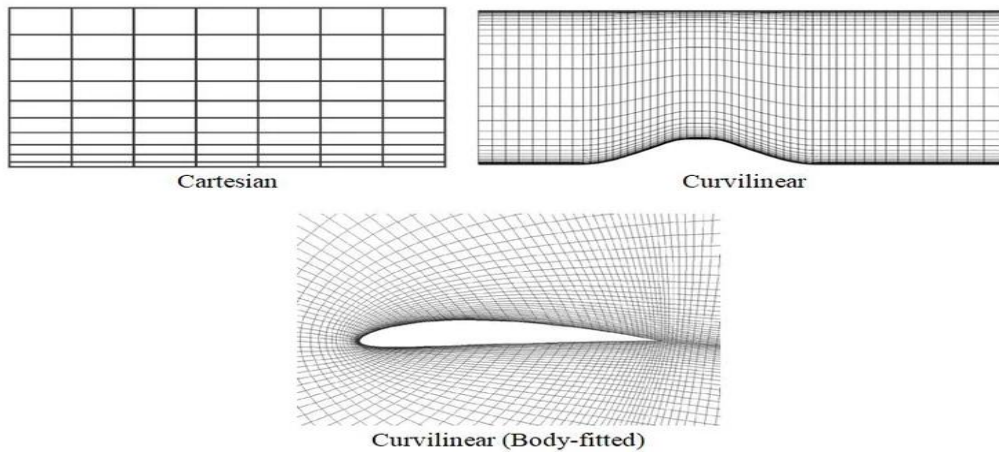

Figure 3-2: Types of structured mesh. [110]

- **Block structured mesh**

The domain (group of node, face and cell zones) is decomposed into small number of regions, the mesh in this region is structured. A common arrangement is that grid lines match at the interface between two blocks so that there are cell vertices that are common to two blocks (matching cells). In some circumstances, the cell counts at the interface do not match, resulting in non-matching cells. Non-matching cells should be avoided as much as possible because they slow down processing. Some solvers also support overlapping blocks (such as chimera grids) with non-aligned cell vertices. At the block boundaries, interpolation is required.Multiple blocks help to keep a structured grid design around difficult border. There are no hard and fast rules, however in crucial and rapidly changing sections of the flow, such as at solid borders, it is generally preferable to avoid dramatic changes in grid direction (which contribute to poor accuracy). It's also a good idea to try to keep the grid's non-orthogonality to a minimum.[110]
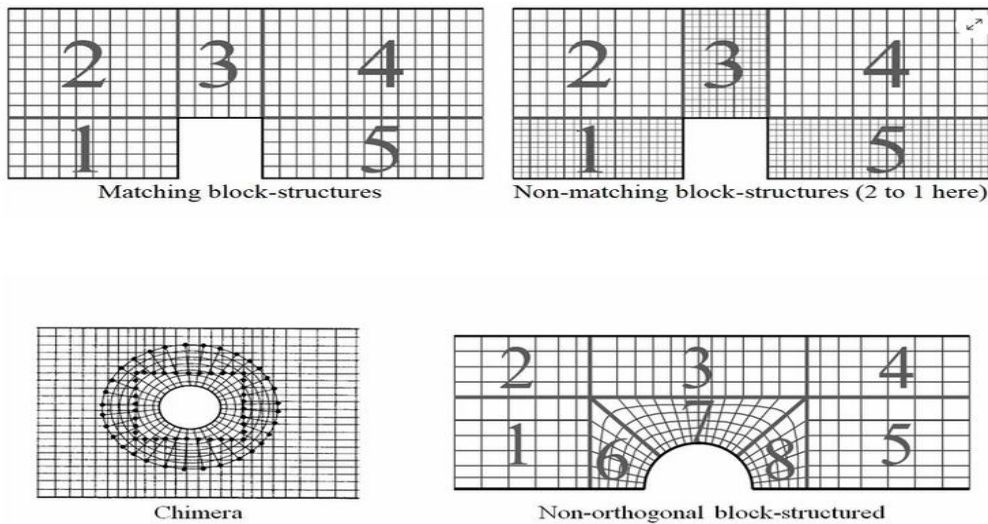
Figure 3-3: Types of block structured mesh. [110]

- **Unstructured Mesh**

Unstructured meshes Triangular (tetrahedral), Quadrilateral (hexahedral), Polygon (polyhedral), Hybrid allow for entirely random geometries to be accommodated. However, this flexibility comes with significant costs, both in terms of connecting data structures and solution algorithms. Grid generators and plotting procedures for such meshes are likewise extremely difficult to develop. [109,110]
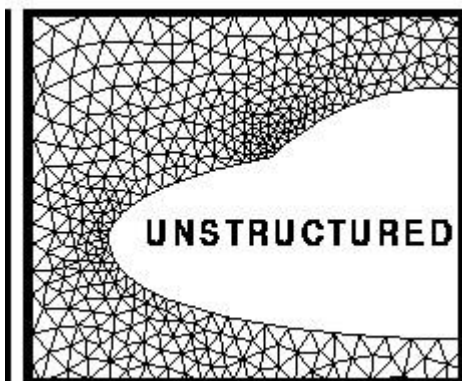

Figure 3-4: Triangular mesh. [112]
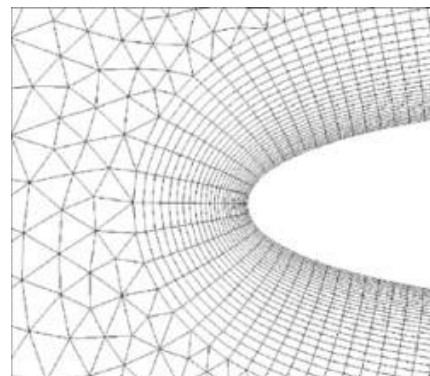
Figure 3-5: Hybrid mesh. [113]

3.3.4 Mesh quality

Aspect ratio, skewness, orthogonality, and smoothness are the four main criteria used to evaluate the solid mesh's qualities. The most significant criterion for evaluating the characteristics of any individual element is the aspect ratio. Skewness, orthogonality, and smoothness, on the other hand, demonstrate the quality prediction for two adjacent elements with the same inner face. Each quality's definition is explored in detail.

- **Aspect Ratio of Triangle (Element)**

A triangle's aspect ratio is 2Ri/Ro, where Ri is the radius of the circle encircling the triangle and Ro is the radius of the circle circumcircle the triangle. A triangle's aspect ratio is between 0 and 1. The higher the aspect ratio, the higher the triangle's quality. The aspect ratio of a triangle with a zero area is 0. In the case of the equilateral triangle, the aspect ratio is 1.[114]

Figure 3-6: Definition of triangle of aspect ratio.

- **Aspect Ratio of Tetrahedron**

The tetrahedron's aspect ratio is 3Ri/Ro, where Ri is the radius of the sphere encircled by the tetrahedron and Ro is the radius of the sphere circumcircled by the tetrahedron. The tetrahedron's aspect ratio is also between 0 and 1, with a bigger aspect ratio implying a higher grade tetrahedron. The aspect ratio of a tetrahedron with zero volume is 0. The aspect ratio of an equilateral tetrahedron is 1. The left one is a front view of an equilateral tetrahedron element with a nice aspect ratio, as seen in the image below. The tetrahedron on the right is created by reducing the height of the equilateral one, which has a poor aspect ratio.[114]
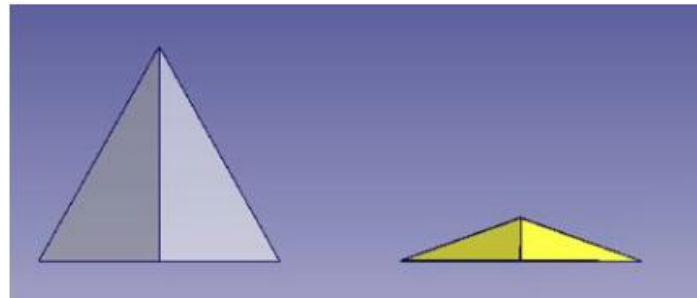

Figure 3-7: Good aspect ratio V.S. poor aspect ratio for tetrahedron element. [114]

- **Skewness**

Skewness is defined as $1 - \dfrac{\overline{ee'}}{\sqrt{A}}$ where e is inner face centre, e' is the connecting centre of $\overline{PE}$ and A is area of face e. The inner faces may be triangles or quadrangles. P and E are centres of cells adjacent to face e. Cells may be tetra, pyramid, prism or hexa solid elements. The quality of skewness indicates the distance between the connecting centre and face centre. And its value is normalized by the square root of inner face area. If these two centres, e and e', are coincident, the skewness is equal to 1. The skewness is influenced by the area of inner

63

face. The smaller skewness implies a bigger distance between two centres. By definition, the skewness may be negative. As shown in below figures, the skewness is good for the left face, and is bad for the right one.[114]
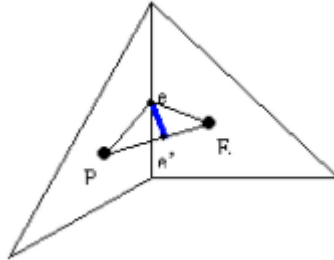

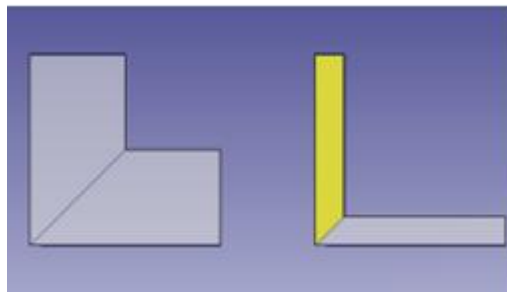Figure 3-8: Definition of Skewness. [114]

Figure 3-9: Good/poor skewness. [114]

- **Orthogonality**

Orthogonality is defined as the angle in degrees between PE connection vector of cell centres and $\vec{n}$ normal vector of inner face. The orthogonality lies between 0 and 180. The value of 0 implies the best situation, and the larger value indicates poor orthogonality.[114]
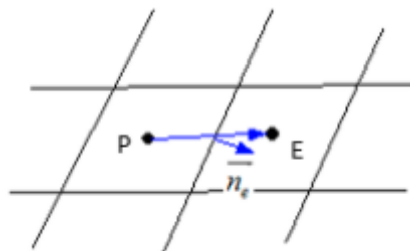
Figure 3-10: Definition of Orthogonality. [114]
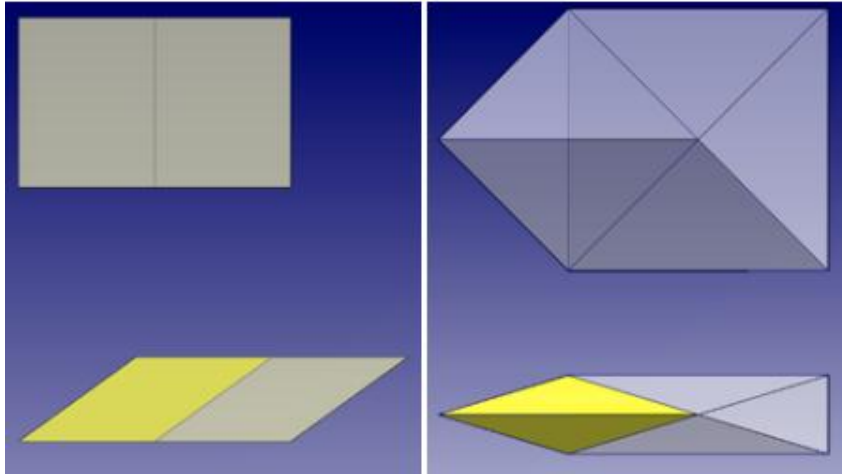
Figure 3-11: Good vs poor orthogonality. [114]

CHAPTER 4

Modelisation and Results

4.1 Design and performance analysis

In this chapter, we are going to present the results obtained from simulating the flow on the thruster that has been designed, the simulation is taking place exactly inside the convergent divergent nozzle. The software used is ANSYS fluent 19.0.

The operation passed through two cases, the first case is to assume that the flow is inviscid, ideal and isentropic, the purpose is to see if the nozzle geometry obtained in MATLAB will give the same performances. The second case study is to assume a viscous flow at high temperature, the purpose from this study is to see how viscosity will reduce performances

4.2   The design of the preliminary thruster's nozzle

The nozzle is considered as an important part of the conception of propulsive system and its design must correspond to the following conditions

- Cheaper, from different nozzles with same performance we must choose the cheapest design to reduce the cost of the project.
- Easy to manufacture
- Simple to be integrated in the total system

According the work done by O'Gara, Michael R., A CFD Investigation of Axisymmetric Micro thruster Nozzles for use on Nano-Satellites (2007) [115] and Lynn A. Arrington et.al, A performance comparison of two small satellite nozzles rocket nozzles (1996) [116] we can see that the conical nozzle performances and efficiency were almost the same as the bell nozzle and the loss was small. For that reason, we use a conical nozzle for our thesis because it matches with the criteria mentioned previously. Nozzle is the convergent-divergent part as shown in Figure 4.1 that provide desired amount of thrust to perform manoeuvres in space. The nozzle is conical such that high-pressure with high injection velocity of H_2O_2 and after the decomposition it enters the nozzle and is compressed as it approaches smallest diameter section, where the gas velocity increases to exactly the speed of sound. A micro-thruster chip is fabricated with a pressure expansion ratio nearly 2 for space condition thought it should be in the range of 2-500, because of design and space constraint, it was kept as 2. Previous literature suggests that the semi divergent and semi convergent angle for micro thruster must close to 28 degrees so as to compensate the dominating viscous effect of propellant over mean free path of the propellant molecules [117,118]. The diameter of the inlet should be such that

the flow must not be interrupted due the friction dominance in micro-level flow passage [119]. The Nozzle design is represented in Figure 4.1.
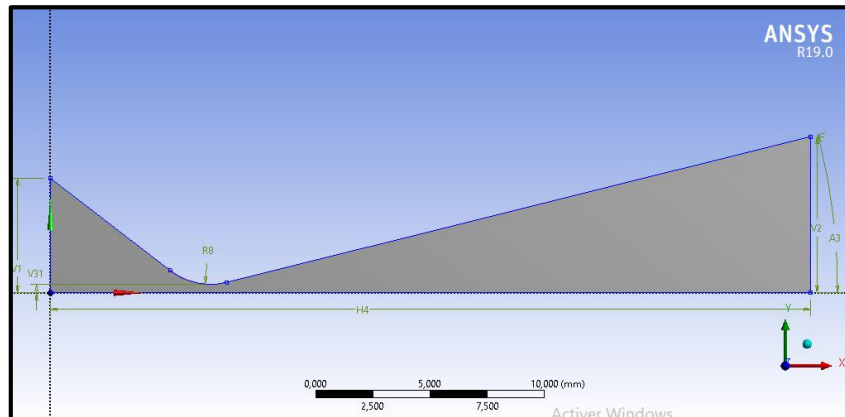

Figure 4-1: Convergent and Divergent nozzle.

As mentioned previously the theoretical correction factor λ can be applied to the nozzle exit momentum of an ideal rocket with a conical nozzle exhaust. This factor is the ratio between the momentum of the gases in a nozzle with a finite nozzle angle 2α and the momentum of an ideal nozzle with all gases flowing in an axial direction:

$$\lambda = \frac{1}{2}(1 + \cos\alpha) \qquad\qquad (2\text{-}62)$$

The variation of λ with different values of α is shown in table 10 for any nozzle that has uniform mass flow per unit exit area. For ideal rockets $\lambda = 1.0$. For a rocket nozzle with a divergence cone angle of 28 ° (half angle $\alpha = 14°$), the exit momentum and therefore the exhaust velocity will be 98.51% of the velocity calculated by the Eq. 2-28:

$$V_e = \left(\left(\frac{2\gamma}{\gamma - 1} \right) \times R \times T_c \times \left\{ 1 - \left(\frac{p_e}{p_c} \right)^{\frac{\gamma-1}{\gamma}} \right\} + V_c^2 \right)^{1/2}$$

Table 4-1: The variation of λ with different values of α.

Nozzle cone divergence half angle α (deg)	Correction factor, λ
0	1.0000
2	0.9997
4	0.9988
6	0.9972
8	0.9951
10	0.9924
12	0.9890
14	0.9851
15	0.9830
16	0.9806
18	0.9755
20	0.9698
22	0.9636
24	0.9567

A small nozzle divergence angle causes most of the momentum to be axial and thus gives a high specific impulse, but the long nozzle has a penalty in rocket propulsion system mass, vehicle mass, and design complexity. A large divergence angle gives short, lightweight designs, but the performance is low. There is an optimum conical nozzle shape and length (typically between 12 and 18 degrees half angle) and it is usually a compromise, which depends on the specific application and flight path. [120]
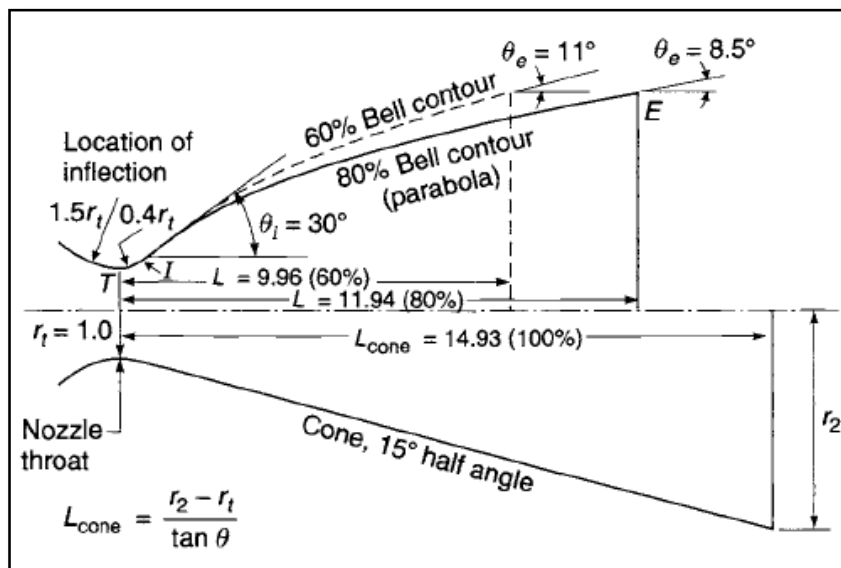
Figure 4-2: Conical and Bell nozzle. [120]

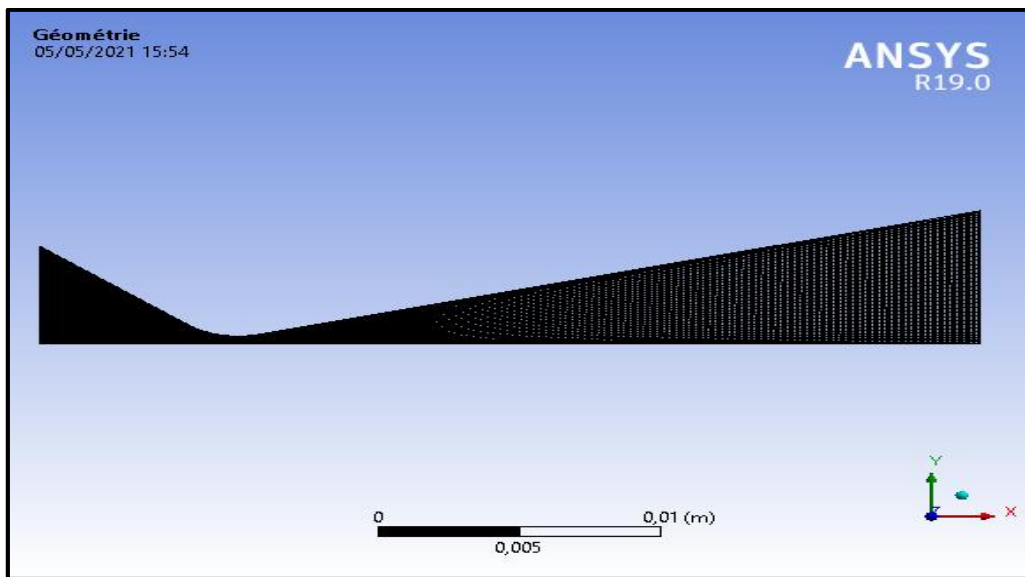## 4.3 Meshing modelisation of the preliminary thruster's nozzle

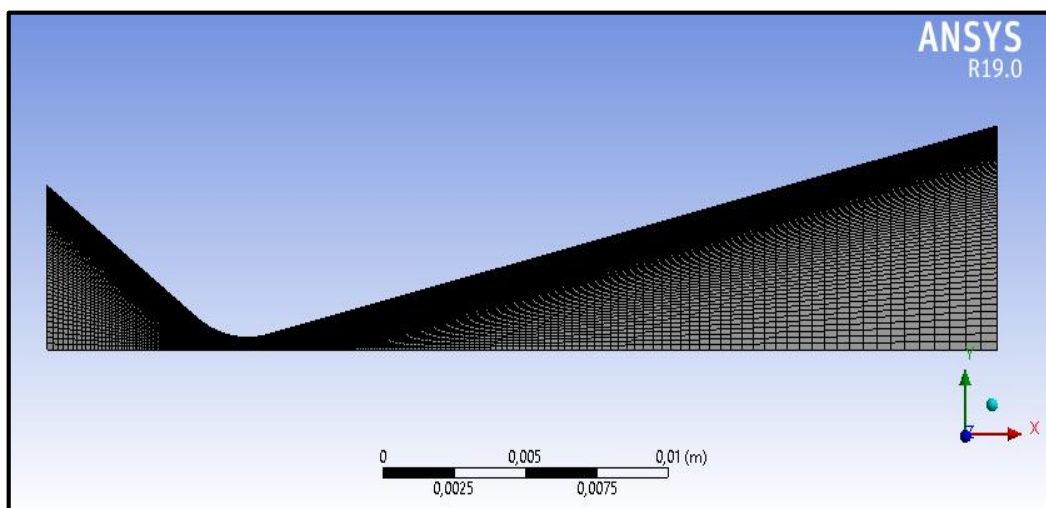Figure 4-3: Meshing modeling for none Viscose flow.

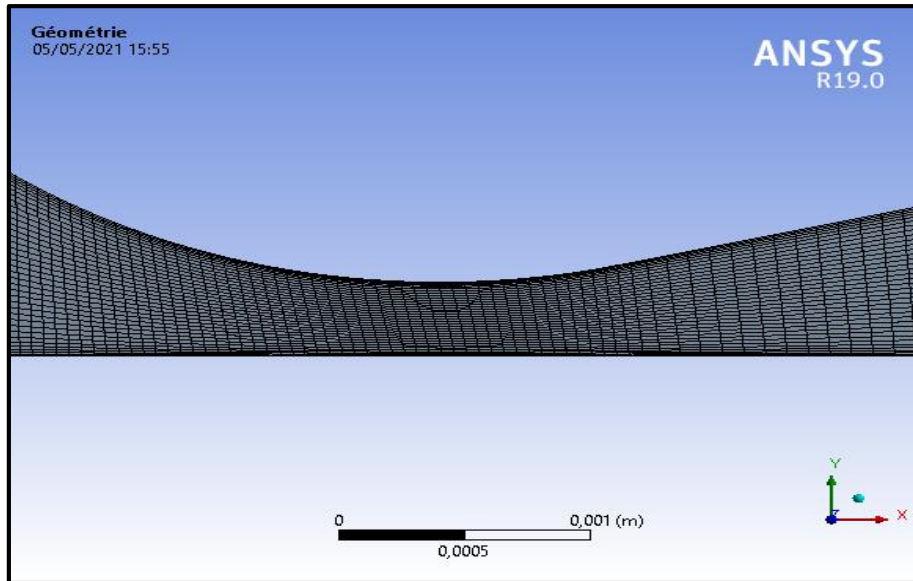Figure 4-4: Meshing modeling for Viscose flow.

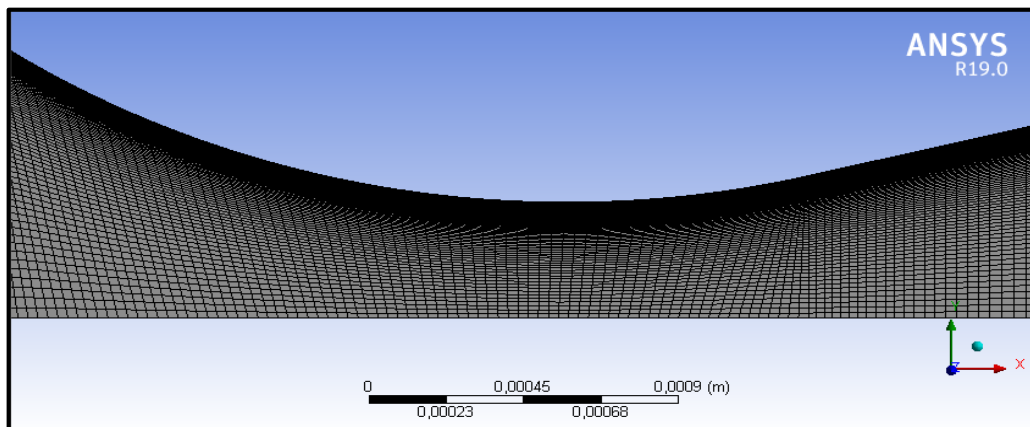Figure 4-5: Meshing modeling in the throat for none Viscose flow.

Figure 4-6: Meshing modeling in the throat for Viscose flow.

ANSYS Mesh Quality Mesh quality recommendations Low Orthogonal Quality or high skewness values are not recommended Generally try to keep minimum orthogonal quality> 0.1, or maximum skewness <0.95. However, these values may be different depending on the physics and the location of the cell Fluent reports negative cell volumes if the mesh contains degenerate cells
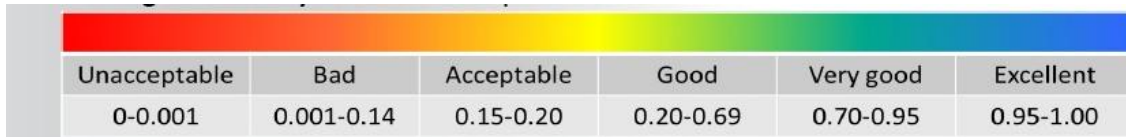
Unacceptable	Bad	Acceptable	Good	Very good	Excellent
0-0.001	0.001-0.14	0.15-0.20	0.20-0.69	0.70-0.95	0.95-1.00

Figure 4-7: Orthogonal quality mesh metrics spectrum.
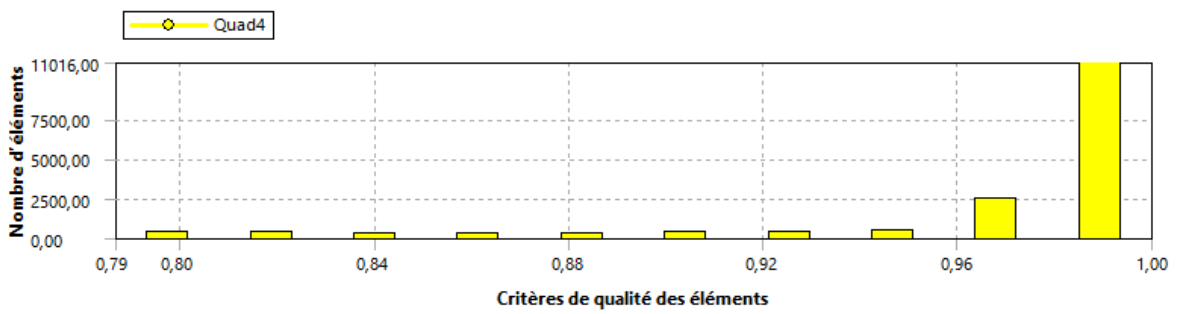
Figure 4-8: Parameter of Orthogonal meshing inclination.

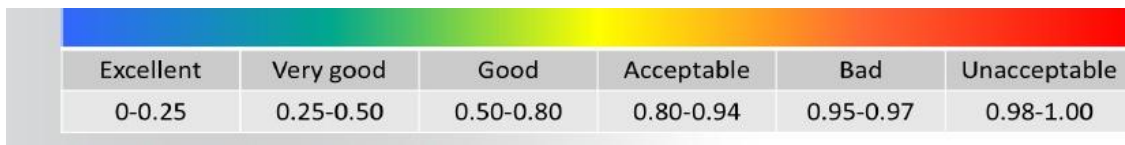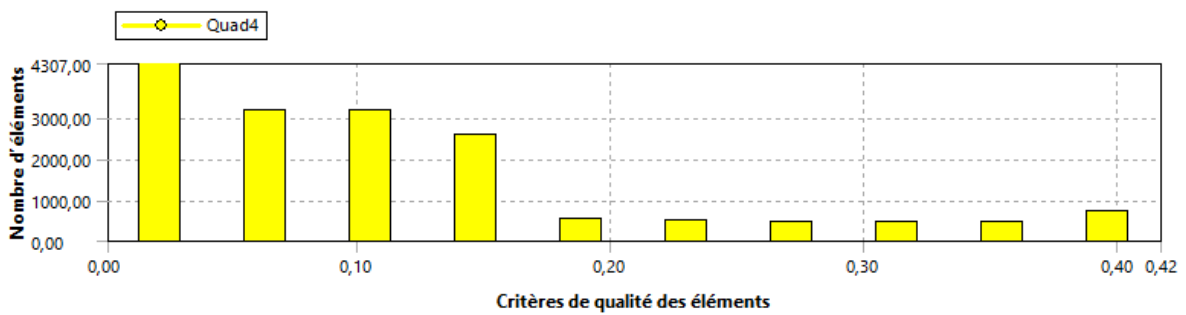| Excellent	Very good	Good	Acceptable	Bad	Unacceptable
0-0.25	0.25-0.50	0.50-0.80	0.80-0.94	0.95-0.97	0.98-1.00

Figure 4-9: Skewness mesh metrics spectrum.

Figure 4-10: Parameter of Skewness meshing quality.

72

4.4 inviscid -isnetropique-ideal gas flow H2O and O2

Case study 1

Boundary/Cell Zone Conditions	
Solver Type	Density-Based Absolute Steady Axisymmetric
Models	Energy (on) Viscous (Inviscid) Species Transport –Mixture Templates
Fluid	mixture: $H_2O + O_2$ Cp: Constant Density: Ideal-gas
Mixture-template	$H_2O + O_2$ Cp: Mixing-law
Operating condition	Pressure = 0 pascal
nozzle zone	**wall**
Inlet Mass flow	**inlet**
	Pressure=1200000 Pascal Liquid mass flow rate=0.599 g/s Liquid temperature = 968 K Species mole fraction: O2=0.2825 H2O=0.7175
Outlet	**Pressure-outlet**
	Gauge pressure = 0 Pa
Methods	**Solution Methods**
Formulation	Implicit formulation
Flux type	Roe-FDS
Flow	Second order Upwind

The simulation was run for 707 iteration and converged by a precise error of 10^{-5}. The simulation results presented in this chapter was obtained at the simulation time approximately 20 minutes.

- **Mesh test**

   For all simulations, mesh is an important feature. Grid design require taking in consideration the shape type, the quality and number of grids, this latter will have a big influence on computational cost and accuracy on simulation analysis results [121].

To avoid the problem of grid influence on the results we must select the optimal number of grids appropriate for the CFD, a mesh test is one of the solutions used to insure the grid independency. A grid independency for a denser or looser mesh the calculation results will change little bit, so the mesh change wont influence on the results obtained [122].

A same test was applied in our simulation in order to observe how refining mesh will change our results and how much mesh adaptation is needed to achieve grid independency. Table 4.2 will represent the different meshes and the results obtained in each one.

Table 4-2: Inviscid flow case study grid independency

Adaptation	Initial mesh	Adaptation 1
Cells	29201	67478
Nodes	29765	68302
Faces	58965	135779
Exit Mach number	7.55	7.5
Exit temperature (K)	96	96.6
Exit pressure (Pa)	88.9	88.8

Because our study in interested in figuring the rocket performance, we will focus our mesh test on viewing how the Mach number is changing
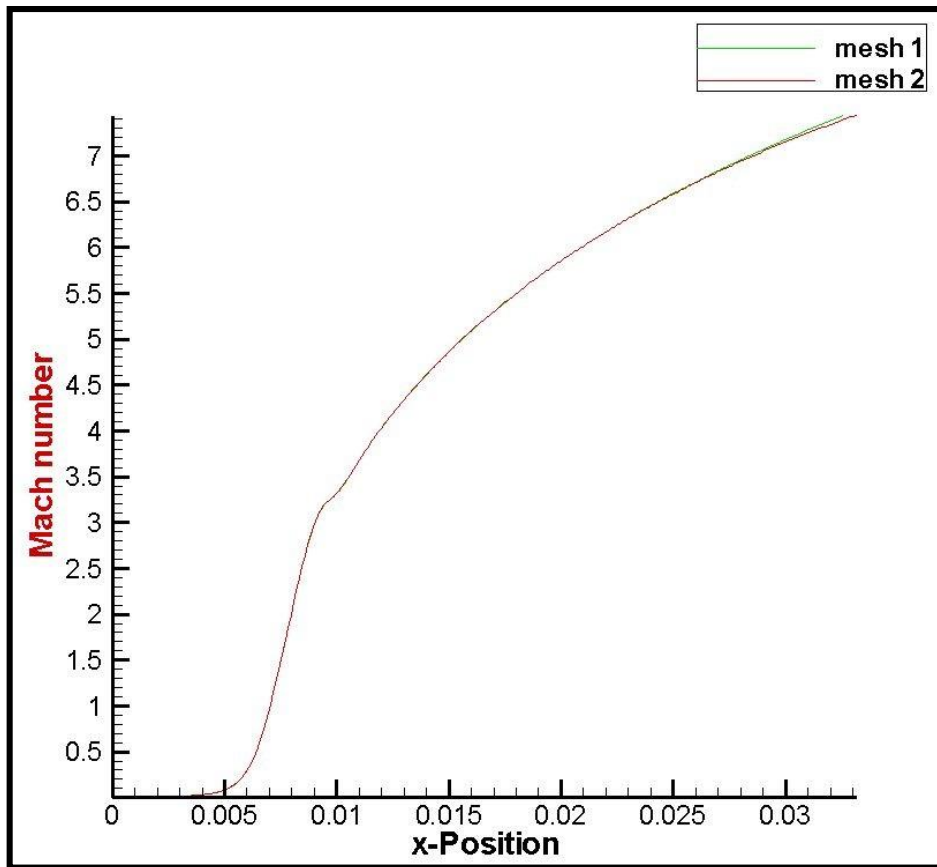
Figure 4-11: Grid independency for Inviscid case, Mach number

From Figure 4.11 we can see that the plots for both meshes are identical at all x-Positions and, so we could achieve grid independency from the second mesh. The plots shows that we have a good result since both gave the same solution.
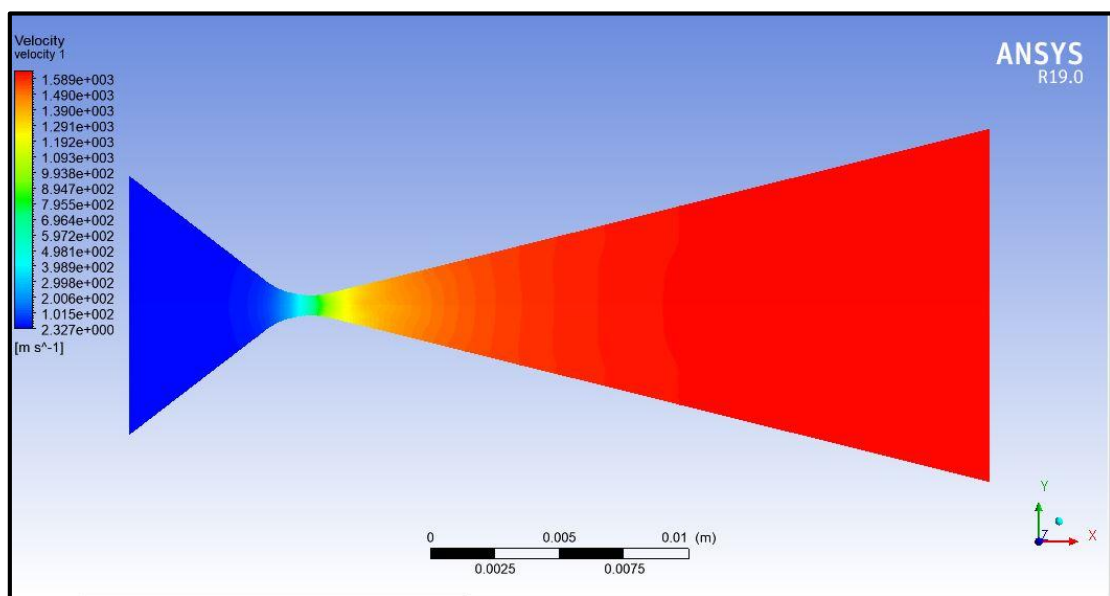
- **Velocity**

Figure 4-12: Full view of Velocity magnitude inside the corps.
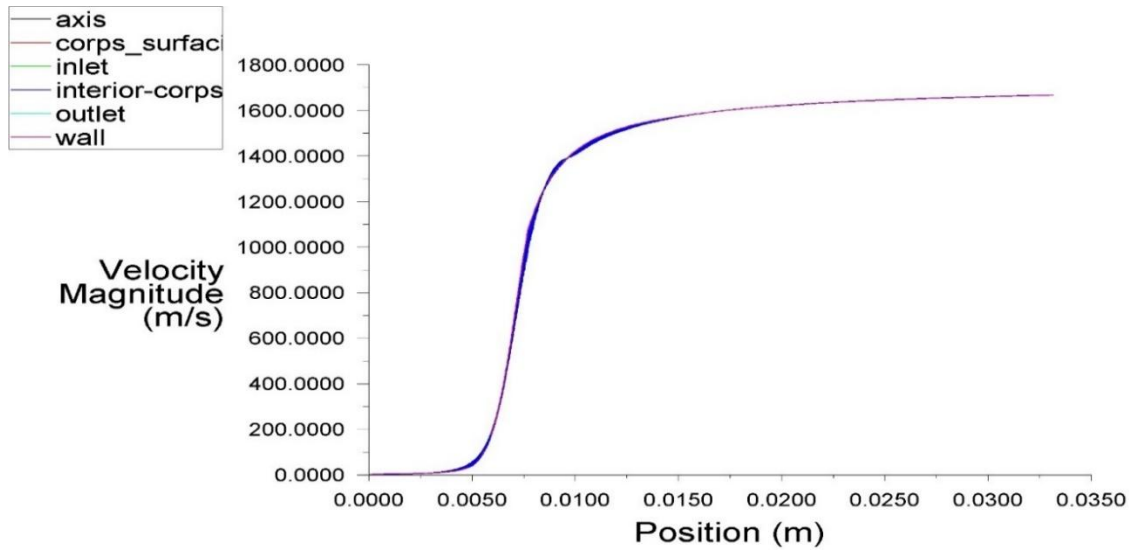
Figure 4-13: Velocity change inside the full corps.

Figures 4.12-4.13 shows the variation of velocity magnitude along the axis of symmetry (X axis).

According to Figures 4.12-4.13, the area surface in decreasing from inlet and reaches its minimum at the throat section. In the same time the subsonic flow velocity is increasing.

From throat to outlet the surface area is increasing, and we can also see that the velocity kept rising and reached $Ve = 1638\ m.s^{-1}$ at the outlet.

Near wall regions and far wall regions have almost the same values, this is due to the inviscid flow.

The Velocity contour start from the color bleu which refers to a low velocity at the inlet $Vi = 2.3\ m.s^{-1}$, then start to change gradually into red which refers to very high values in the nozzle outlet.

We can see from the Plot (Figure 4.13) obtained by ANSYS fluent 19.0 that the speed increased in convergent then sharply rises in the throat, the flow then is expanded throw the divergent and the velocity rises gradually.

These obtained results correspond to Hugoniot law which states that the speed is inversely proportional to are section for subsonic flow, and it is proportional to area section for supersonic flows.
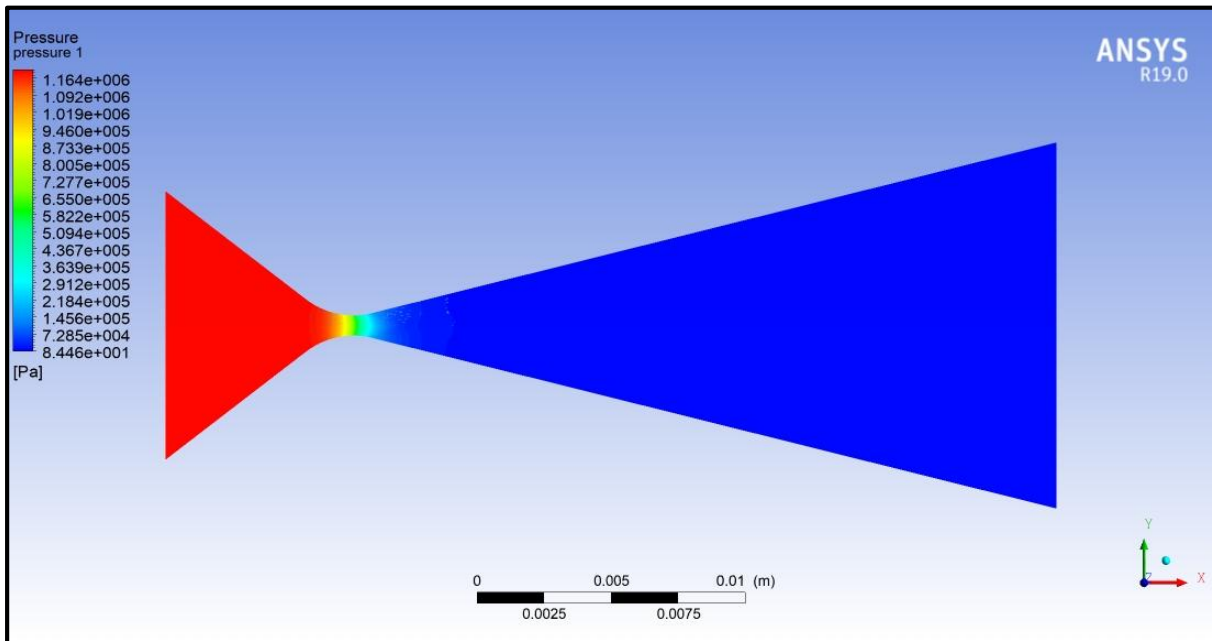
- **Pressure**

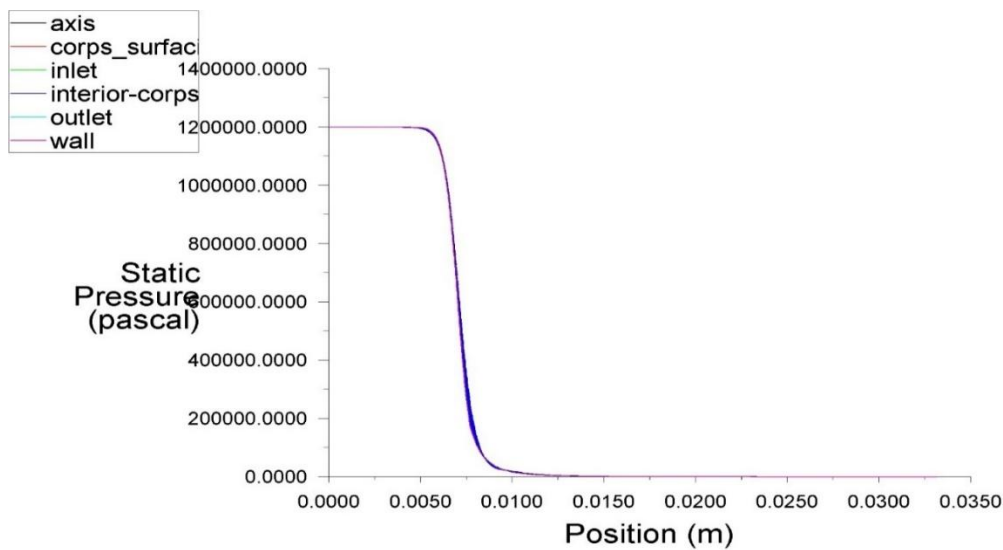Figure 4-14: Full view of Static Pressure inside the corps.

Figure 4-15: Static Pressure changes inside the full corps.

Figures 4.14-4.15 shows the variation of Static Pressure along the axis of symmetry (X axis). Static pressure is measured when the fluid is at rest relative to the measurement.

In contour of Figure 4.14, the pressure is red (high pressure) in inlet and decreases gradually until becoming bleu (low pressure) on the nozzle outlet in an isentropic way.

In plot of Figure 4.15 we can see that the pressure at inlet is very high Pi= 12e5 pascal which is the pressure coming from the catalysts chamber, after that we notice a significant decrease of static pressure in the throat area. And keep going down in the divergent zone with a value of Pe=73 pascal at the outlet.This rapid decrease is transformed into very quick increase in velocity seen previously. Pressure transformed into kinetic energy.
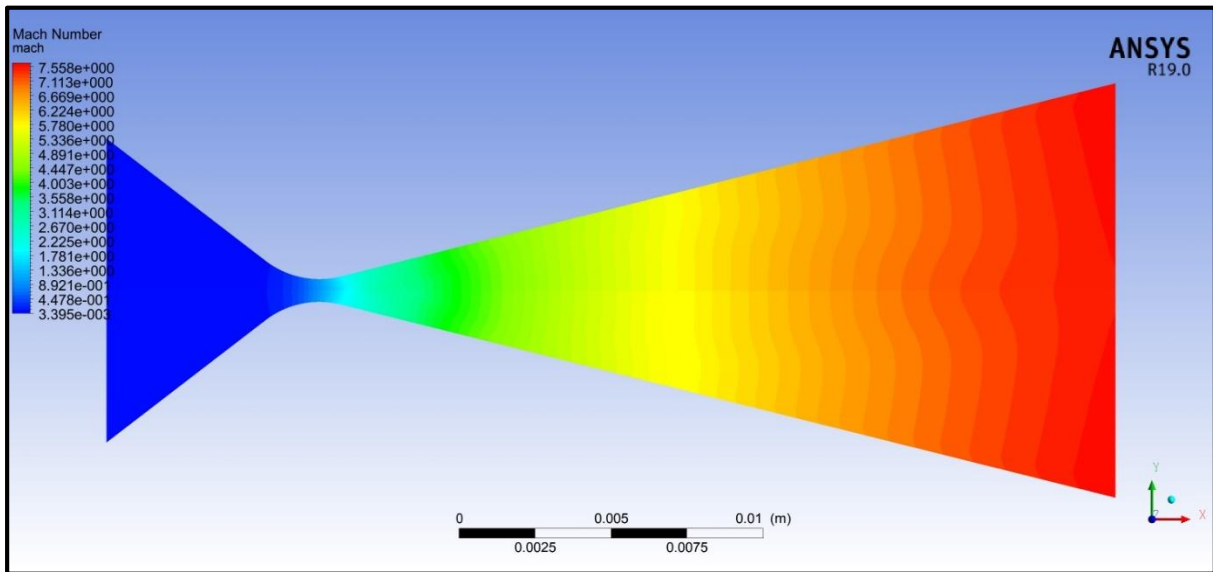
- **Mach number**

Figure 4-16: Full view of Mach number inside the corps.
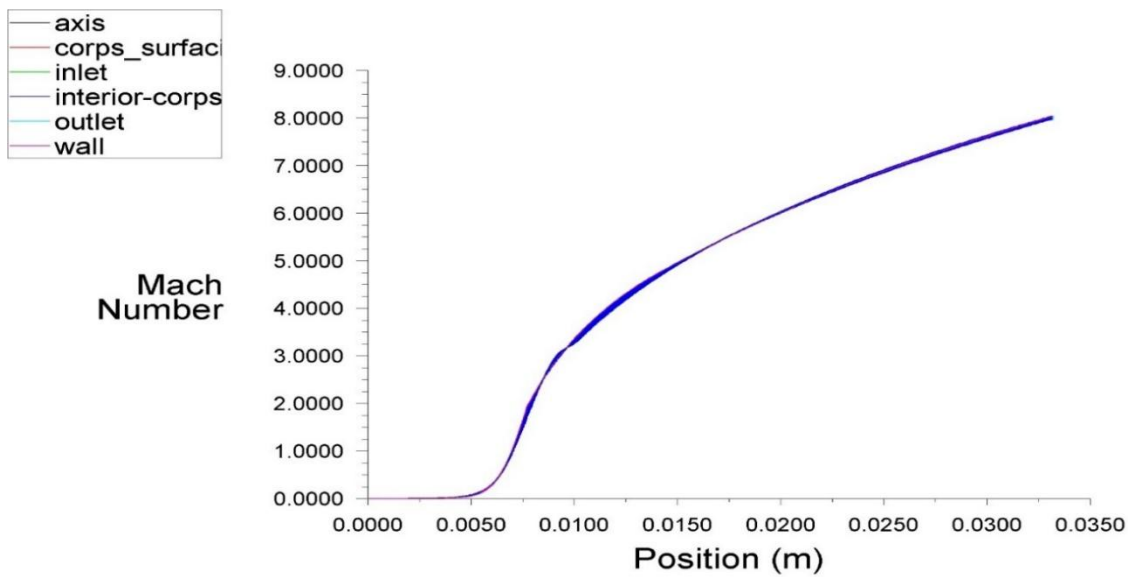

Figure 4-17: Mach number change inside the full corps.

Figures 4.16-4.17 shows the variation of Mach number along the axis of symmetry (X axis). Figure 4.16 shows that the Mach number obtained in the inlet is subsonic and very low ($Mi=3.4e-3$), we can observe that the Mach contour is bleu in the inlet and start changing in color and turn into light blue in throat area which refers to $Mt=1$, the color in the divergent region of the nozzle keeps changing and it becomes red in the outlet (high Mach number).

Plot of Figure 4.16 shows that the Mach number was very low (subsonic flow) in Inlet and increase rapidly in the throat area, we can notice that the flow is sonic in the throat, and that

what make the flow become supersonic in the divergent zone where the Mach increases until it reaches Me=7.55 at the outlet.

These obtained results correspond to Hugoniot law which states that the Mach number is inversely proportional to area section for subsonic flow, and it is proportional to area section for supersonic flows.
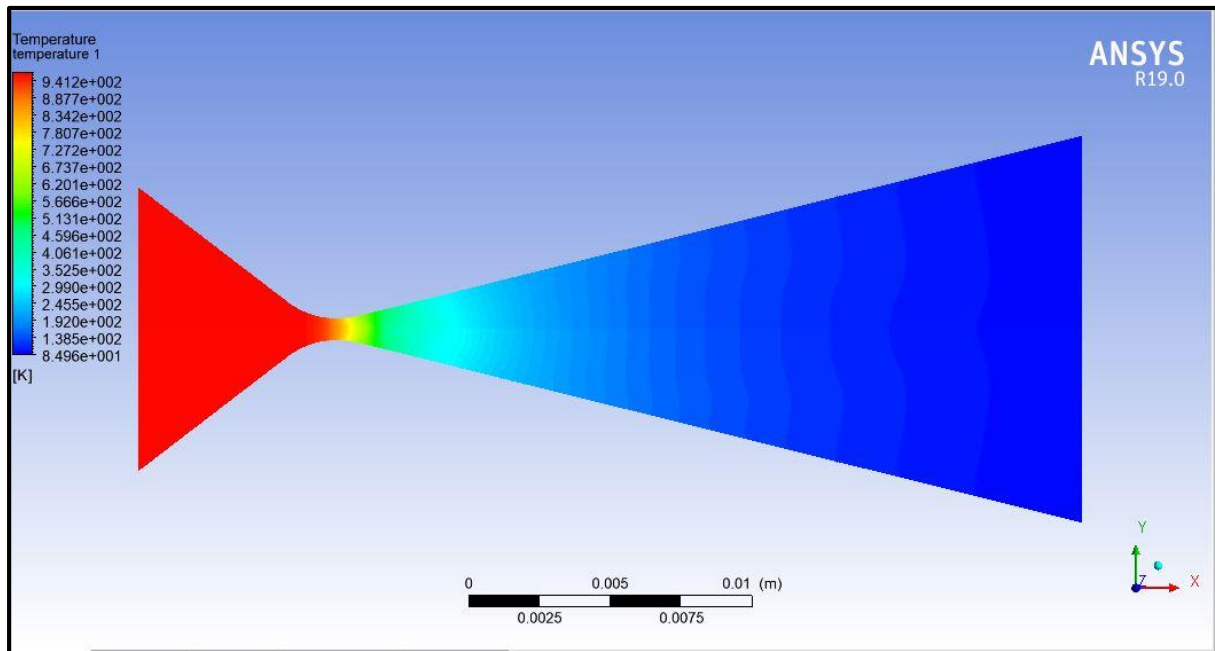
- **Temperature**

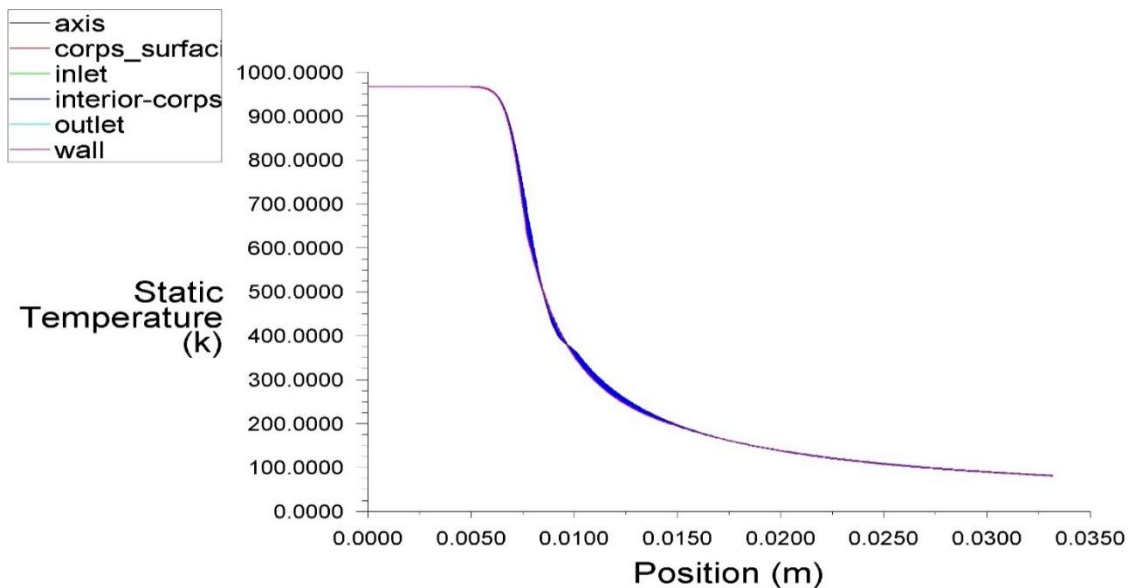Figure 4-18: Full view of Static temperature inside the corps.

Figure 4-19: Static temperature change inside the full corps.

Figure 4.18 shows the contour of static temperature along the convergent divergent nozzle, the contour is red in the inlet because of high temperature obtained from the decomposition of H_2O_2 ,the red color is becoming lighter while the flow passes from inlet through convergent arriving to throat, which means that the temperature decreased. In the divergent part of the nozzle the temperature contour changes its color and become bleu at the outlet (low temperature).

The temperature gradient is the same near wall and far from wall, this is due to the inviscid flow and the absence of thermal boundary layer.

Because the flow is isentropic, the evolution of temperature is proportional to the pressure, and this correspond with the perfect gas law. We can obviously see it in Figure 4.18 where the temperature in the nozzle keeps going down while we go from inlet to outlet.

In Plot of Figure 4.19 the temperature is high Ti=968 K at the inlet, and then decreases rapidly in throat region, then gradually in the divergent nozzle Te = 84 K.

4.5   <u>Viscous flow H2O and O2</u>

Real nozzles have a viscous boundary layer next to the nozzle walls, where the gas parameters meet some conditions, which make it differ much more than the free-stream gas in the inviscid flow regions. A clear schematic view of a boundary layer is presented in Figure 4.20, right after the wall the flow parameters are consequently derivative with boundary layer that can be considered as being built up of successive annular shaped thin layers until the we reached the exit area.

The gaseous boundary layer has a profound effect on the overall heat transfer to nozzle and chamber walls. It also has an effect on the rocket performance, particularly in applications with relatively long nozzles with high nozzle area ratios, where a relatively high proportion of the total mass flow (2 to 25%) can be in the lower-velocity region of the boundary layer. The high gradients in pressure, temperature, or density and the changes in local velocity (direction and magnitude) influence the boundary layer as they will be seen in the upcoming figures for the second case. [29]

Scaling laws for boundary layer phenomena have not been reliable. Theoretical approaches to boundary layer performance effects can be found in Chapters 26 to 28 of Reference [123]. A truly satisfactory theoretical analysis of boundary layers in rocket nozzles has not yet been

developed. Fortunately, the overall effect of boundary layers on rocket performance has been small. For most rocket nozzles the loss seldom exceeds 1% of specific impulse. [29]
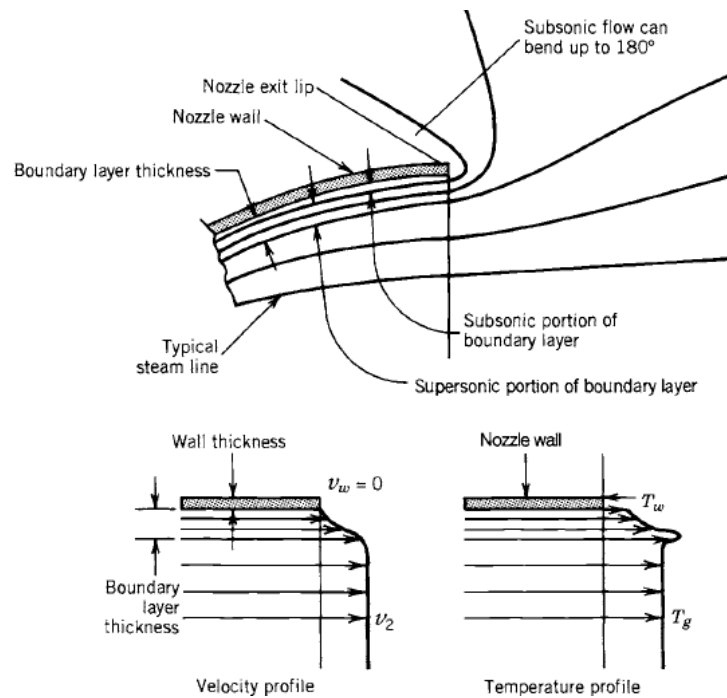

Figure 4-20: Flow conditions at a nozzle exit lip at high altitude, showing streamlines. [64]

Case study 2

The boundary conditions used in case two of the three-step simulation is found in Table ….

Boundary/Cell Zone Conditions

Solver Type	Density-Based
	Absolute
	Study – Axisymmetric
Models	Energy (on)
	Viscous (K-omega-SST)
	Species Transport –Mixture Templates
	- volumetric Reaction
	- Inlet diffusion – Finite Rate /Eddy-dissipation
Fluid	mixture : $H_2O + O_2$
	Cp : piecewise-linear
	: Mixing Law
Operating condition	Pressure = 0 Pa
Wall-Porous and nozzle zone	**wall**

	Heat transfer coefficient = 20 w/m2-K
	Free stream Temperature = 288 K
	External Emissivity = 0.3
	External Radiation Temperature = 288 K
	Wall Thickness = 0.002425 m
	Wall material = Steel

Inlet Mass flow	inlet
	Pressure = 1200000 Pa
	Turbulence intensity = 5%
	Viscosity ratio = 10
	Liquid mass flow rate=0.599 g/s
	Liquid temperature = 968 K
	Species mole fraction:
	H_2O=0.7175
	O_2=0.2825

Outlet	Pressure-outlet
	Gauge pressure = 100 Pa

Methods	Solution Methods
	Second order Upwind – Turbulent kinetienergy (k)
	Second order Upwind – Specific Dissipation rate (omega)
	Second order Upwind – Flow
	Roe – FDS – Flux type
	Implicit Formulation

The simulation was run for 5200 iteration and converged by a precise error less than 10^-5. The simulation results presented in this chapter was obtained at the simulation time approximately 120 minutes

82

- **Mesh test**

As for the previous case, the second study case simulations need a mesh test independence, for that reason we did our check in order to see if our results are good enough and to see how the mesh adaptation will influence them. In this case the near wall region is the region that needs more focus because of boundary layer effects and because the gradient change in this region is significant. Table 4.3 will show us results obtained from different meshes.

Table 4-3: Viscous low case study grid independence.

Adaptation	Initial mesh	Adaptation 1
Cells	29250	117000
Nodes	29666	117800
Faces	58915	234830
Exit Velocity (ms^{-1})	1654.912	1655.08
Exit Mach number	7.15	7.16
Exit temperature (K)	104.59	104.6
Exit pressure (Pa)	100	100
Y+	1.35	0.68

From the table we can see that the results for the initial mesh and after mesh adaptation are perfectly matched, this leads to conclude that our results are correct and are not affected by mesh refinement.
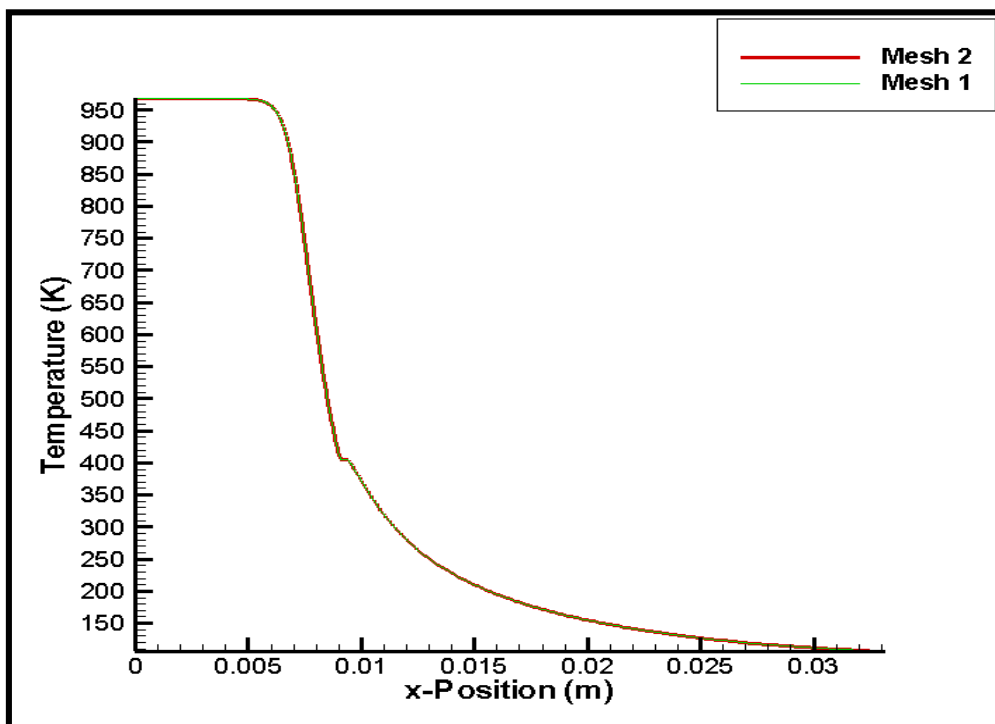

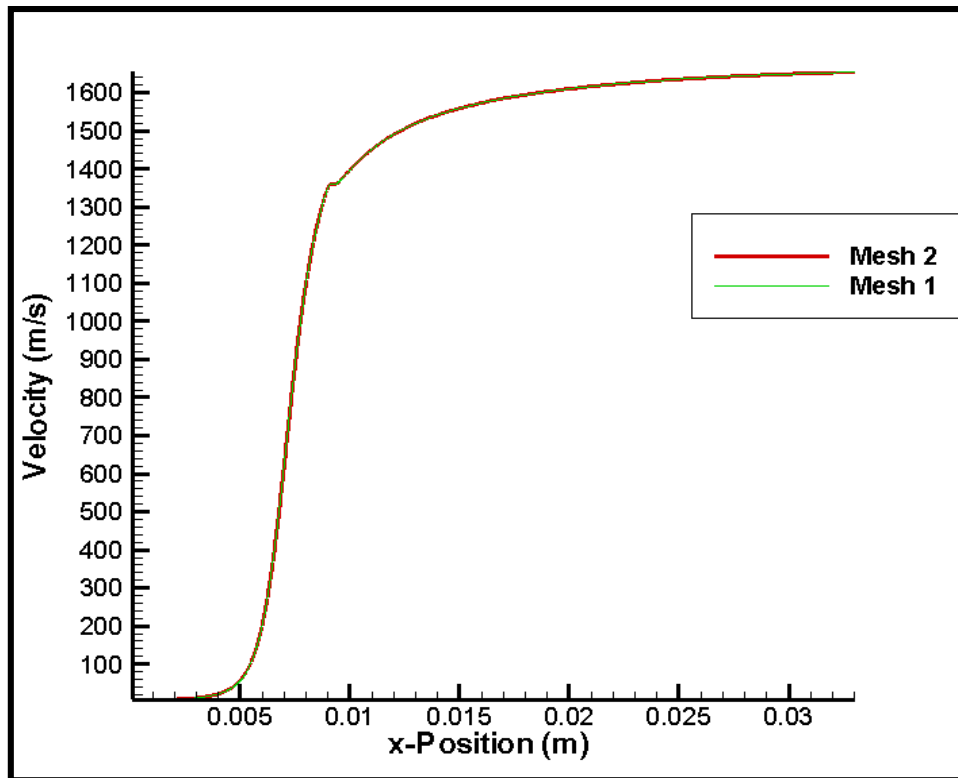Figure 4-21: Grid independency for viscous case, temperature.

Figure 4-22: Grid independency for viscous case, velocity.

As the previous case, the plots are identical for both meshes and the mesh test approved that the obtained results are good. A one remark can be mentioned is that for the second mesh (adaptation 1) the time taken for the simulations was long, almost 8 hours comparing to the first mesh 2 hours, this time difference will lead us to make a choice in order to pick a good mesh that gives good results in less time.

- **Velocity**

Figure 4.23 is a good representation of velocity change in the full corps. Meanwhile, Figure 4.24 present a detailed changes, right after the wall the flow velocity is zero and then the boundary layer can be considered as being built up of successive annular shaped thin layers of increasing velocity until the free-stream velocity is reached figure 4.25 demonstrate the change of velocity in x-axis . The low-velocity flow close to the wall is laminar and subsonic, but in the higher-velocity regions of the boundary layer, the flow is supersonic and can become turbulent. The velocity near to the wall is facing the no-slip condition, it is there by fulfilled more. We increase the distance away from the wall the velocity degradation increase and the shear stress were the boundary layer decrease.

Close to the nozzle exit an increased velocity of the oxygen and water vapor plume. It can be seen that the velocity of mixture attends its maximum injection speed at the exit region attending a velocity equal to 1655 m/s.
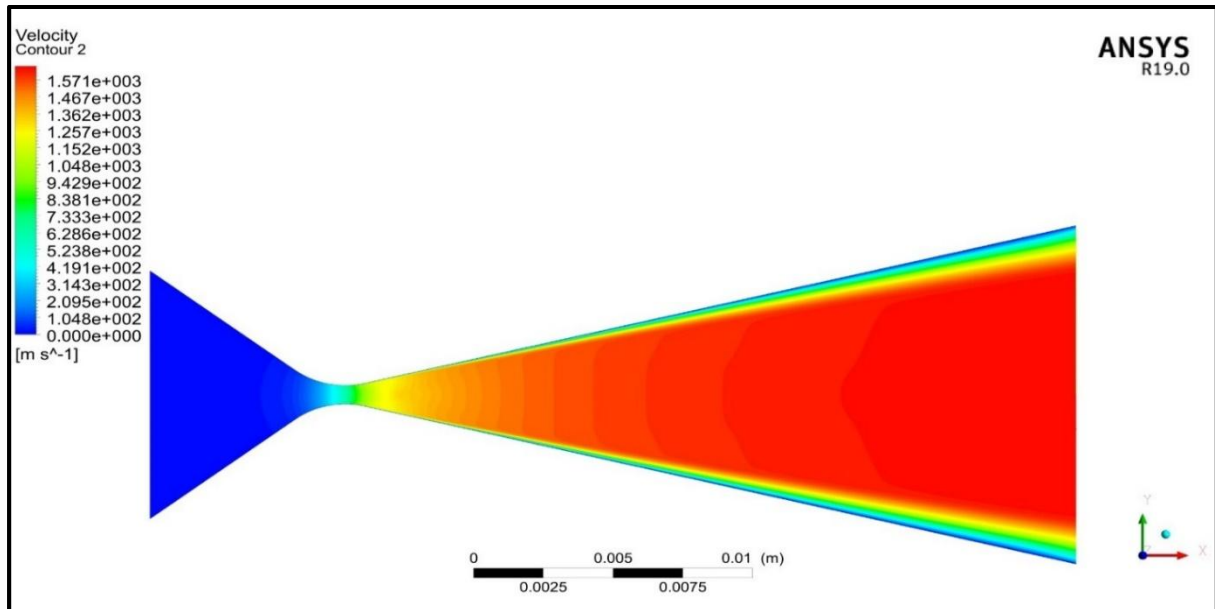

Figure 4-23: Full view of Velocity magnitude inside the corps.
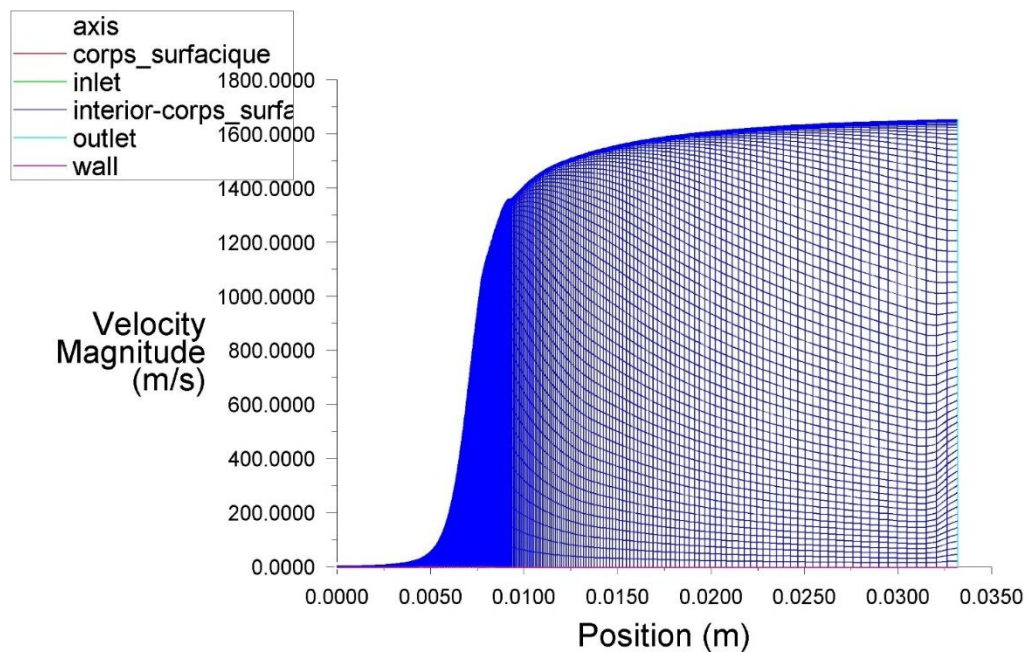

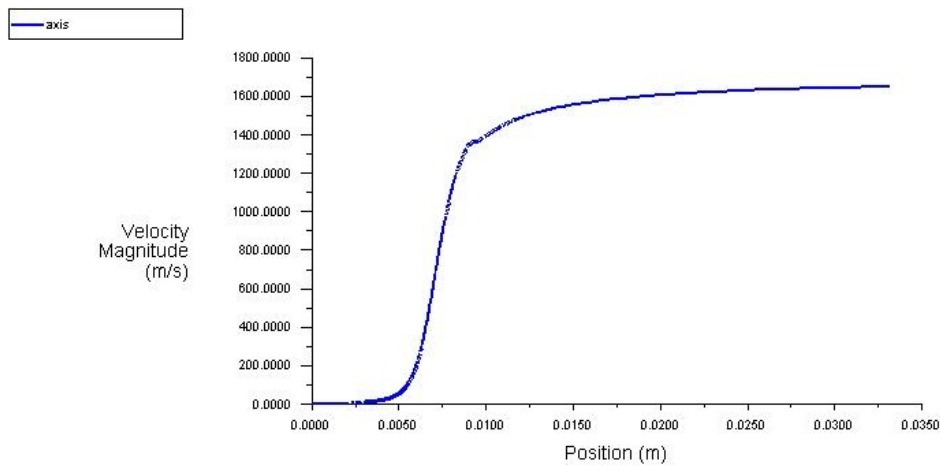Figure 4-24: Velocity change inside the full corps.

Figure 4-25: Velocity change in x-direction.

- **Mach number**

From the contour plot of the Mach number Figure 4.26 it is clear that there is an existence of boundary layer, where the Mach number approach to zero $3.31 * 10^{-5}$ at the wall and its increase slightly more we pull away from the wall.

In the converging section, we have a subsonic flow approximately, 0.453 without any boundary layer, then can be seen that the Mach number reaches rapidly to sonic flow 1 in the nozzle throat region, and the nozzle is thereby choked.

From the nozzle throat region to the nozzle exit, the gas phase has entered into a hypersonic speed regime. In this region, the gases are accelerated towards the exit, which concur with the Hugoniot theory of a supersonic convergent divergent nozzle where it achieved M = 7.157.

Mach number along the axis of the nozzle, a small bump can be seen in Figure 4.28. The reason for this was found to be caused by a small offset in the conical form in the nozzle divergent section. With this error accounted for, the results show that they concur with the theory of a supersonic convergent divergent nozzle [121].
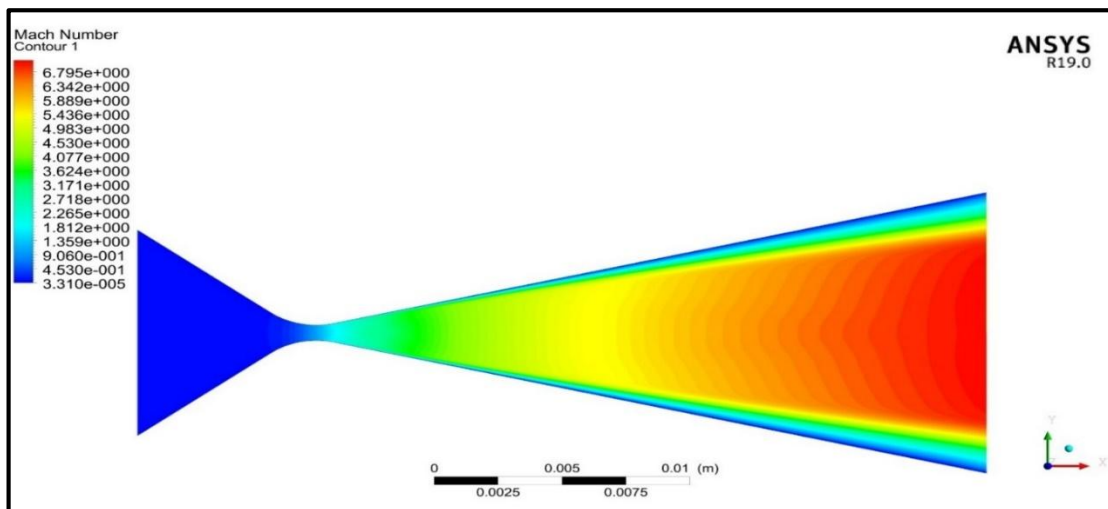

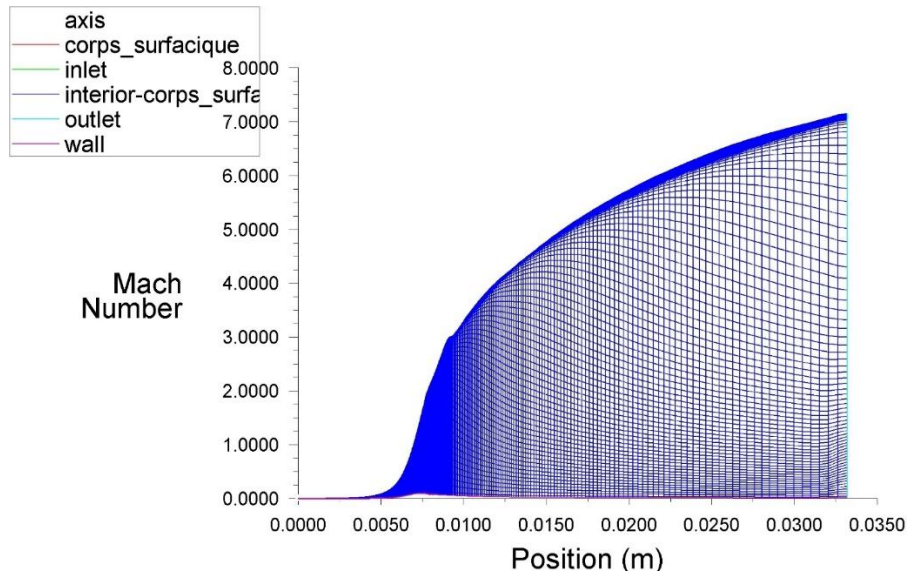Figure 4-26: Full view of Mach number change.

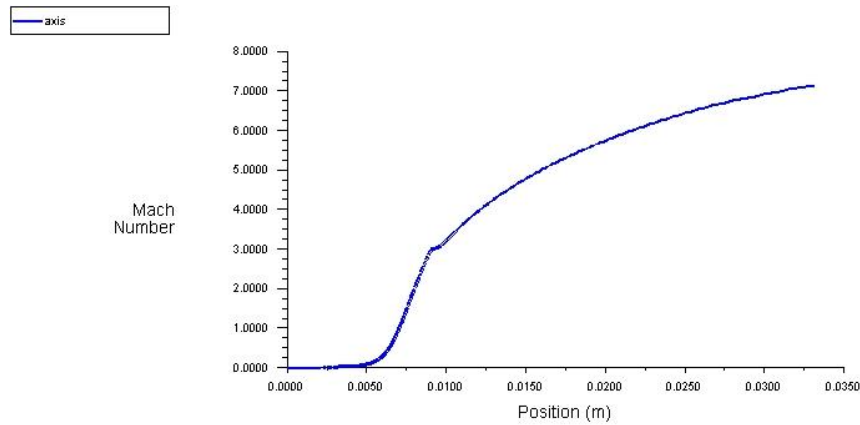Figure 4-27: Mach number change inside the full corps.

Figure 4-28: Mach number change in x-direction.

- **Temperature**

The plot of the gas phase static temperature is found in Figure 4.26 & Figure 4.27, it is seen that the static temperature remains maximum 968 K and constant in the converging part until the flow reaches the nozzle throat and transitions to supersonic flow, it is worth that the static temperature decreases towards the nozzle exit where it reached approximately 104.6 K.

The local temperature in part of the boundary layer can be substantially higher than the free-stream temperature Figure 4.27 because of the conversion of kinetic energy Figure 4.29 into thermal energy as the local velocity is slowed down and as heat is created by viscous friction. The layer right next to the wall will be hotter because of friction.

However, if the system were considered as insulated, wall temperature would be higher than our case study because of the absence of convection heat exchange between exterior surroundings and nozzle, and because of the non-emissivity of radiation from wall surface.

For our case study the simulation is not isentropic, this change can be accorded for by the heat loss at the walls of the thruster. In the nozzle region the stagnation temperature remains constant which is in accordance with supersonic nozzle flow.
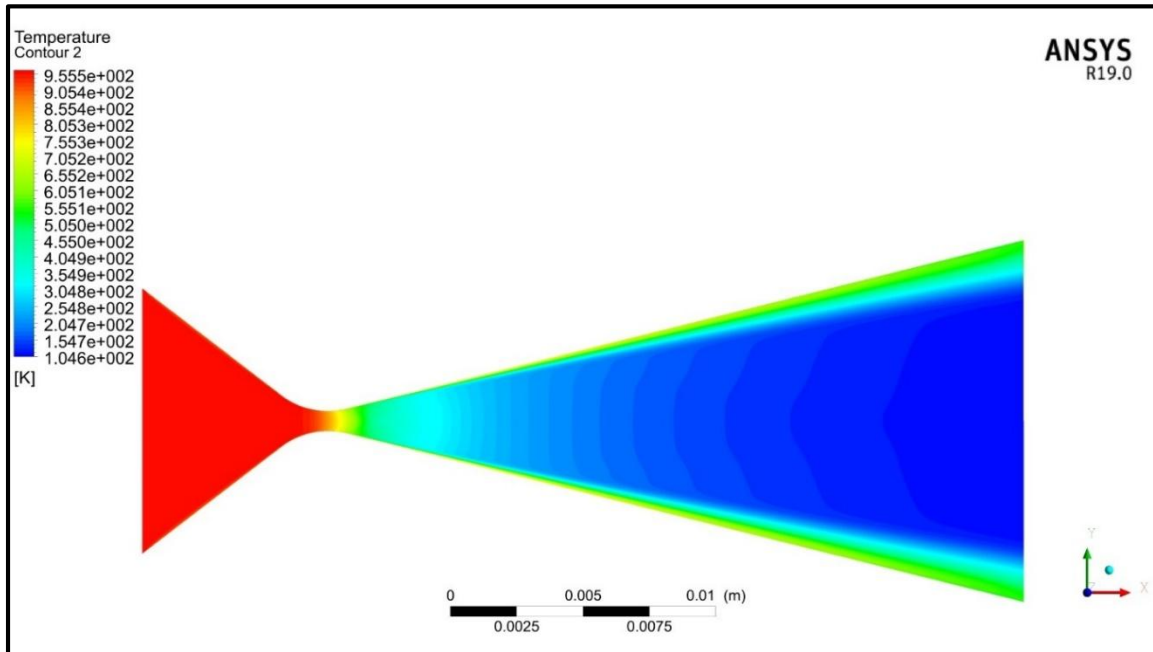

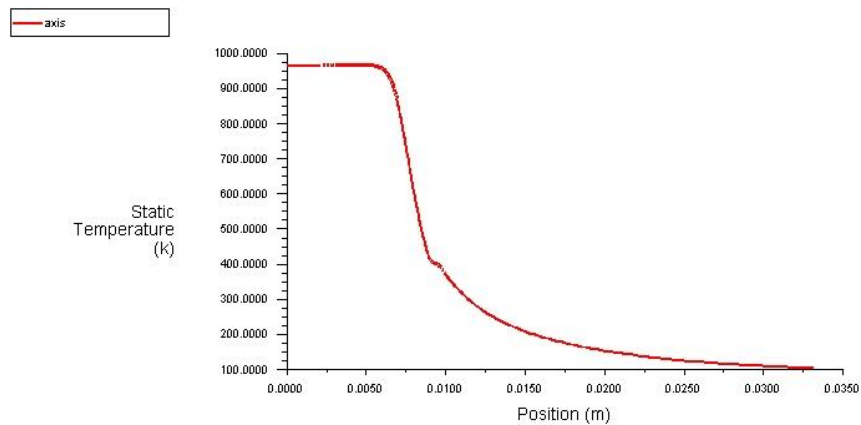Figure 4-29: Full view of Static Temperature change.

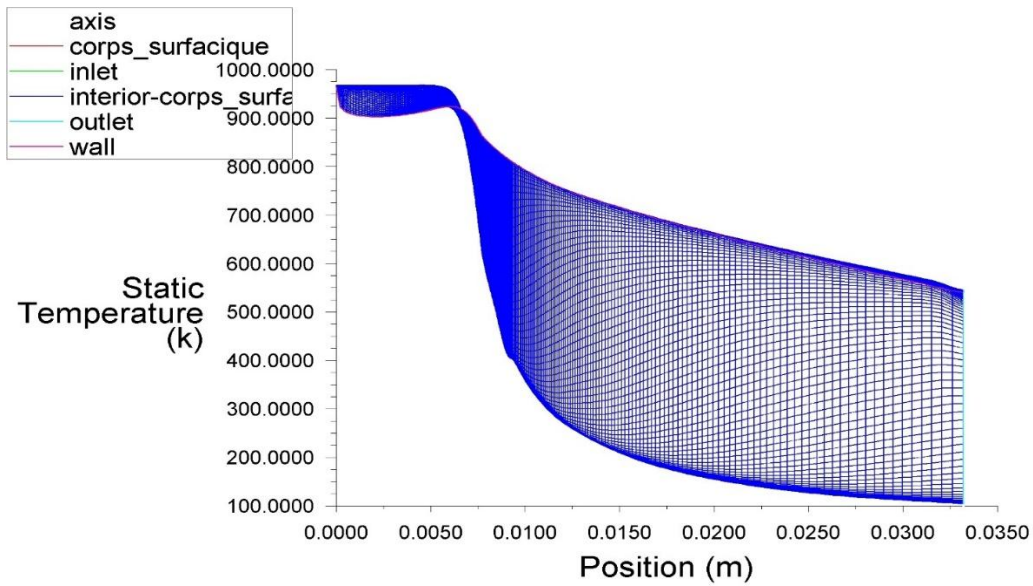Figure 4-30: Static Temperature change for x-axis.

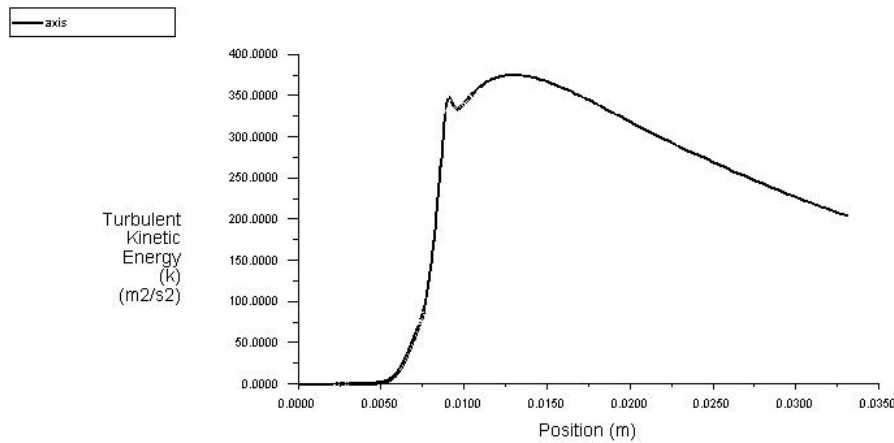Figure 4-31: Static Temperature change for all the corps.

Figure 4-32: Turbulent kinetic energy on the x-axis vs position.

- **Pressure Distribution**

The change of the absolute pressure field in the thruster found in Figure 4.33 does not has a difference with pressure distribution in the first case Figure 4.14. The pressure max is meant to be at inlet section represented by red color $12 * 10^5$ Pascal (converging section) and it decrease gradually through the nozzle convergence and meet a critical change in the throat until the flow enters the diverging nozzle section where it meets a transitions flow into a supersonic flow. The pressure decreases sharply in the divergence side until the nozzle exit where it reached 100 Pascal representing the reference value of this study, and the gradient of pressure in the y-axis is constant. And this match with boundary layer theory when solving the momentum equation in Y-axis.
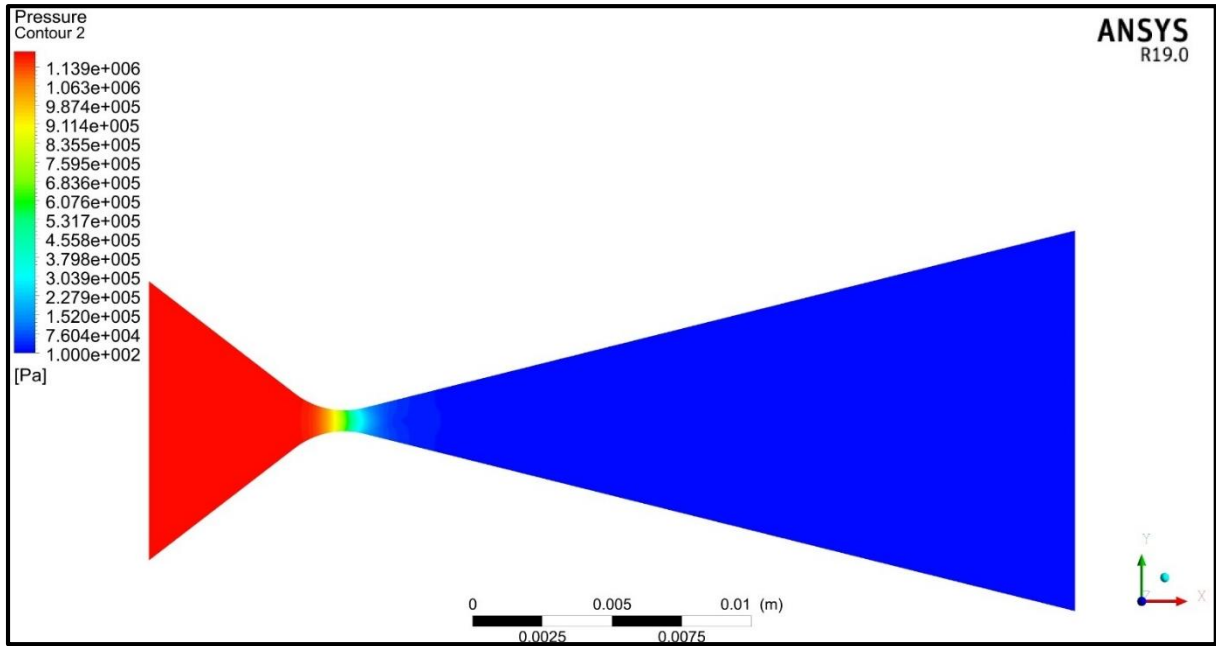
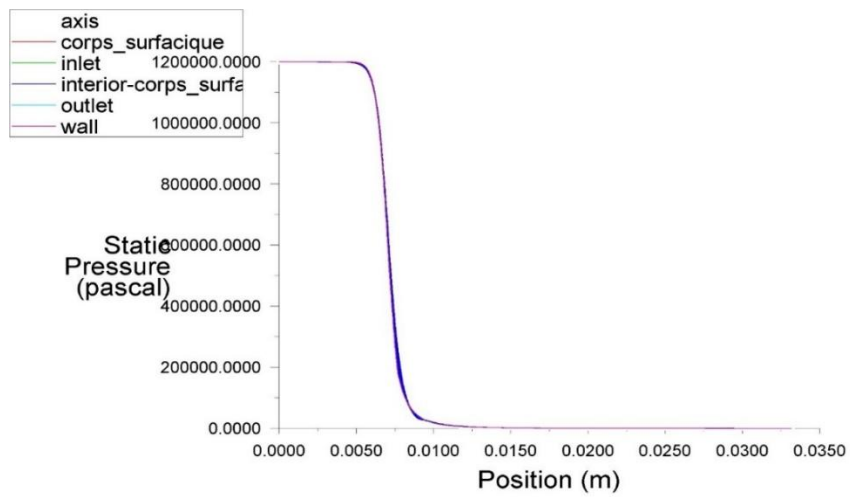Figure 4-33: Full view of static pressure change

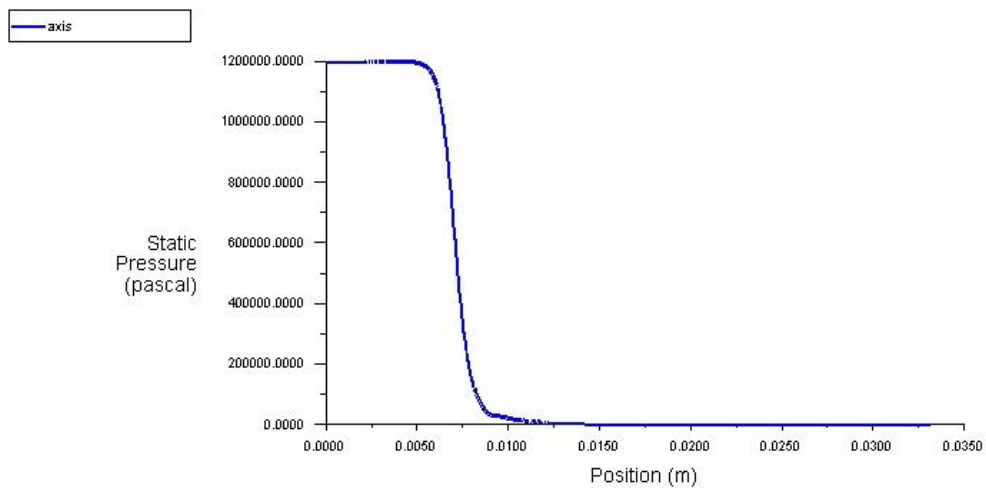Figure 4-34: Static pressure changes inside the full corps.

Figure 4-35: Static pressure changes in x-direction

- **Turbulence**

In fluid dynamics, turbulence or turbulent flow is fluid motion characterized by chaotic changes in pressure and flow velocity. It is in contrast to a laminar flow, which occurs when a fluid flows in parallel layers, with no disruption between those layers.[53]

Turbulence is caused by excessive kinetic energy in parts of a fluid flow, which overcomes the damping effect of the fluid's viscosity. For this reason, turbulence is commonly realized in low viscosity fluids. In general terms, in turbulent flow, unsteady vortices appear of many sizes which interact with each other, consequently drag due to friction effects increases. This increases the energy needed to pump fluid through a pipe.

The onset of turbulence can be predicted by the dimensionless Reynolds number, the ratio of kinetic energy to viscous damping in a fluid flow. However, A region where these forces change behavior in boundary layer, such as the bounding surface in the interior of a pipe, turbulence has long resisted detailed physical analysis, and the interactions within turbulence create a very complex phenomenon. [125]

In the contour plot of Figure 4.36-4.37, we measure the change of Reynolds number. it is well known that for a fluid through pipe should exceed 2300 in order to have a turbulent flow.

However, in our case study let us start to analyze the change. it is remark that the change depends on the section, the first section the converging part at the wall part the Re is too low that attend a value of 4.78, more we move forward to the center of the converging part the Reynolds increase until 239, it noted that the flow is in a laminar state in the wall and in the middle of the section.

next we analyze the throat part we remark that the maximum value of Re is attended in the center of the throat (red color) Figure4.32 achieving a value equal to 377.677 until then the value achieved is still in the laminar range. Finally, in the diverging section Re decrease dramatically until it achieves $1.609 * 10^{-6}$. We conclude from the analysis that our flow was laminar in the entire nozzle sections and that is due to the low thrust recommended.
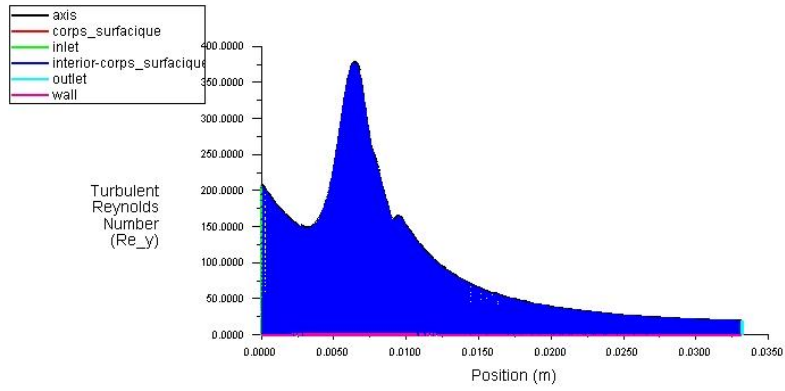
Figure 4-36: Reynolds number Turbulence full change.
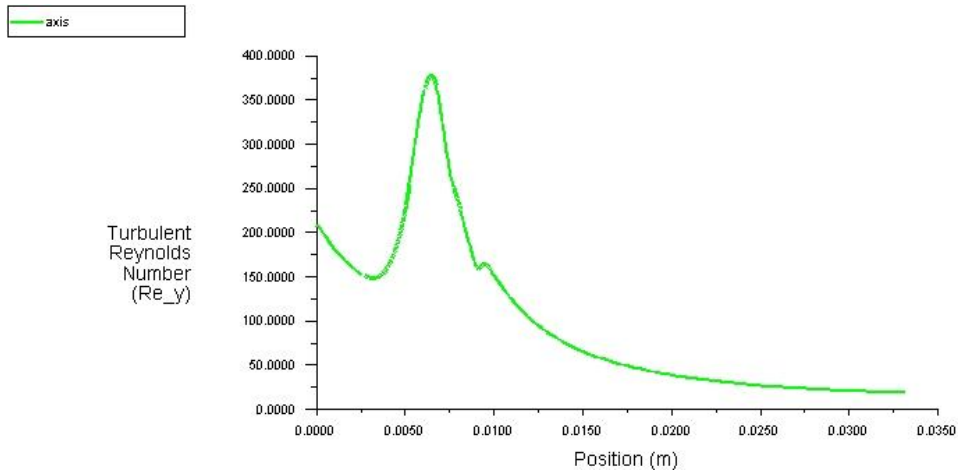
Figure 4-37: Reynolds number Turbulence appearance in x-axis.
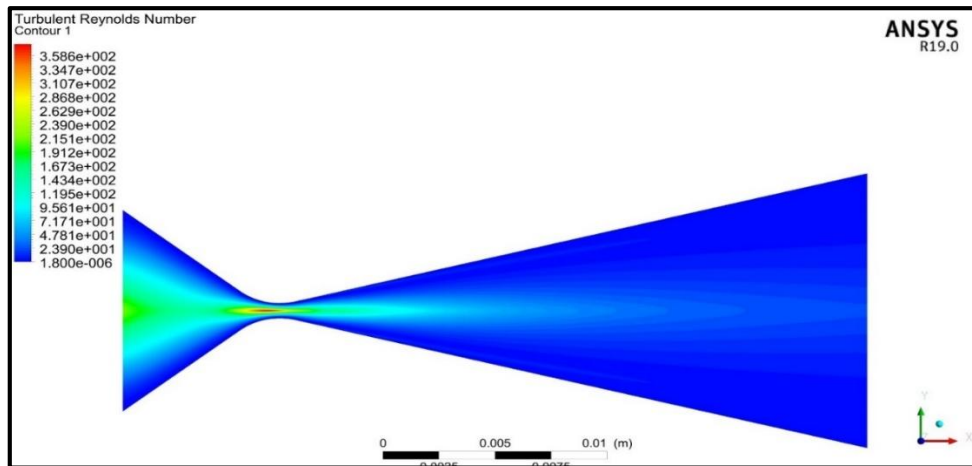
Figure 4-38: Reynolds number Turbulence appearance.

- **Yplus**

y+ is a non-dimensional distance. It is often used to describe how coarse or fine a mesh is for a particular flow pattern. It is important in turbulence modeling to determine the proper size of

the cells near domain walls. The turbulence model wall laws have restrictions on the y+ value at the wall (Schlichting and Gersten 2001)

$$y+= \frac{y u\tau}{v} \quad (4\text{-}1)$$

$$u\tau = \sqrt{\frac{\tau_{wall}}{\rho}} \quad (4\text{-}2)$$

1. u_τ is the so-called friction velocity
2. y is the absolute distance from the wall
3. v is the kinematic viscosity

as can be seen in Figure 4.33 the y+ depends on the type of layer should be studied.
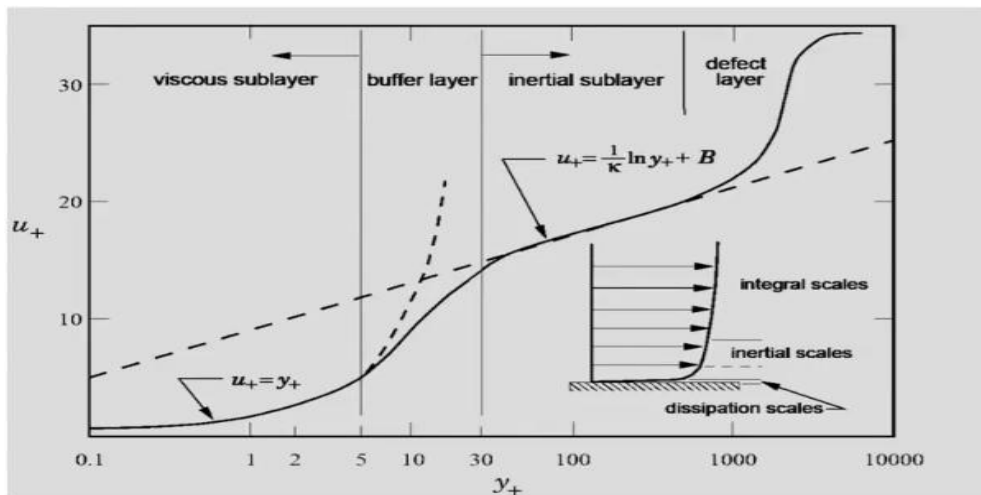
Figure 4-39: Dependency of layer with y+
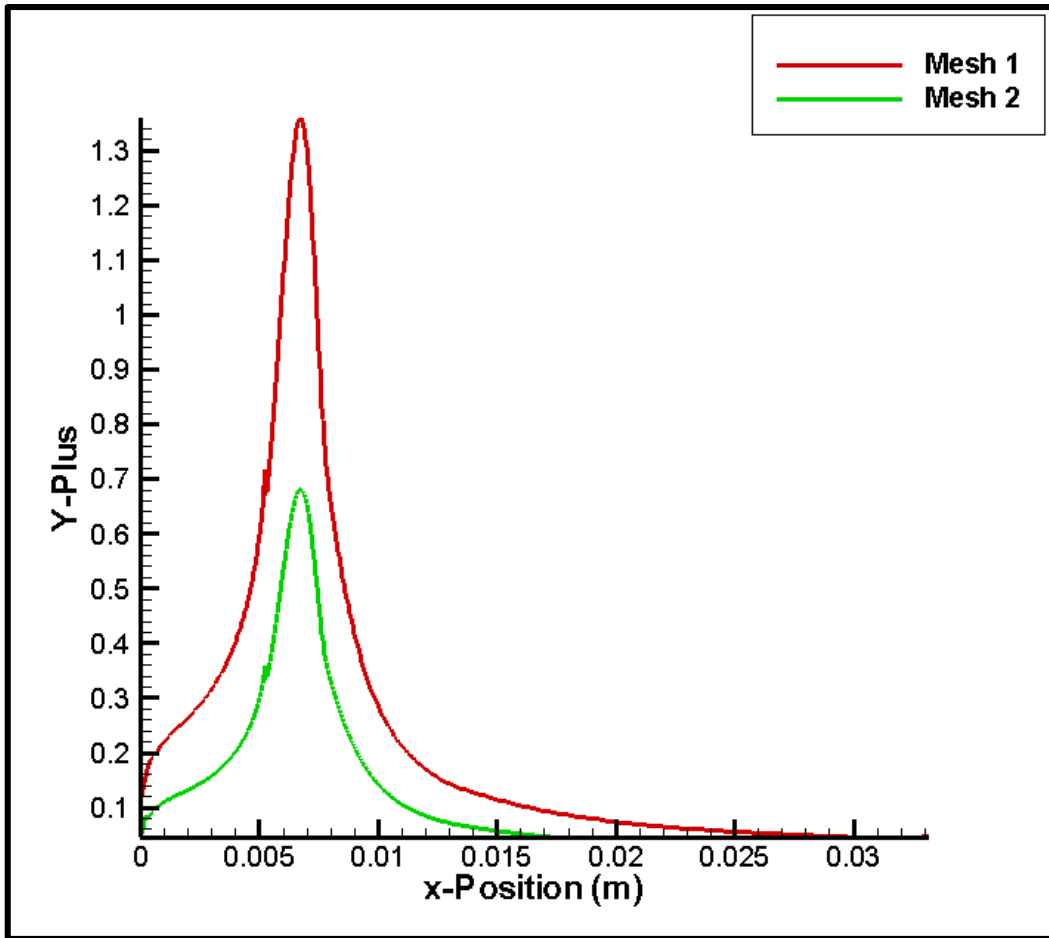
Figure 4-40: Grid independency for viscous case Y+ .

From Figure 4.40, we choosed the K-ω SST turbulence model because it is a good model to determine the boundary layer near wall. We can see from the plots that the Y+ values didn't cross the maximum value which is Y+ =5 so the choice of the model was good.

For our case study it can be seen from Figure 4.35 that y+ attend it maximum value 1.358483 , however it change with change in position but does not exceed the range between [0,5].
With respect to the standard wall law the viscous sub-layer (y + <5) with the Reynolds tensor is equal to 377.677 we conclude the absence of pressure gradient in Y- axis which give low degradation of shear stresses which means the speed evolves linearly with the distance from the wall.
It is a proof that our work has the credibility to be validated since K-Omega-SST model for the simulation is respecting the rules of being 0 < y+ < 5.
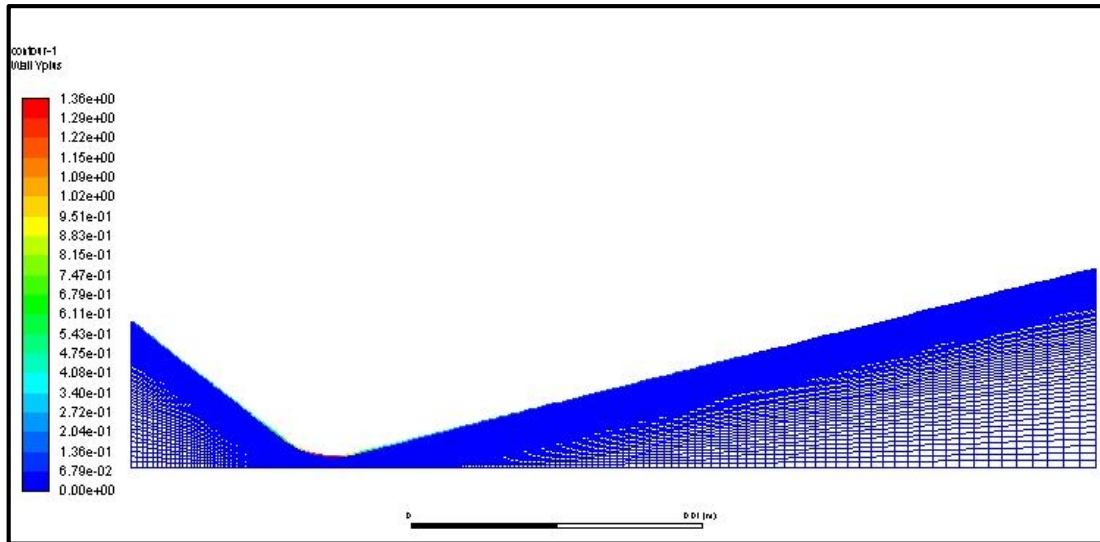
Figure 4-41: Y+ distribution inside the nozzle.
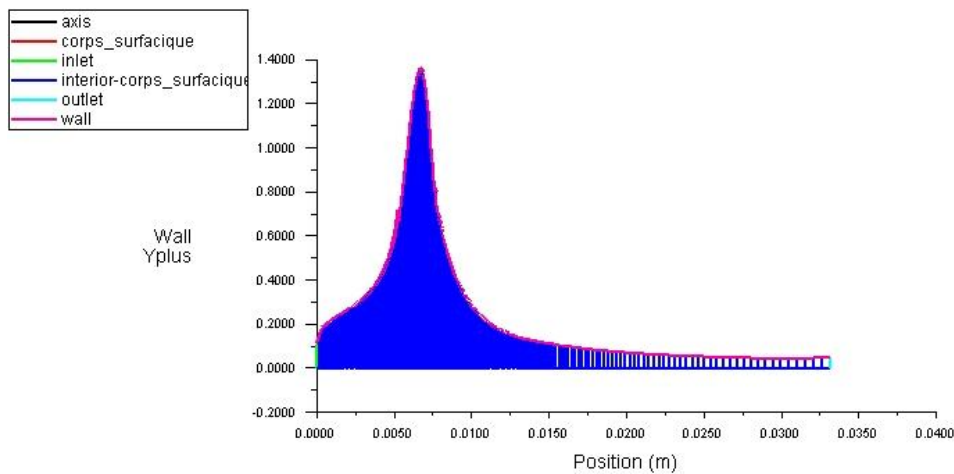
Figure 4-42: Y+ distribution for different position.

4.6 Check rocket performance

To check rocket thrust obtained by simulation in the viscous flow, case study number two. We divided the outlet of the nozzle into 1000 circular section. Using ANSYS FLEUNT CFD POST we imported the values of density, axial velocity and velocity of each section in a MICROSOFT OFFICE EXCEL file.

With MICROSOFT OFFICE EXCEL we calculated the area section, mass flow and thrust in each part. The following equations are used for the calculation.

$$\dot{m} = \rho.A.V \tag{4-3}$$

$$Thrust = \dot{m}.V_{axial} \tag{4-4}$$

95

To obtain the total thrust delivered from the thruster we summed all the partial thrusts calculated previously.

$$T_{TOT} = \sum_{i=1}^{1000} T_i \qquad (4\text{-}5)$$

We found that the total thrust is equal to $T_{TOT} = 0.933$ N

Comparing to the ideal performance of the rocket which is 1N, we can see that there is 0.067N lost. this loss is due to divergence of the flow at the exit and also because of the viscosity and the frictional loss inside the boundary layer.

Table 4-4: Performance comparaison

$Ideal$ thrust$[N]$	$Obtained$ thrust$[N]$	$LOSS[N]$	$Change\%$
1	0.933	0.067	99.3

4.7 **Results and comparison**

This part represents test conception and performance comparison, the results were found using Matlab®2017 and ANSYS FLUENT 19.0, the basic idea of this comparison is to find out how study conditions effect the outcome.

Table 4-5: Test conception and performance comparison

Element	MATLAB	ANSYS Inviscid		ANSYS Viscous	
		Value	Change %	Value	Change %
Exit Velocity (m/s)	1669.1	1638	-1.84	1655	-0.85
Exit Mach	7.23	7.5	+3.73	7.15729	-1.1
Exit Temperature (K)	107	84	-21.5	104.49	-2.43
Exit Pressure (Pascal)	100	73	-27	100	0

Through the entire analysis using different programs and several conditions its noteworthy to come to the conclusion that the outcome gained supposed to be valid and integrated into the high accuracy.

- Starting with the exit velocity change, it is found that in the program MATLAB is the highest comparing to the result in ANSYS using the Inviscid and viscous conditions respectively and the order of change is approximately 2%. The exit velocity found in the Inviscid and the Viscous conditions vary with MATLAB due to the difference between the standard constant value of specific heat given by ANSYS and the one found in the programme, and because of considering gases at high temperature, respectively.

- Following, the exit Mach number we get a little increase between the value from MATLAB and the Inviscid case. Meantime, obtaining slight decrease comparing to Viscous case due the exit temperature difference between three cases, it is concluded that the exit temperature effect Mach number, the change of temperature is resulted from the appearance of turbulent kinetic energy created from viscous condition. The exit Mach number in Viscous case study is the lowest which was anticipated due to the friction apparition caused by the boundary layer.

- Finally, for the exit pressure for the MATLAB study it was found 100 Pascal, in the other side we got 100 Pascal in the viscous condition, which means that our study in vacuum level has been approved.

CONCLUSION

The thruster is the most important part in propulsion system. This system criterion differs with mission requirement starting from altitude, weight and payload. This master thesis is a study of a thruster that produce one Newton (1 N) of thrust using green propellant H_2O_2 with concentration of 87.5 % that should be used in research satellite and it is composing of four parties.

The first part was dedicated to space propulsion history from the time of developing idea; after all, we mentioned different applications, stating some state of art models and giving their advantage and drawback maintaining our objective of the thesis.

Secondly, in order to evaluate the chosen thruster. The first step is to define the geometry, which means the dimensions of different parties of thruster and the type of nozzle used, With the help of the numerical method program Matlab-2017 to obtain these dimensions it is obligatory to pass through three steps starting from Thermochemistry analysis using Pricewise method, Theoretical Rocket Performance to Preliminary Thruster Design. Where we considered in the analysis that the flow is frozen, adiabatic, permanent, one-dimensional, and the fluid is considered as perfect non-Viscous. This hypothesis are sufficient in order to get the exact dimensioning, Chamber Temperature, Exit Velocity, Exit Mach number, and Mass flow. The second step is to select the right catalyzer so that to obtain a maximum accuracy while the chemical reaction is occurring, in this project we select gauze based silver catalyst after a set of comparisons with different types of catalysts maintaining a set of valuable characterization.

In the third part, we presented a brief definition on how SNSYS Fluent work, starting from continuity and moment equation, to turbulence models, until meshing characteristics. This section is so important to understand the exact algorithm of how the simulation should be done.

In the fourth part, we presented our model conception in ANSYS Fluent 19.0 program to simulate it, this model was presented in the program under atmospheric conditions, many tests have been done with different case of study (Viscous case & non-Viscous case, Vacuum & non-Vacuum) in this thesis. So from The outcome gained it has been proven that our education is credible comparing to previous work done by Dr.Amri Reda from university of Blida-Algeria and Dr.Matt Palmer from University of Southampton-England , which gave us the opportunities to manufacture our products precisely with correct measures of merits.

Finally, we modelled our result into CAD using Solid-works 2017 as it is presented in annex. Finally yet importantly, our research has been promoting some conditions to achieve approximately ideal results. However, our aim to the upcoming work is to consider some optimal perspective, which reinforce our work:

- Porous medium

- Eliminate the frozen flow assumption.

- If significant levels of contaminate are present within the propellant, feedsystem, or chamber, the effects of these impurities has to be modelised

- During the reaction through the catalyst, the entirety of hydrogen peroxide will not dissociate. The completeness of dissociation is dependent upon the catalyst and operational conditions. An optimal model would account for incomplete dissociation

- At high concentrations (>87.5%) of hydrogen peroxide aqueous solutions, the dissociation would also result an amount of OH, and other gaseous products.

REFERENCES

[1] M.J.L.Turner. History and principles of rocket propulsion.

[2] https://www.britannica.com/biography/Konstantin-Eduardovich-Tsiolkovsky

[3]https://www.larousse.fr/encyclopedie/personnage/Konstantine_Edouardovitch_Tsiolkovski/147593

[4] https://www.nasa.gov/audience/foreducators/rocketry/home/konstantin-tsiolkovsky.html

[5] https://www.britannica.com/biography/Robert-Goddard

[6] https://www.nasa.gov/missions/research/f_goddard.html

[7]https://www.linternaute.fr/science/biographie/1778038-wernher-von-braun-biographie-courte-dates-citations/

[8] https://www.universalis.fr/encyclopedie/lancement-de-spoutnik-1

[9] George P. Sutton. Rocket Classifiacion, Liquid Propellant Rockets, Engine Selection, and Heat Transfer. W.H.T.Loh. Jet,Rocket,Nuclear,Ion and Electric Propulsion:theory and desing.California.Springer

[10] Redha Amri.Etude et developement des systems de propulsion pour les applications spatiales.University of Blida,Institut of aeronautics,PHD thesis,2013

[11] Ahmed F.EL-Sayed. Fundamentals o aircraft and rocket propulsion. Zagzig Egypt: Springer

[12] Mojtaba Ghasemi.et.al. Design and Development of a Flight-model Cold Gas Propulsion System.tehran, Iran.2011

[13]Michael Zaberchik.et.al Fabrication and Testing of the Cold Gas Propulsion System Flight Unit for the Adelis-SAMSON Nano-Satellites.Haifa,Palestine.2019

[14]Assad Anis. Cold Gas Propulsion System – An Ideal Choice for Remote Sensing Small Satellites. NED University, Pakistan.

[15] AIAA, SAE, ASME, and ASEE, Joint Propulsion Conference and Exhibit, 28th, Nashville, TN, July 6-8, 1992. 8 p.

[16] Akshay Reddy Tummala et.al. An Overview of Cube-Satellite Propulsion Technologies and Trends. Wichita State University, USA.2017

[17] Ahmed.F.EL-Sayed. Chemical Rocket Engines

[18] Martin J.L.Turner. Rocket and spacecraft propulsion principles practice and new developments.2nd edition.leicester,UK.Springer.2005

[19] Mohamed Abd-Elghany et.al. Performance of advanced composite solid rocket propellants based on novel oxidizers. IOP Publishing

[20] Shalini Chaturvedi et.al. Solid propellants: AP/HTPB composite propellants. Arabian Journal of Chemistry.2014

[21] Nazumuddin Shaik. Design and Geometrical Analysis of Propellant Grain Configurations of a Solid Rocket Motor.India.2020

[22] Richard Nakka's.Experimental Rocketry.nakka-rocketry.net

[23]B.P.MASON et.al.SOLID PROPELLANTS.RUBBER CHEMISTRY AND TECHNOLOGY, Vol. 92, No. 1, pp. 1–24.(2019)

[24] Alessandro de laco veris.Fundamental Concepts of liquid-propellant rocket engines.Rome,Italy.Springer.2021

[25] Dieter K.Huzel and David H.Huang.Design of Liquid Propellant Rocket Engines.Natioanl aeronautics and space administration.Washington DC.1967

[26] Oscar Biblarz.Liquid Propellant rocket engine fundamentals.Rocket propulsion elements.8th edition.John wiley edition.2010

[27]Europeanspaceagencyeducation.Solidandliquiddfuelrockets..esa.int/Education/Solid_and _liquid_fuel_rockets

[28]Goerge.P.Sutton.History of Liquid PropellantRocket Enaines.American institute of Aeronautics and Astronautics

[29]Goerge.P.Sutton.Classification.Rocket propulsion elements.7th edition.

[30]Paweł Surmacz et.al.Hybrid Rocket Propulsion Development and Application.Institute of Aviation, Al. Krakowska,Poland.2009

[31]Goerge.P.Sutton.ELECTRIC PROPULSION.Goerge.P.Sutton.Rocket propulsion elements.8th edition.

[32]S.G.Forbes.Electric and Ion Propulsion.W H.T.Loh.Jet, Rocket, Nuclear, Ion and Electric Propulsion:Theory and Design.NORTH AMERICAN ROCKWELL CORPORATIONDOWNEY, CALIFORNIA.Springer.1968

[33]Dan M.Goebel and Ira Katz.Propulsion:Ion and Hall thrusters.jet propulsion laboratory california.(2008)

[34]Niels E. Jensen.ELECTRIC PROPULSION.Europian space agency.2002

[35]Magdi Ragheb et.al.NUCLEAR PROPULSION CHOICES FOR SPACE EXPLORATION.researchgate.2010

[36]Edward J. Zampino et.al.The Challenge of Space Nuclear Propulsion and Power Systems Reliability.reaserchgate.2004

[37]James R. Downey et.al.FLYING REACTORS: THE POLITICAL FEASIBILITY OF NUCLEAR POWER IN SPACE.Maxwell Air Force Base, Alabama.2004

[38]T. W. Price et.al.The Status of Monopropellant Hydrazine Technology.Technical Report 32-7227.NATIONAL AERONAUTICS AND SPACE ADMINISTRATION.JET PROPULSION LABORATORY CALIFORNIA INSTITUTE OF TECHNOLOOY PASADENA, CALIFORNIA.1968

[39]ECHA European Chemicals Agency. Candidate List of Substances of Very High Concern for Authorisation. 20 June 2011.

[40]HIKARU URAMACHI et.al.Green Propulsion Systems for Satellites - Development of Thrusters and Propulsion Systems using Low-toxicity Propellants -.Mitsubishi Heavy Industries Technical Review Vol. 56 No. 1.(2019)

[41]Ahmed E. S. Nosseir et.al.Review of State-of-the-Art Green Monopropellants:For Propulsion Systems Analysts and Designers.

[42]Amir S.Gohardani et.al.Greenspacepropulsion:Opportunitiesandprospects.Elsevier.2014

[43]E. Wernimont et.al.Past and Present Uses of Rocket Grade Hydrogen Peroxide.

[44]GrzeGorz rarata et.al.THE SAFE PREPARATION OF HTP And CONCENTRATEd H2O2 SAmPlES.Warsaw 2011

[45]Andrews, David, "The Industrial History of the Ansty Rocket Department, 19467 to 1971," July 26, 1998

[46]https://military.wikia.org/wiki/Black_Knight_(rocket)

[47]https://discovery.nationalarchives.gov.uk/

[48]C. N. Hill.A Vertical Empire History of the British Rocketry Programme,chapter13.2nd edition.Imperial College Press.Formerly Charterhouse, UK

[49]Donald C.Reaction control system THrusters for space shuttle orbiter.California.2021

[50]Calvin R.jarvis.Operational experience with the X-15 reaction control and reaction augmentation systems.NASA TN D-2864

[51]Chemical and Material Sciences Department Research Division.HYDROGEN PEROXIDE HANDBOOK.July 1967

[52]Advanced Space Transportation Program:Paving the Highway to Space.NASA.https://www.nasa.gov/centers/marshall/news/background/facts/astp.html

[53]K. C. Tseng et.al.Development of Satellite Propulsion Components for Hydrogen Peroxide Propellant.reaserch gate.May 2016

[54]Grzegorz Rarata.Research on Preparation and Propulsive Applications of Highly Concentrated Hydrogen Peroxide.Journal of Aerospace Science and Technology 1.David publishing.2016

[55]One-stage method for production of HTP for propulsion applications and system for production thereof. Description 12.07.2016.

[56]Charles N. Ryan et.al .Experimental Validation of a 1-Newton Hydrogen Peroxide Thruster. JOURNAL OF PROPULSION AND POWER.

[57]Angelo Cervone et.al. DEVELOPMENT OF HYDROGEN PEROXIDE ROCKETS AT ALTA S.P.A.: THE PAST, THE PRESENT AND THE FUTURE.63rd International Astronautical Congress, Naples, Italy.2012

[58]Bastien Boust et.al .Catalytic Ignition of Hydrogen Peroxide for Storable Bipropellant Thrusters.8TH EUROPEAN CONFERENCE FOR AERONAUTICS AND SPACE SCIENCES

[59] Perez Luna, Jaime. *Modélisation et diagnostics d'un propulseur à effet Hall*. Diss. Université de Toulouse, Université Toulouse III-Paul Sabatier, 2008.

[60] Kundu, Pijus, Tarun Kanti Bhattacharyya, and Soumen Das. "Design, fabrication and performance evaluation of a vaporizing liquid microthruster." *Journal of micromechanics and microengineering* 22.2 (2012): 025016.

[61] Liu, Z. G., et al. "The flow resistance and heat transfer characteristics of micro pin-fins with different cross-sectional shapes." *Nanoscale and Microscale Thermophysical Engineering* 19.3 (2015): 221-243.

[62] Denny, Mark, and Alan McFadzean. "Theory: The Rocket Equation and Beyond." *Rocket Science*. Springer, Cham, 2019. 55-102.. https://slideplayer.com/slide/12577751/

[63] Huang, David H., and Dieter K. Huzel. *Modern engineering for design of liquid-propellant rocket engines*. American Institute of Aeronautics and Astronautics, 1992.

[64] Sutton, George P., and Oscar Biblarz. *Rocket propulsion elements*. John Wiley & Sons, 2016.

[65] Cauvin, Daniel. Aérodynamique, Mécanique du vol. Institut aéronautique Jean Mermoz, 1983.

[66] Davis, N. S., and James C. McCormick. "Design of catalyst packs for the decomposition of hydrogen peroxide." *Liquid Rockets and Propellants* (1960).

[67] Levenspiel, Octave. *Chemical reaction engineering*. John Wiley & Sons, 1999.

[68] Ryan, Charles N., et al. "Experimental Validation of a 1-Newton Hydrogen Peroxide Thruster." *Journal of Propulsion and Power* 36.2 (2020): 158-166..

[69] Hirshfield, Laura J., and Heather B. Mayes. "Incorporating Inclusivity and Ethical Awareness Into Chemical Reaction Engineering." *Chemical Engineering Education* 53.4 (2019): 215-219.

[70] Hirshfield, Laura J., and Heather B. Mayes. "Incorporating Inclusivity and Ethical Awareness Into Chemical Reaction Engineering." *Chemical Engineering Education* 53.4 (2019): 215-219.

[71] Krejci, David, et al. "Hydrogen peroxide decomposition for micro propulsion: Simulation and experimental verification." *47th AIAA/ASME/SAE/ASEE Joint Propulsion Conference & Exhibit*. 2011.

[72] Kappenstein, Charles, et al. "Catalytic decomposition of energetic compounds-Influence of catalyst shape and ceramic substrate." *42nd AIAA/ASME/SAE/ASEE Joint Propulsion Conference & Exhibit*. 2006.

[73] m.chemxin-en.com/inert-alumina-ceramic-ball/17-23-inert-ceramic-ball/3-19mm-17-23-inert-ceramic-ball-for-bed.html

[74] Baharudin, Luqmanulhakim, and Matthew James Watson. "Monolithic substrate support catalyst design considerations for steam methane reforming operation." *Reviews in Chemical Engineering* 34.4 (2018): 481-501.

[75] Jacobs, Stan. "Observations of change in the Southern Ocean." *Philosophical Transactions of the Royal Society A: Mathematical, Physical and Engineering Sciences* 364.1844 (2006): 1657-1681.

[76] phae.kipandale.icu/wire-gauze-diagram.html

[77] Richardson, J. T., Y. Peng, and D. Remue. "Properties of ceramic foam catalyst supports: pressure drop." *Applied Catalysis A: General* 204.1 (2000): 19-32.

[78] Bartholomew, Calvin H. "Mechanisms of catalyst deactivation." *Applied Catalysis A: General* 212.1-2 (2001): 17-60

[79] Chan, Y. A., et al. "Development and hot-firing test of a hydrogen peroxide thruster for Formosat-7 project."

[80] Maia, Fernanda Francisca, et al. "Development and optimization of a catalytic thruster for hydrogen peroxide decomposition." *Journal of Aerospace Technology and Management* 6.1 (2014): 61-67.

[81] Whitehead, John. "Hydrogen peroxide propulsion for smaller satellites." (1998).

[82] Robles, Robert Anthony. *THERMOCHEMICAL ANALYSIS OF HYDROGEN PEROXIDE WITH APPLICATIONS TO ROCKET DESIGN*. Diss. San Jose State University, 2002.

[83] Chan, Y. A., et al. "Preliminary development of a hydrogen peroxide thruster." *Proceedings of World Academy of Science, Engineering and Technology*. No. 79. World Academy of Science, Engineering and Technology (WASET), 2013.

[84] Robles, Robert Anthony. *THERMOCHEMICAL ANALYSIS OF HYDROGEN PEROXIDE WITH APPLICATIONS TO ROCKET DESIGN*. Diss. San Jose State University, 2002.

[85] TAYEB, Imad, and Farid BOUFRAINE. *Étude d'un propulseur pour satellite de 20N fonctionnant aux H2O2*. Diss.

[86] Hill, Philip G., and Carl R. Peterson. "Mechanics and thermodynamics of propulsion." *Reading* (1992).

[87] TAYEB, Imad, and Farid BOUFRAINE. *Étude d'un propulseur pour satellite de 20N fonctionnant aux H2O2*. Diss.

[88] Long, Matthew, and John Rusek. "The characterization of the propulsive decomposition of hydrogen peroxide." *36th AIAA/ASME/SAE/ASEE Joint Propulsion Conference and Exhibit*. 2000.

[89] Delery, J. "Tuyères et arrières corps." *Polycopié du cours, ENSAE* (1998).

[90] Wernimont, E., et al. "Past and present uses of rocket grade hydrogen peroxide." *General Kinetics, LLC Aliso Viejo, CA* 92656 (1999).

[91] CHARACTERISTIC VELOCITY WRITTEN BY JERRY RATZLAFF ON 05 APRIL 2020. POSTED IN CLASSICAL MECHANICS

[92] BENAROUS, Abdallah. "Prédiction Numérique des Performances d´ une Tuyère de Propulsion." *Congrès français de mécanique*. AFM, Maison de la Mécanique, 39/41 rue Louis Blanc, 92400 Courbevoie, France (FR), 2013.

[93] Santi, Marco, et al. "Design and Testing of a 3D Printed 10 N Hydrogen Peroxide Monopropellant Thruster." *AIAA Propulsion and Energy 2019 Forum*. 2019.

[94] Pasini, Angelo, et al. "Experimental characterization of a 5 N hydrogen peroxide monopropellant thruster prototype." *43rd AIAA/ASME/SAE/ASEE Joint Propulsion Conference & Exhibit*. 2007.

[95] Torre, L., et al. "Performance of a monopropellant thruster prototype using advanced hydrogen peroxide catalytic beds." *Journal of Propulsion and Power* 25.6 (2009): 1291-1299.

[96] Amri, Redha. *Etude et developpement des systemes de propulsion pour les applications spatiales*. Diss. Blida, 2013.

[97] Continuity and Momentum Equations;Guide, ANSYS Fleunt Teory. "ANSYS Fleunt Teory Guide." (2013).

[98]Invisicd flows;Manual, U. D. F. "ANSYS FLUENT 12.0." Theory Guide. Canonsburg, PA (2009).

[99] Compressible flows;Fluent, A. N. S. Y. S. "ANSYS fluent theory guide 15.0." ANSYS, Canonsburg, PA 33 (2013).

[100] Vestnes, Frida. A CFD-model of the Fluid Flow in a Hydrogen Peroxide Monopropellant Rocket Engine in ANSYS Fluent 16.2. MS thesis. NTNU, 2016.

[101] Speties transport equations;Fluent, A. N. S. Y. S. "ANSYS fluent theory guide 15.0." ANSYS, Canonsburg, PA 33 (2013).

[102] Peter Davidson. Turbulence - An introduction for Scientists and Engineers. OxfordUniversity Press, 2nd edition edition, 2015.

[103] Frank M. White. Fluid Mechanics. McGraw-Hill, New York, USA, 7th edition edition, 2006.

[104] Choosing a turbulance model,Manual, U. D. F. "ANSYS FLUENT 12.0." Theory Guide. Canonsburg, PA (2009).

[105] Yusuf, Siti Nurul Akmal, et al. "A Short Review on RANS Turbulence Models." CFD Letters 12.11 (2020): 83-96.

[106] A. Balabel, A.M. Hegab, M. Nasr, and Samy M. El-Behery. Assessment of turbulence modeling for gas flow in two-dimensional convergent–divergent rocket nozzle. Applied Mathematical Modelling, 35:3408–3422, 2011.

[107] Amrom, Victor. Lois de paroi pour les écoulements turbulents présentant des gradients de pression adverses. Diss. École Polytechnique de Montréal, 2018.

[108] https://simutechgroup.com/why-is-meshing-important-for-fluid-simulations

[109] Bakker, André. "Lecture 7-Meshing Applied Computational Fluid Dynamics." (2002).

[110] https://www.manchestercfd.co.uk/post/all-there-is-to-know-about-different-mesh-types-in-cfd

[111] https://www.cfd-online.com/Wiki/Mesh_classification

[112] https://www.nas.nasa.gov/Software/FAST/RND-93-010.walatka-clucas/htmldocs/chp_16.surferu.html

[113] Zhang, Laiping, et al. "A 3D hybrid grid generation technique and a multigrid/parallel algorithm based on anisotropic agglomeration approach." Chinese Journal of Aeronautics 26.1 (2013): 47-62.

[114] Moldex 3D softawre help manual, mesh quality.

[115] Sutton, George P., and Oscar Biblarz.NOZZLE THEORY ANDTHERMODYNAMIC RELATIONS Rocket propulsion elements. John Wiley & Sons, 2016.

[116] M. Cecotti, La propulsion spatiale, 2003

[117] Tsiolkovsky_rocket_equation//en.wikipedia.org/wiki

[118] Engineering ToolBox. 2003. Specific Heat and Individual Gas Constant of Gases. [https://www.engineeringtoolbox.com/specific-heat-capacity-gases-d_159.html]. Accessed Feb 19, 2018.

[119] Santi, Marco, et al. "Design and Testing of a 3D Printed 10 N Hydrogen Peroxide Monopropellant Thruster." AIAA Propulsion and Energy 2019 Forum. 2019.

[120] Shapiro, Ascher H. *The dynamics and thermodynamics of compressible fluid flow*. No. BOOK. John Wiley & Sons, 1953.

[121] Frank M. White. Fluid Mechanics. McGraw-Hill, New York, USA, 7th edition edition, 2006.

[122] Eames, Ian, and Jan-Bert Flor. "New developments in understanding interfacial processes in turbulent flows." (2011): 702-705.

[123] Đào, Anh. *MÉMOIRE POUR L'OBTENTION DU DIPLÔME DE MASTER*. Diss. 2007.

<u>Annex-1</u>: CAD Model design for the final conception

Based on the output parameters of our model a 3-D CAD model was made by SolidWorks 2017, the design was based on the most critical part of thruster component which are nozzle, injectors, bed loading catalyst, and the tubes used to measure pressure and temperature.
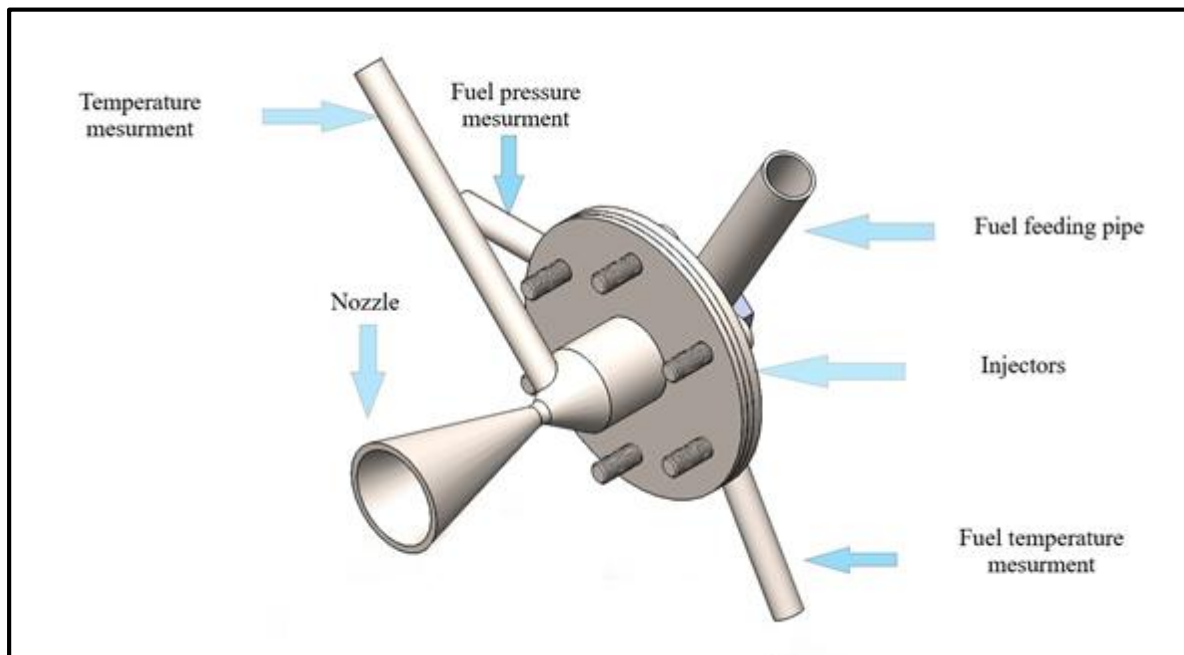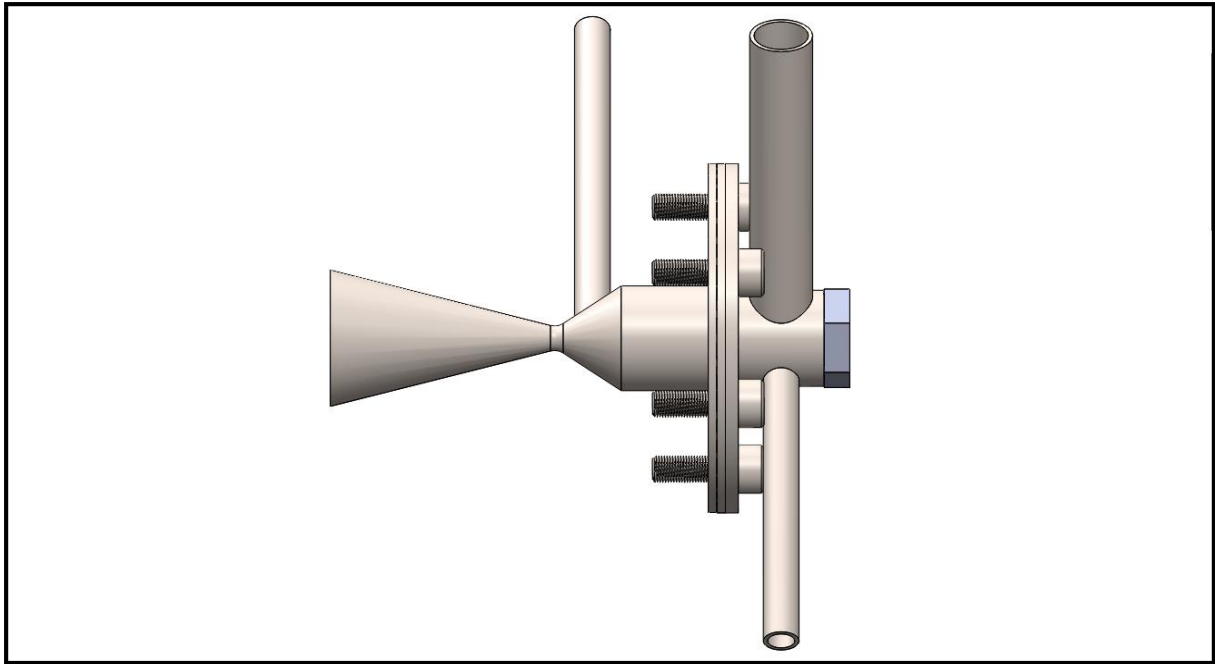

Figure 1: Axisymmetric view of thruster.

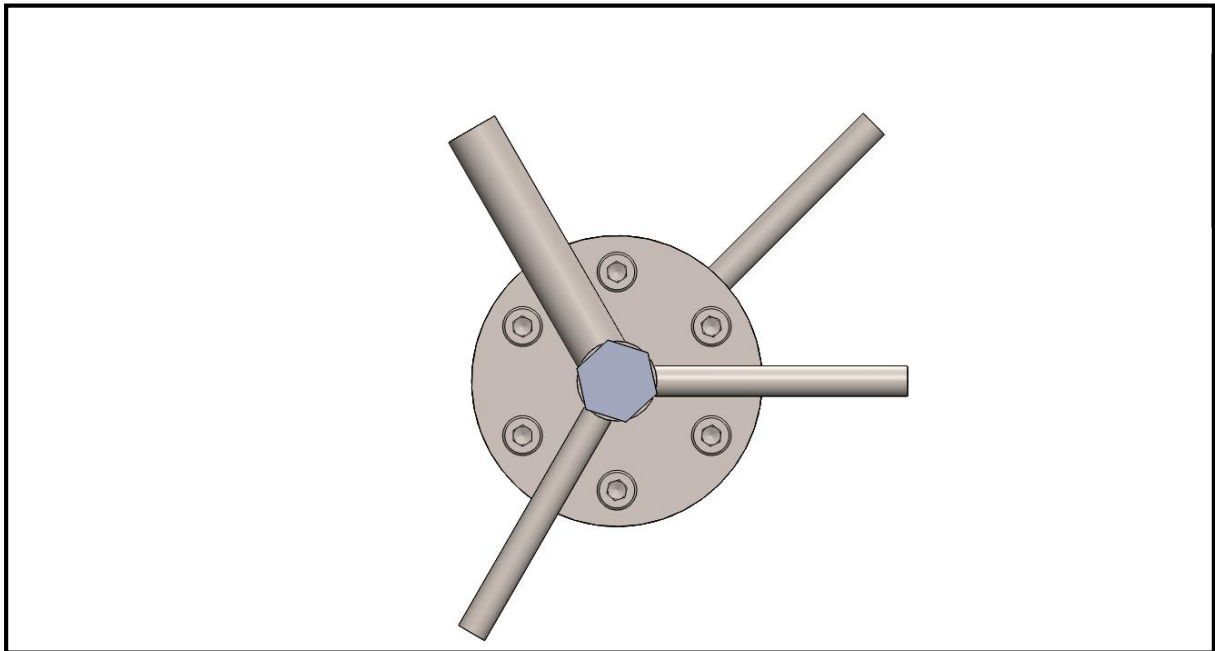Figure 2: Left side view of Thruster.
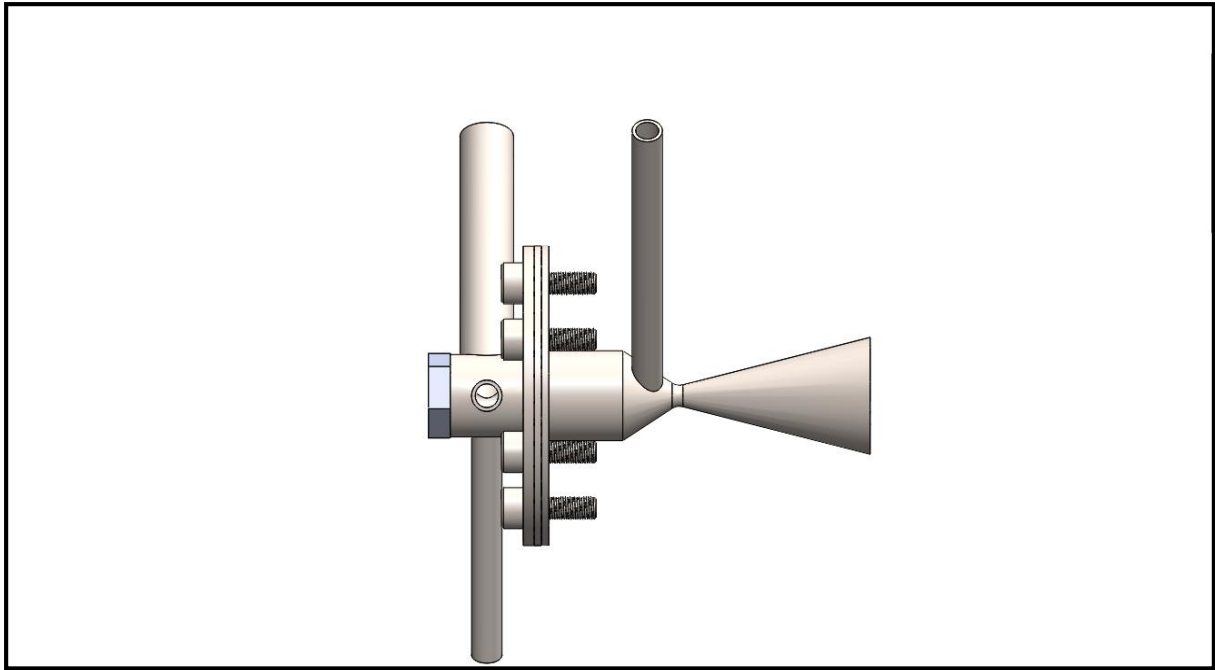

Figure 3: Back view of thruster.

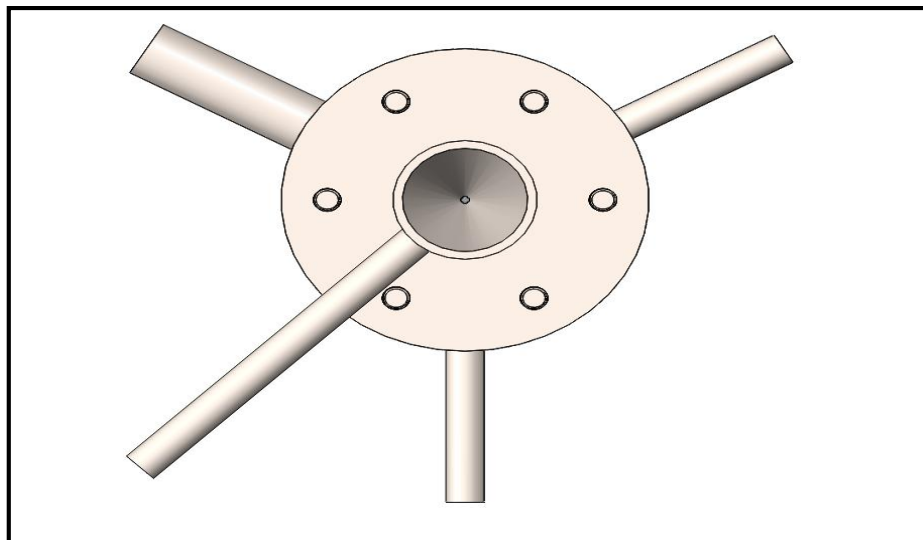Figure 4: Right side view of Thruster.

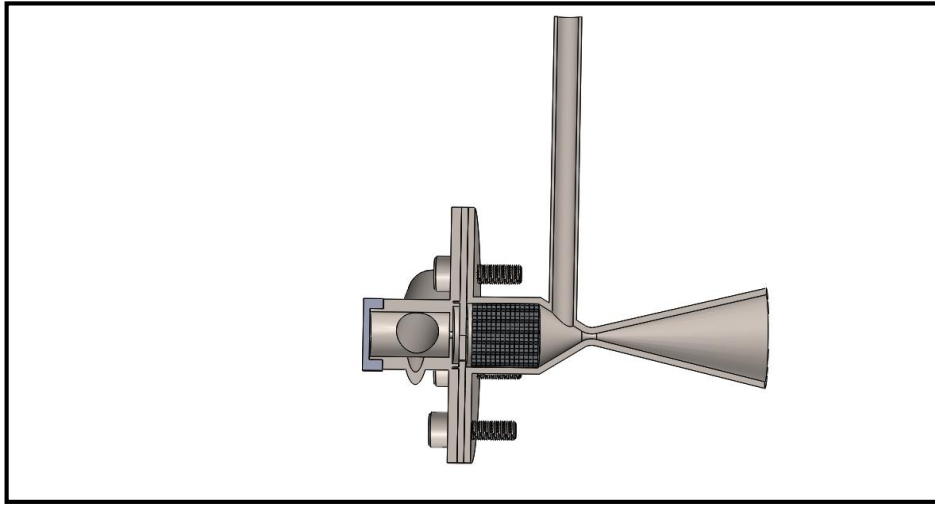Figure 5: Front side view of Thruster.
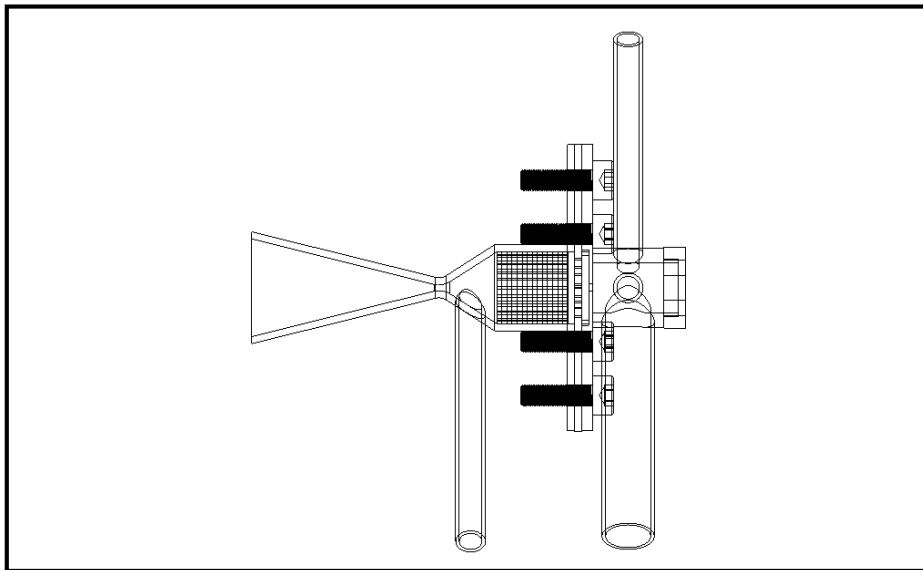
Figure 6: Left side inner view of Thruster.

Figure 7: Axisymmetric inner view of thruster.

Annex-2: **Algorithm to calculate chamber temperature**

$$T = [300:100:2000]$$

$$\Delta H_{H2O} = [\Delta H_{H2O}(1), \Delta H_{H2O}(2), \dots, \Delta H_{H2O}(N)]$$

$$\Delta H_{O2} = [\Delta H_{O2}(1), \Delta H_{02}(2), \dots, \Delta H_{O2}(N)]$$

Q_{avail}= - DrHo

[z,N] = size(Temp)

For i=1,N

$$Q(i) = \frac{c}{a}\Delta H_{H2O}(i) + \frac{d}{a}\Delta H_{O2}(i)$$

z=i

If Q(i) < Q_{avail}

If Q(i)>Q_{avai}

Else

Q(i)=Q_{avail}

Stop, use z=i from previous case

Z=i

$$T_c = Temp(z)$$

$$T_c = \left(\frac{Q_{avail} - Q_Z}{Q_{Z+1} - Q_Z}\right) * (T_{Z+1} - T_Z) + T_Z$$